PERFORMANCE ASSESSMENT OF CARBON-FIBER REINFORCED ELASTOMERIC ISOLATORS INCORPORATED WITH POLYURETHANE CORES

by

Miah Mohammed Riyadh

B.Eng., International Islamic University Malaysia, 2018

A THESIS SUBMITTED IN PARTIAL FULFILLMENT OF

THE REQUIREMENTS FOR THE DEGREE OF

MASTER OF APPLIED SCIENCE

in

THE COLLEGE OF GRADUATE STUDIES

(Civil Engineering)

THE UNIVERSITY OF BRITISH COLUMBIA

(Okanagan)

February 2022

The following individuals certify that they have read, and recommend to the College of Graduate Studies for acceptance, a thesis/dissertation entitled:

PERFORMANCE ASSESSMENT OF CARBON-FIBER REINFORCED ELASTOMERIC ISOLATORS INCORPORATED WITH POLYURETHANE CORES

submitted by Miah Mohammed Riyadh in partial fulfillment of the requirements of the degree of Master of Applied Science in Civil Engineering.

Dr. Shahria Alam, School of Engineering

Supervisor

Dr. Kasun Hewage, School of Engineering

Supervisory Committee Member

Dr. Abbas Milani, School of Engineering

Supervisory Committee Member

Dr. Sina Kheirkhah, School of Engineering

University Examiner

Abstract

Elastomeric isolators dissipate the earthquake energy by providing lateral flexibility, increasing public safety, and reducing the expense of rehabilitation. Steel reinforced elastomeric isolators (SREIs) are the most well-known passive earthquake protection systems which are used in widespread applications of buildings and bridges. SREIs consist of alternate layers of elastomer and steel reinforcement and are usually heavy and expensive. Therefore, they are often limited to expensive and important structures. In seek of broadening the usage of elastomeric isolators by improving their performance, as well as making them lighter and inexpensive, carbon-fiber reinforced elastomeric isolators (C-FREIs) were introduced. C-FREIs consist of carbon fiber sheets instead of steel as the reinforcement and they show satisfactory performance in both vertical and horizontal directions. They can also be used in both bonded and unbonded applications due to the fiber reinforcement having a lack of flexural rigidity. However, C-FREIs undergo premature delamination when used in bonded applications and possess a low energy dissipation capability in unbonded applications. Using polyurethane material in the form of circular cores is a partial solution to overcome the described limitations of C-FREIs. Polyurethane due to its high abrasion resistance and energy dissipation capability makes them an excellent candidate for energy dissipation applications. The objective of this thesis is to introduce and test a novel usage of polyurethane cores in C-FREIs. First, the carbon-fiber reinforced elastomeric isolators with polyurethane cores (C-FRPEs) were designed and fabricated. Then, the C-FRPEs were tested under a series of vertical and compressive-shear loadings to evaluate their vertical and horizontal performance characteristics. Based on the experimental observations, the results showed that incorporating the C-FREIs with polyurethane cores improves their re-centering capability, and noticeably enhances their energy dissipation capacity. It was also revealed that the polyurethane cores in C-FREIs were able to significantly improve the delamination behavior in bonded applications.

Lay Summary

Carbon-fiber reinforced elastomeric isolators (C-FREIs) have the advantage to be used in both bonded and unbonded applications since the carbon fiber sheets have almost negligible flexural rigidity. However, previous experimental studies showed premature delamination occurring at lower lateral strains when used in bonded applications, and lower energy dissipation capability of lower aspect ratio C-FREIs when used in unbonded applications. In seek of improving their energy dissipation capability and delamination behavior, a novel form of C-FREIs incorporated with polyurethane cores was designed and tested in vertical and horizontal directions. The carbon-fiber reinforced elastomeric isolators with the polyurethane cores (C-FRPEs) showed an enhanced recentering capability compared to the plain C-FREIs. Moreover, the C-FRPEs also showed enhanced energy dissipation capabilities, and improved delamination behavior compared to plain C-FREIs.

Preface

The contents presented in this thesis are based on original work carried out at the University of British Columbia (Okanagan campus) by the author. The literature review, collection of literature data, specimen design and test setup, testing, analysis of data, and thesis writing was the sole responsibility of the author. Dr. Shahria Alam provided guidance and supervision throughout the entire process. Peer-reviewed journal and conference papers related to the research topic was submitted as listed below:

1) Riyadh, M.M., Osman, S.M., and Alam, M.S. (2022). “Experimental investigation of novel carbon-fiber reinforced elastomeric isolators with polyurethane cores under vertical and lateral loading”. Journal of Structural Engineering, American Society of Civil Engineers (ASCE). (submitted)
2) Riyadh, M.M., Hedayati, F.H., and Alam, M.S. (2021). “Parametric study on the vertical operational characteristics of carbon fiber reinforced elastomeric isolators using Taguchi approach”. Structures, Elsevier. (Published)
3) Riyadh, M.M., Rodriguez, J., and Alam, M.S. (2021). “Shape factor influence of fiber reinforced elastomeric isolators on the seismic response of a bridge pier”. Canadian Society of Civil Engineers Annual Conference 2021. (Accepted)
4) Riyadh, MM., Hedayati, F.H., and Alam, M.S. (2020). “Parametric study on the lateral stiffness of carbon-fiber reinforced elastomeric isolators against cyclic loads”. IABSE-JSCE Joint Conference in Advances in Bridge Engineering. (Published)

.

Table of Contents

List of Tables

List of Figures

List of Symbols

μ_{st}	=	Static co-efficient of friction
μ_{st}	=	Dynamic co-efficient of friction
S_F	=	Primary shape factor
S_{F2}	=	Secondary shape factor
${S_{F2}}^{-1}$	=	Slenderness ratio
L	=	Length of bearing
W	=	Width of bearing
t_e	=	Thickness of individual elastomer layer
n_e	=	Number of elastomer layers
T_e	=	Total elastomeric height
n_f	=	Number of fiber reinforcement layers
t_f	=	Thickness of each fiber reinforcement sheet
A	=	Surface area of the bearing
P_v	=	Design Compressive pressure
F_v	=	Compressive force
K_v	=	Vertical stiffness
E_c	=	Compression modulus
ξ	=	Equivalent viscous damping
v_{max}	=	Maximum vertical deflection
F_{V2}	=	Maximum vertical force
F_{V1}	=	Minimum vertical force
δ_{V2}	=	Maximum vertical displacement
δ_{V1}	=	Minimum vertical displacement

K_h	=	Effective horizontal stiffness
F_{h2}	=	Maximum horizontal force
F_{h1}	=	Minimum horizontal force
δ_{h2}	=	Maximum horizontal displacement
δ_{h1}	=	Minimum horizontal displacement
G_h	=	Effective shear modulus
γ	=	Lateral strain
W_d	=	Energy dissipated per cycle
W_s	=	Energy restored per cycle
δ_{avg}	=	Average lateral displacement
F_h	=	Horizontal force
δ_h	=	Horizontal displacement
δ_v	=	Vertical displacement
f_v	=	Lateral cyclic frequency

List of Abbreviations

SREI	Steel Reinforced Elastomeric Isolator
C-FREI	Carbon-Fiber Reinforced Elastomeric Isolator
C-FRPE	Carbon-Fiber Reinforced Elastomeric Isolator with Polyurethane Cores
FREI	Fiber Reinforced Elastomeric Isolator
FRP	Fiber Reinforced Polymer
PE	Polyurethane
SMA	Shape Memory Alloy
ISO	International Standard of Organization
LDEI	Low Damping Elastomeric Isolator
HDEI	High Damping Elastomeric Isolator
LRB	Lead Rubber Bearing
PTFE	Polytetrafluoroethylene
FP	Friction Pendulum
BC-FREI	Bonded Carbon-Fiber Reinforced Elastomeric Isolator
U-CFP	Unidirectional Carbon-Fiber Polymer
B-CFP	Bidirectional Carbon-Fiber Polymer
UC-FREI	Unbonded Carbon-Fiber Reinforced Elastomeric Isolator
U-FREI	Unbonded Fiber Reinforced Elastomeric Isolator
ADRI	Added Damping Rubber Isolator
EQS	Eradi-Quake System
CHBDC	Canadian Highway Bridge Design Code
ALAMS	Applied Laboratory for Advanced Materials and Structures
LVDT	Linear Variable Differential Transformer
HSS	High Strength Steel

SRD	Stable Rollover Deformation
B	Bonded
UB	Unbonded

Acknowledgements

I would like to express my deepest appreciation to my supervisor Dr. Shahria Alam for his continuous support and feedback throughout my master's degree. Dr. Alam's optimistic attitude and immense knowledge have enabled me to improve my critical thinking and improve the quality of my work.

I would like to express my sincerest gratitude to my parents who have always supported me throughout my years of education, morally, financially, and emotionally.

I would like to thank the University of British Columbia and the School of Engineering for providing me with an excellent environment for completing my degree. The financial contributions of Mitacs were critical to conducting this research and gratefully acknowledged.

I also acknowledge the support of my research teammates who gave their valuable time whenever I needed their help and all my friends who were with me during my study. I would like to give my special thanks to Sherif M. Osman who provided me with a lot of support and time for concluding my experiments and Peng Zhang who guided me during the design and thesis writing phase.

Dedication

I would like to dedicate this thesis to my dear father Ziauddin, and my dear mother Tahmina for their endless love and support. I deeply appreciate my siblings for always being there with me and making my journey easier. I would like them to always know that all my achievements are theirs too. Thank you very much.

Chapter 1: Introduction and Thesis Organization

1.1 Background

A major challenge of earthquake engineering is understanding the behavior of the structural components as earthquakes are one of the most unpredictable naturally occurring phenomena and can have disastrous repercussions to human civilization. Earthquakes having high magnitudes can have devastating consequences such as the loss of human lives and financial consequences. For instance, the 2011 Tohoku earthquake in Japan had resulted in an economic loss of more than 300 billion USD and a loss of human lives of more than 19,500 (Daniell et al., 2011; Khazai et al., 2011).

A higher level of consequence is given to important structures such as bridges, and emergency control centers (e.g. Hospitals, fire stations), for them to remain fully functional during a seismic event. For this reason, a significant amount of research has been conducted in the past 50 years to persuade designers to consider high levels of structural performance with reasonable construction costs (Tsai & Kelly, 2002). Different seismic protection systems have been developed which can be active, passive, or even hybrid. Passive protective systems are widely implemented in civil engineering applications since no external power supplies are required for them to function (Ozbulut et al., 2007). A traditional example of a passive seismic protective system is the steel-reinforced elastomeric isolators (SREIs), which consist of alternating layers of elastomers and steel reinforcement (Madera Sierra et al., 2019).

1.2 Seismic Isolation

Seismic isolation refers to the uncoupling of the superstructure from the substructure by the placement of a flexible damping system between them. The flexible damping system possess a low horizontal stiffness which brings the fundamental frequency of a structure lower than the ground motion predominant frequencies (James M. Kelly & Konstantinidis, 2011a). This significant reduction in the fundamental frequency of the structure limits the seismic damages and

prevents the structure from collapsing. Many isolation systems have been developed and installed throughout the years to mitigate the aftereffects of seismic actions (Kim et al., 2019). One of the most common devices for seismic isolation is elastomeric bearings.

Elastomeric isolators constitute alternating layers of a flexible elastomer material and a suitable reinforcement (Amin et al., 2006). The reinforcement enables the isolator to limit the lateral bulging of the elastomer layers to be able to take large vertical loads (Milani & Milani, 2012), while the elastomer layers provide the required flexibility to attenuate the course of the lateral component of a seismic action (Warn et al., 2007a). The flexibility of the isolator in the horizontal direction increases the period of the structure, thereby limiting the earthquake energy transferred to it. Figure 1 shows a schematic of the behavior of structure when isolated by elastomeric isolators. It is observed that for the isolated structure, the superstructure remains almost rigid by containing the deformation entirely at the isolation level.

As mentioned previously, the most common type of elastomeric isolators used are the steel-reinforced elastomeric isolators, SREIs (also commonly known as laminated isolators) (Farzad Naeim, 2000). The bonding between the layers of these traditional isolators is achieved using a hot vulcanization method which is a labor-intensive and expensive manufacturing process, limiting their application to only large and expensive structures (Spizzuoco et al., 2014).

The application of elastomeric isolators can be extended to smaller projects such as residential buildings or to developing regions with the development of fiber-reinforced elastomeric isolators (FREIs). In FREIs, the reinforcement used consists of an appropriate fiber-reinforced polymer (FRP), instead of steel shims used in traditional elastomeric isolators. The manufacturing process of FREIs is much more cost-efficient and allows easy handling and transportation due to the lower weight of the fiber reinforcement. FRP has a much higher strength-to-weight ratio compared to steel, which makes FREIs an efficacious alternative to the traditional SREIs (James M Kelly, 1999b).

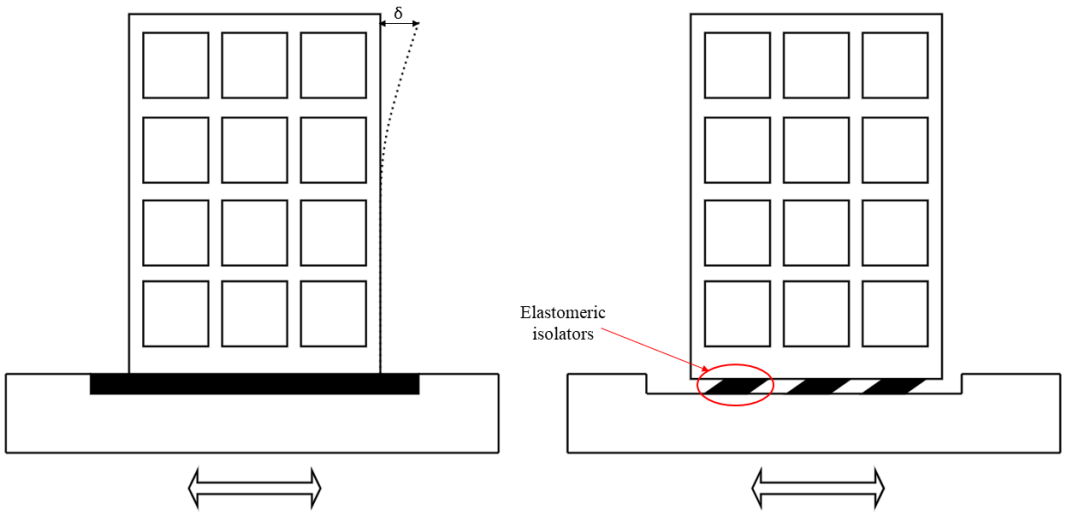

Figure 1: Behavior of a structure during a seismic action (a) fixed base (b) isolated with elastomeric isolators

Several studies have revealed superior or satisfactory performance of FREIs when compared to SREIs. For example, Bakhshi et al. (2014) determined that FREIs have a slightly lower vertical stiffness but has a more efficient energy dissipation capability when compared to SREIs. The functionality of differenttypes of fiber sheets as reinforcement to be used in elastomeric bearings has been investigated by Moon et al. (2002). They found out that the highest vertical stiffness corresponds to that of carbon fiber compared to the other types of fiber material. Therefore, carbon-fiber reinforced elastomeric isolators (C-FREIs) have been chosen for this study.

Carbon fiber sheets when used as reinforcement have almost no flexural rigidity and are prone to a unique horizontal deformation known as the rollover deformation, occurring at larger strain values. Due to this characteristic, C-FREIs can be used in both bonded and unbonded applications with each application having certain limitations. For bonded C-FREI applications, delamination and unrecoverable deformations occur at lower horizontal displacements (Farshad Hedayati Dezfuli & Alam, 2016). For unbonded applications, the isolators are susceptible to slip, disabling the isolators to transfer tensile forces under certain loading conditions and have lower

energy dissipation capacity (Van Engelen et al., 2019). To overcome the aforementioned limitations, a method of improving the recentering capability, energy dissipation capacity, and delamination of C-FREIs have to be explored. It is also important that the method used for improving the energy dissipation and delamination behavior of the C-FREIs has a minimal effect on the shear modulus as an increase in shear modulus will deplete the lateral flexibility of the isolators.

Naturally, neoprene rubber is the most common for the elastomer material in elastomeric isolators. They are generally soft which results in a relatively low compressive stiffness and low damping properties (Choi et al., 2017). Given the need to improve the energy dissipation capacity of elastomeric isolators, several studies have explored the use of rubber cores in elastomeric isolators. In one study, the lead plug used in LRBs was replaced with a rubber cylinder enclosed with steel rings where the mechanical properties depicted a lower lateral stiffness and a superior energy dissipation. Rahnavard & Thomas (2019) explored the behavior of circular SREIs containing single or multiple rubber cores. Their study revealed that the rubber cores improve the energy dissipation of the isolators at large lateral strains. In contrary to rubber cores, polyurethane cores can be used for higher energy dissipation. Polyurethane has been used as the elastomer material in many Civil engineering applications due to its high compressive stiffness and high abrasion performance (Qi & Boyce, 2005). Furthermore, it was also determined that polyurethane presents an ideal self-centering capability when tested with a precompression. The flag-shaped hysteresis behavior of pre-compressed polyurethane is similar to superelastic shape memory alloys (SMA), which are often referred to as smart materials (Choi et al., 2017; Rahman Bhuiyan & Alam, 2013). The excellent re-centering, high energy dissipation, high abrasion performance capabilities deem polyurethane as a potential material to be used in elastomeric bearings. To the best of the authors' knowledge, there are no studies that examine the effect of viscous material cores to improve the energy dissipation capability of C-FREIs, and therefore, this study aims to address this topic.

1.3 Research Objectives

With the goal of seeking an improvement in the energy dissipation and delamination behavior of carbon-fiber reinforced elastomeric isolators (C-FREIs), the primary goal of this thesis is to introduce and evaluate a novel configuration of carbon-fiber reinforced elastomeric isolators integrated with polyurethane cores (C-FRPEs). Experimental tests are done in order to establish a sufficient understanding of the behavior of C-FREIs when polyurethane cores are placed in them and to accurately perceive their advantages/limitations in both types of applications (bonded and unbonded). Thus, the primary objectives of this work include:

- Developing a novel configuration of carbon-fiber reinforced elastomeric isolators containing polyurethane cores (C-FRPEs).
- Determining the vertical/horizontal stiffness and energy dissipation capabilities of the C-FRPEs by subjecting them to a series of vertical and compression-shear loadings.
- Comparing the vertical/horizontal stiffness and energy dissipation capabilities of the C-FRPEs with those of the plain C-FREI for both bonded and unbonded applications.

In order to carry out the aforementioned objectives, the C-FREIs and C-FRPEs are designed and fabricated using a cold vulcanization method which is a cost-effective and quicker alternative compared to the typically used hot vulcanization method. The effectiveness of the fabricated isolators is explored by conducting a series of vertical and compression-shear testing complying with the methods specified by the International Organization of Standardization ISO 22762:2018. The series of tests are carried out at the Applied Laboratory for Advanced Materials and Structures (ALAMS) at the University of British Columbia.

1.4 Thesis Layout

Chapter 2 presents the literature review on the different aspects of the concept of base isolation and various kinds of elastomeric isolators, including but are not limited to the traditional

steel-reinforced elastomeric isolators (SREIs), carbon-fiber reinforced elastomeric isolators (C-FREIs), and the self-centering capability of polyurethane (PE).

Chapter 3 concentrates on the design features and fabrication of the C-FREIs and the novel C-FRPEs. This chapter also briefly describes the testing program and the test setup used for conducting the series of vertical and compressive-shear tests. The parameters of interest and the mechanical properties are also discussed in this chapter.

Chapter 4 describes the results obtained from carrying out the experimental tests. The performance specifications of interest such as the vertical and horizontal stiffness, energy dissipation, equivalent viscous damping are discussed and compared from the obtained results.

Chapter 5 presents the summary and the concluding remarks. The prime findings of this thesis are discussed, along with the limitations of the current work with recommendations for future research.

Chapter 2: Literature Review

2.1 General

It is not always economically feasible to design structures that remain within the elastic range during a seismic event. With the objective to mitigate the disastrous effects of seismic action, several devices to dissipate seismic energy have been developed in the past. These energy dissipation devices can be classified as active, passive, and hybrid systems. In civil engineering applications, passive energy dissipation devices are preferred and heavily used in the past due to the simplicity of not having an external power source (Ozbulut et al., 2007). Recent passive control systems are based on energy dissipation and seismic isolation techniques (Dolce et al., 2000). The primary aim of these devices is to eliminate or reduce the plastic deformations the structure experiences during strong seismic events.

Isolation techniques decouple some of the parts along the height to introduce one or more discontinuities. The discontinuities are made between the superstructure and substructure level and are designed to undergo relatively large horizontal displacements, typically in the range of 100-200mm (Dolce et al., 2000). Elastomeric isolators and sliding isolators are the most common isolation techniques currently in use (Buckle, 2000). Elastomeric isolators are placed between the superstructure and the substructure for both bridge and building applications. They allow the superstructure to remain sufficiently rigid during a seismic action. In some regions, there are lateral pressures from the soil due to the inclined ground surface for residential buildings. This will not affect the isolator and the superstructure performance given that the foundation is designed to be rigid enough to withstand the lateral pressures of the soil.

2.2 Elastomeric Isolators

Currently, elastomeric isolators provide the simplest method of isolation. Elastomeric isolators introduce significant flexibility into an isolated structure by exhibiting large strains (B. M. Constantinou et al., 1990). Elastomeric bearings consist of alternating layers of elastomer and

suitable reinforcement material. The function of the reinforcement is to support the vertical loads of the superstructure and to keep the structure sufficiently stiff, while the function of the elastomer layers is to influence the shear modulus of the elastomeric bearing (Warn et al., 2007b). Thus, the addition of the elastomeric isolators having a low horizontal stiffness between the superstructure and substructure lowers the fundamental frequency of the structure compared to the ground motion's predominant frequencies. (James M. Kelly & Konstantinidis, 2011b;Cenan, 2010). Figure 2 shows how the acceleration of the structure is affected by base isolation.

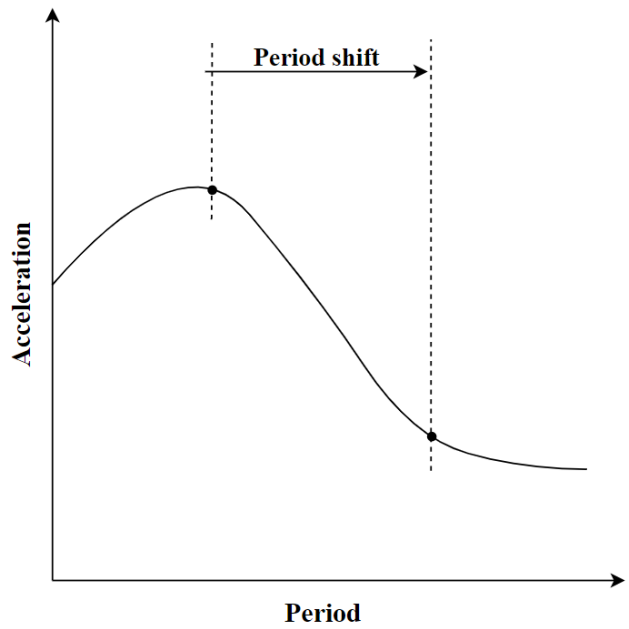

Figure 2: Effect of the structural period due to base isolation on the acceleration response

Steel-reinforced elastomeric isolators (SREIs), which are the conventional isolators in use have the reinforcements made of steel shims (Farshad Hedayati Dezfuli & Alam, 2017). Figure 3 shows the main components of an elastomeric isolator and the schematic of a bridge behavior when isolated with elastomeric isolators. As shown in the figure, the isolators are placed between the superstructure (e.g., deck) and the substructure (e.g., pier).

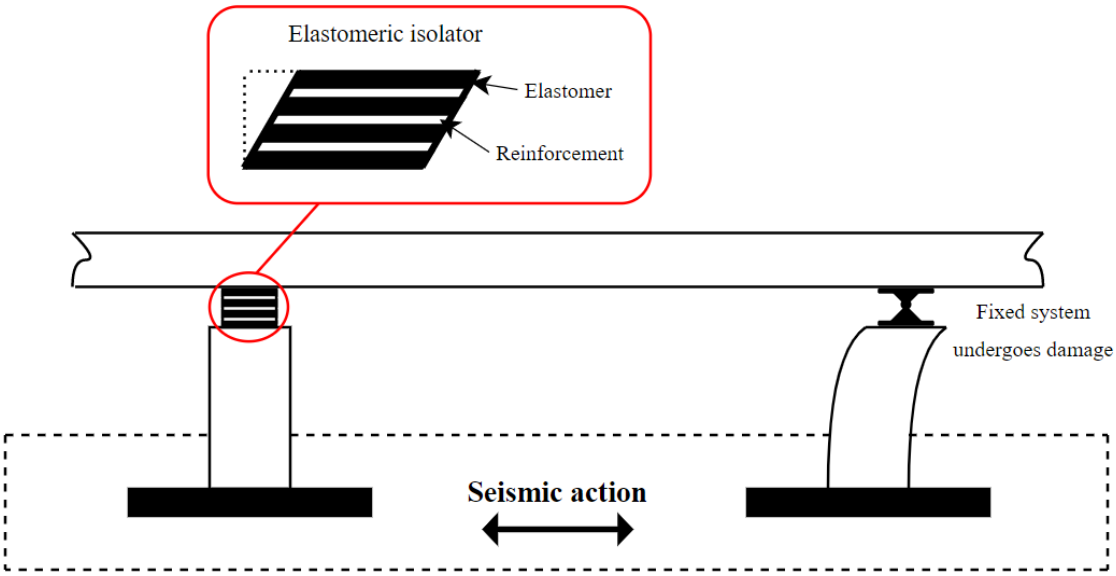

Figure 3: Behavior of base isolation system in a bridge

Bridge infrastructures represent a key role in the transportation network of any country or region. The vulnerability of bridges in any seismic event is a major consideration and significant challenges underly to keep the bridges safe during such catastrophic events. Any loss of functionality of major route bridges during a seismic event will compromise public safety (such as rescue operations or medical services). Furthermore, extensive direct or indirect economic losses can prevail depending on the post functionality of bridges. Large residual deformations of bridge piers can cause expensive repairs or even demolition. In Japan, more than 100 bridge piers were demolished due to undergoing large residual deformations following the aftermath of the Kobe 1995 earthquake (Billah & Alam, 2015). The concept of base isolation using elastomeric bearings is a well-understood concept and widely utilized for alleviating the consequences following a seismic event. The base isolation system with elastomeric isolators can improve the seismic performance of a structure and thus reduce the cost of rehabilitation after a seismic event (Siqueira et al., 2014). With the energy dissipation capability of the elastomeric bearings, the main aim of their application is to provide continuous operation in important bridges and buildings

during an earthquake, keeping the structural damage to a minimum for moderate events, and preventing the collapse of structures in severe events.

2.2.1 Traditional steel-reinforced elastomeric isolators (SREIs) / Laminated isolators

SREIs are the most conventional type of elastomeric isolators in use. Figure 4 shows the cross-section of the main components of an SREI. As observed, the main components of the SREI are the alternating layers of elastomer and steel reinforcement and are supported by thick end plates.

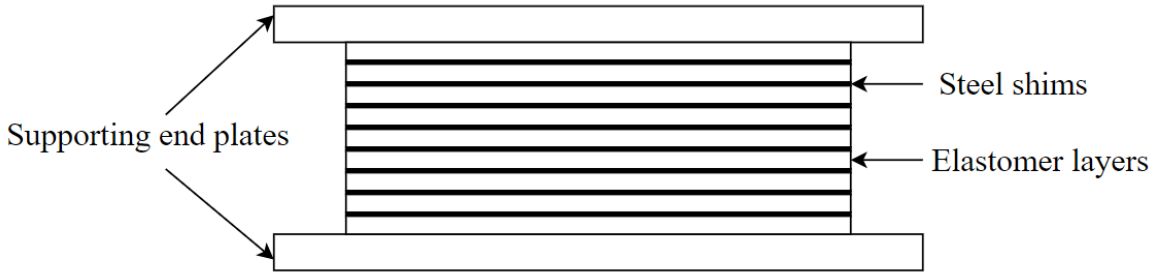

Figure 4: Components of a steel-reinforced elastomeric isolator (SREI)

As depicted in figure 4, the majority of the weight of SREIs comes from the use of steel shims as reinforcement and the use of thick steel end plates. Therefore, they are generally heavy and difficult to transport. Due to their high cost and weight, SREIs are typically installed in critical infrastructure such as fire stations or hospitals to avoid any post-disaster service interruptions (Farshad Hedayati Dezfuli, 2015). The cost of SREIs is high mainly due to the labor-intensive manufacturing process used to bond the elastomer layers and the steel shims. This manufacturing process involves a hot vulcanization process involving a mold to achieve desirable bonding strength between the varying elastomer and reinforcement layers. Therefore, limited application of conventional rubber bearings is justified (Markou et al., 2016; Kelly & Konstantinidis, 2011b). These kinds of isolators have different properties depending on the elastomer material used or through the use of an external energy dissipating system. They are characterized in the preceding sections.

2.2.1.1 Low damping elastomeric isolators (LDEIs)

These isolators are also commonly known as synthetic isolators. The elastomer is normally produced with natural rubber or neoprene. The damping ratio and the energy dissipation capacity of LDEIs are low and typically range within 2-3% (Cenan, 2010). For this very reason, an external device to increase the energy dissipation capacity of LDEIs is often used accordingly. High damping elastomeric isolators (HDEIs) and lead rubber bearings (LRB) are common examples where the energy dissipation has been magnified.

2.2.1.2 High damping elastomeric isolators (HDEIs)

HDEIs are high energy dissipation bearings that when compared to LDEIs, are enhanced in the damping performance. The order of damping capability of HDEIs is several times larger than that of their low damping counterpart, ranging from 10-20% (Marioni, n.d.). The high damping elastomer material is fabricated using vulcanized rubber synthesized with explicit materials such as extra-fine carbon black, oil, plasticizer, and other exclusive fillers (Yuan et al., 2016). As a result, the augmented elastomeric material possesses the capability to withstand higher magnitudes of strain and higher equivalent viscous damping properties (Yuan et al., 2016; Liu et al., 2014).

HDEIs are very feasible and effective as they do not require any supplementary energy dissipation due to their initial high damping property. The seismic response of such isolated structural systems enhanced by the addition of high damping isolators causes the natural period of the structure to elongate attaining a significant reduction to its seismic response (Markou et al., 2016). The enhancement in the damping property of HDEI is achieved through the manipulation of the viscosity of the elastomer material, and therefore their sensitivity of the operational characteristics becomes more prominent due to temperature changes (Okui et al., 2019), which can become significant in extreme conditions. Figure 5 depicts how the shear modulus of high damping elastomer varies through a range of temperatures (Z-Tech, 2010).

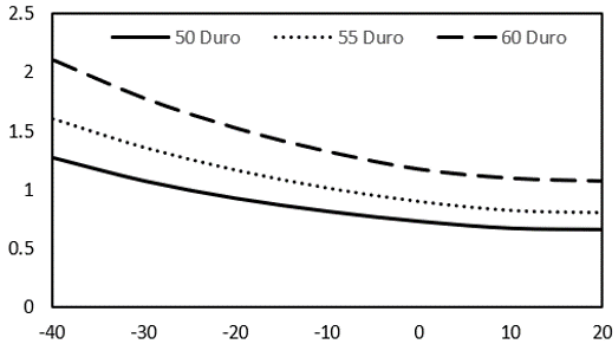

Hardness	Shear Modulus at 20°C (MPa)
50	0.63
55	0.81
60	1.06

Figure 5: Relationship in the shear modulus of high damping elastomer material with respect to temperature at three hardness levels and shear modulus at 20°C (adapted from (Z-Tech, 2010))

HDEIs also display higher shear modulus compared to LDEIs (Skinner et al., 1993). HDEIs can also undergo very large lateral displacements during a seismic excitation of around 400% (expressed with respect to the total height of the elastomer in the bearing) (Yoshida et al., 2002). Figure 6 compares how the hysteresis curves can be classified for low damping and high damping bearings. As observed, the area enclosed within the loop for high damping bearing is much higher denoting a much higher energy dissipation capacity (International Organization for Standardization BS ISO 22762-1:2018).

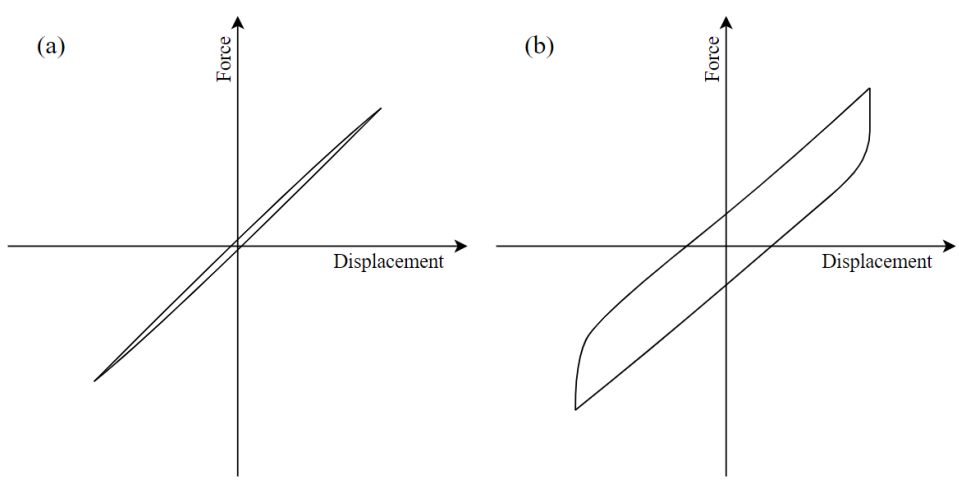

Figure 6: Shear force vs displacement hysteresis loop for (a) low damping elastomeric bearing (b) high damping elastomeric bearing

2.2.1.3 Lead Rubber Bearing (LRB)

Lead rubber bearings (LRBs) are manufactured from traditional SREIs by placing a circular portion at the center with a lead plug. This lead-core undergoes substantial plastic deformation and thus facilitating large energy dissipation, to support the deformations experienced during a seismic action. The lead core returns to its initial position with the assistance of the elasticity of the rubber layers, recrystallization, and the interrelated process of recovery (Lu et al., 2020; Robinson & Greenbank, 1976). The main components of an LRB cross-section are shown in Figure 7.

The very first LRB was used to isolate a building in New Zealand in 1981. This particular LRB experienced the 1994 Northridge and the 1995 Kobe earthquakes and was able to successfully mitigate the disastrous consequences of the ground motions, thus confirming their suitability (Jangid, 2007). Figure 8 displays the hysteresis loop of LRB when compared to that of traditional SREIs (Govardhan & Paul, 2016). It is observed that by placing a lead core, the area enclosed within the hysteresis loop becomes much more prominent implying much higher energy dissipation.

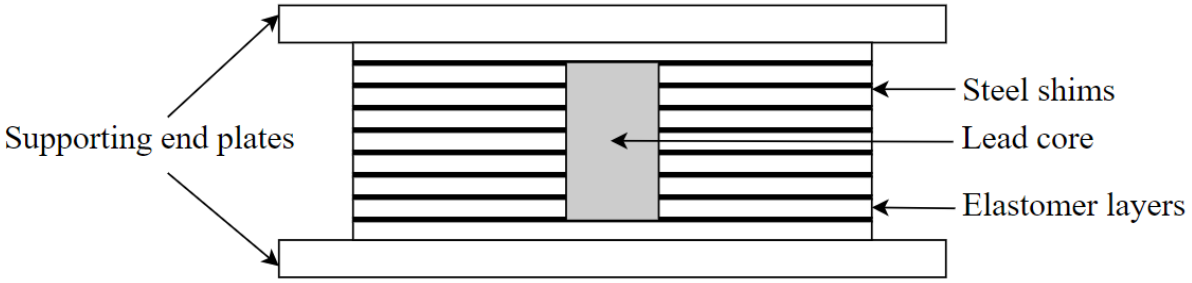

Figure 7: Main components of a lead rubber bearing (LRB)

It is also observed that at a lower level of strain (Figure 8a), the LRB follows almost an ideal hysteresis behavior. This assumption of using the bilinear model to depict the hysteresis behavior of LRBs was used in many studies, for example, the study performed by Ahmadipour & Alam (2017). At larger strain (Figure 8b), a stiffening behavior is observed which happens

primarily due to the non-linear characteristics of the elastomer material. This primary hysteretic behavior is typically modeled analytically using a rate-independent plasticity model or a Bouc Wen model (Satish et al., 1991). However, it should be noted that the lead core heating becomes a concern during successive load cycles which can cause degradation of the operational characteristics of the LRB (Kalpakidis & Constantinou, 2009a). The Bouc Wen model does not take into account the effect of heating of LRBs, and theoretical models to account for this thermal effect have already been introduced which have been experimentally verified (Kalpakidis & Constantinou, 2009b).

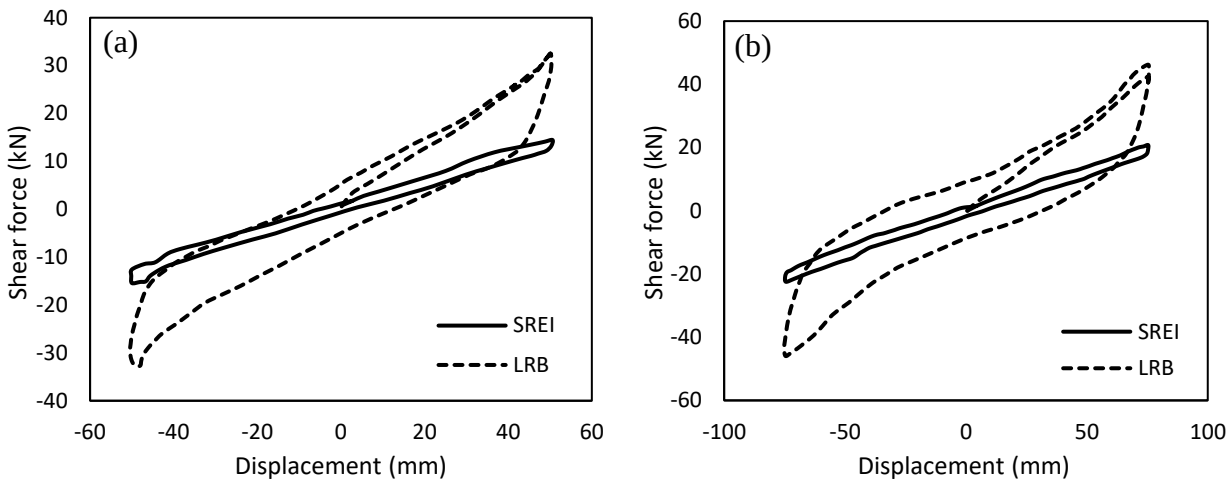

Figure 8: Shear force vs. displacement hysteresis loop comparison for SREI and LRB for (a) low strain (b) high strain (adapted from (Govardhan & Paul, 2016))

The addition of the lead core further augments the vertical stiffness of the bearing and also adds an initial rigidity to the bearing to make it more rigid against wind loads. Amongst the components of LRB, the diameter of the lead core has the highest effect on their performance characteristics (Ahmadipour & Alam, 2017). Zhao et al (2011) determined that the LRB's performance is highly dependent on the yield strength and initial shear stiffness. The restoring force of the LRBs is also more sensitive to the vertical pressure when compared to low damping and high damping isolators (Masato et al., 2004).

2.2.2 Sliding isolators

In sliding isolators, the superstructure is decoupled from the substructure by placing an isolator dependent on the sliding or friction-based interface of the isolator. Sliding isolators work by the sliding of a Polytetrafluoroethylene (PTFE) surface on a stainless-steel plate. Figure 9 shows the main components for a sliding bearing. The co-efficient of friction of the sliding interface is low which provides limited resistance to the horizontal stiffness but is adequate to support large vertical loads. As shown in Figure 9, the curved surface of the concave dish provides the restoring force like a pendulum system, and therefore commonly known as the single friction pendulum system (FP) (Warn & Ryan, 2012). The sliding isolators are often accompanied by elastomeric layer backings to accommodate rotations or the dissipation of vibrations within the structure.

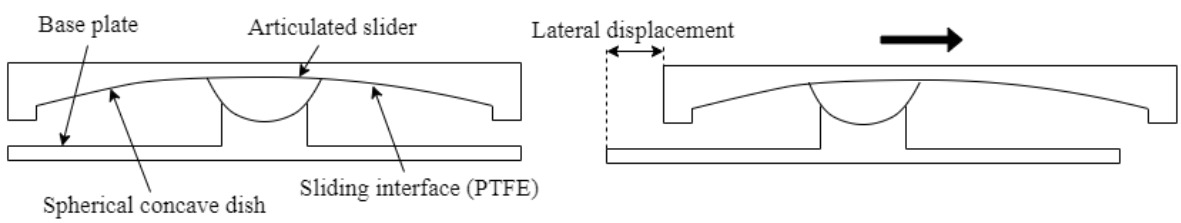

Figure 9: Main components of a sliding isolator

The FP isolators show a bilinear hysteresis behavior similar to the LRBs. M. Constantinou et al. (1990) proposed an analytical equation for FP isolators which deduce the coefficient of friction from the influence of the dead load bearing and the instantaneous velocity. Sliding isolators are also affected by heating due to successive cycles as the LRBs, although a higher number of parameters determines the heating effect for sliding isolators. The service temperature due to successive cycles is dependent on the vigorous sliding velocity, as well as the ambient and bulk temperature due to the co-efficient of friction between the sliding interfaces (Warn & Ryan, 2012). The dependence of the co-efficient of friction on the sliding velocity is depicted in Figure 10. It can be observed that during sliding, the co-efficient of friction changes from a static value (μ_{st}) to a dynamic value (μ_{dy}). The μ_{st} provides an opposing force prior to sliding and the μ_{dy} increases exponentially as the sliding velocity is increased. This large co-efficient of friction for

sliding isolators and the heating during successive cycles are the main disadvantages of sliding isolators.

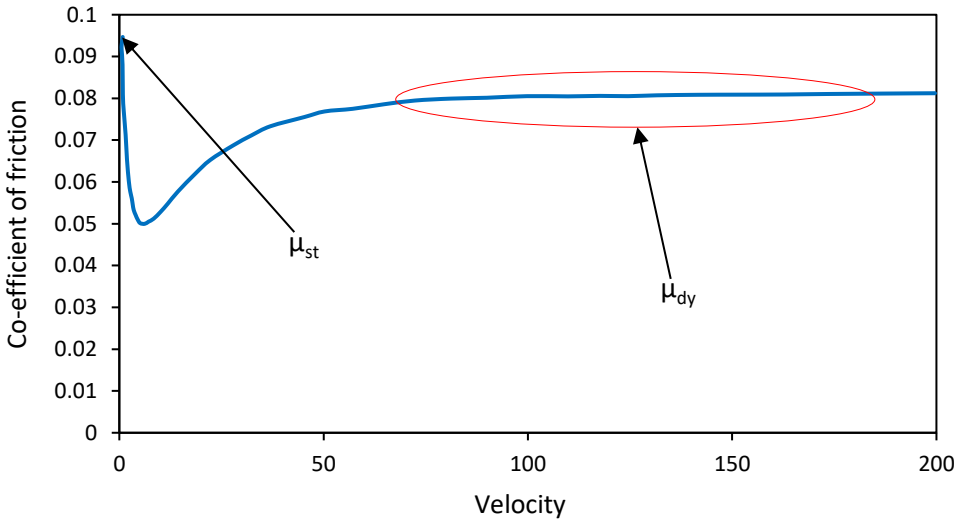

Figure 10: Dependency of the co-efficient of friction of the sliding velocity of sliding isolators (adapted from (Calabrese et al., 2020))

2.3 Carbon-fiber reinforced elastomeric isolators (C-FREIs)

Till date, steel reinforced elastomeric isolators (SREIs) are the most common isolators in use. However, according to Kelly (2002), the traditional SREIs are heavy and expensive which restricts their use to be expanded to low-rise commercial or residential buildings. Their limitations of having a high cost and weight make them be adopted in only important structures in North America, such as in hospitals, bridges, and fire stations. The steel shims used in the isolator to facilitate the vertical loads of the structure are responsible for its heavy weight. Furthermore, as stipulated by Kelly (2002) and Kelly & Konstantinidis (2011b), the weight of such individual isolators can reach up to 1 ton and is also enhanced by using thick steel end-plates. The hike in the cost arises majorly from the labor-intensive manufacturing process to bond the elastomer and the reinforcement layers. This manufacturing process involves a hot vulcanization process involving a mold to achieve desirable bonding strength between the varying elastomer and reinforcement layers. Therefore, limited applications of SREIs are justified (Markou et al., 2016).

There is a need for a reduction in the weight and cost of elastomeric isolators to be expanded to housing or even masonry structures in developing countries. Their application could be further extended to regions where structures may be subjected to moderate seismic events. The functionality of these elastomeric bearings should be attained through a less demanding manufacturing process comprising of reduced weight for easy handling during transportation and construction. In addition, the shipping freight cost can be significantly reduced when shipped at large volume, and will also allow easier handling and installation. These issues have been dealt with by the development of fiber-reinforced elastomeric isolators (FREIs). FREIs consist of elastomer layers and fiber sheets as the reinforcement. The fiber reinforcement limits the lateral bulging of the elastomeric layers when put through compression loadings (Osgooei et al., 2014). The density of fiber materials are much lower than steel which makes them much lighter. The vertical stiffness also remains adequate as fiber materials possess a high strength-to-weight ratio and can have a larger or similar elastic stiffness compared to steel. The mechanical properties of fiber materials depict a high elastic modulus and high tensile strength, satisfactory fatigue behavior, and not prone to any creep or relaxation. Carbon fibers particularly have an elastic modulus ranging from 200GPa to 800Gpa and a tensile strength ranging from 2500MPa to 6000MPa. These desirable properties make fiber reinforcement very desirable candidates for reinforcing elastomeric isolators (Moon et al., 2002).

One aspect of FREIs is that they can be used in unbonded applications due to the fiber reinforcement lacking flexural rigidity and free to rollover. Several studies such as the study performed by Toopchi-Nezhad et al. (2011) have shown that the tensile stresses acting during cyclic loading are reduced by the unique rollover deformation. The orientations of the fiber in the fiber sheets can be modified and manipulated during design to establish superior performance under respective loads. Another advantage of fiber materials is the non-corrosive property which gives them a higher service life compared to steel material (Kelly, 1999a; Osgooei et al., 2014). All these advantages described above make FREIs a remarkable alternative to traditional SREIs

which allow the use of elastomeric isolators to be extended to moderately low seismic regions and residential households.

Besides the performance, the major difference between carbon-fiber reinforced elastomeric isolators (C-FREIs) and the traditional SREIs is the type of reinforcement used. Under bending, the carbon-fiber sheets show no flexural rigidity and are completely flexible. Therefore, under a lateral displacement, C-FREIs undergo a unique rollover deformation. This unique property makes C-FREIs be used in 'bonded' or 'unbonded' configurations. In bonded applications, the compression is within the overlap region of the top and bottom platens, while the tensile stresses created by the unbalanced moments are carried by the region outside the overlap. For unbonded applications, the moment from the applied shear balances the moment created by the offset of the compressive forces. This phenomenon under compressive-shear loading is depicted in Figure 11 (Spizzuoco et al., 2014).

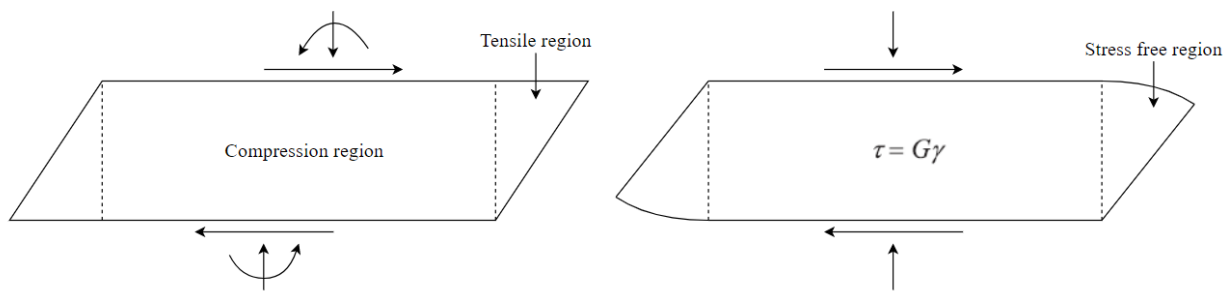

Figure 11: Compressive-shear loading on (a) bonded isolator (b) unbonded isolator

Following a strong seismic event, bonded and unbonded isolators undergo different levels of damage and might have to be replaced. This is done by lifting the superstructure replacing the old isolator for unbonded applications and opening the bolted connections for the replacement for bonded applications. In China, installing unbonded isolators is a common practice for small to medium span highway bridges, where majority of the failure occurs by the unseating of the deck. However, in Japan bonded applications of elastomeric isolators are preferred which are bolted through the superstructure and substructure (Xiang et al. 2018).

2.3.1 Bonded carbon-fiber reinforced elastomeric isolators (BC-FREIs)

In bonded carbon-fiber reinforced elastomeric isolators (BC-FREIs), two thick steel mounting plates are bonded to the top and bottom surface of the isolator, such as the traditional SREIs. The BC-FREIs have their steel mounting plates bolted to the superstructure and the substructure during installation. Figure 12 shows the main components of a BC-FREI.

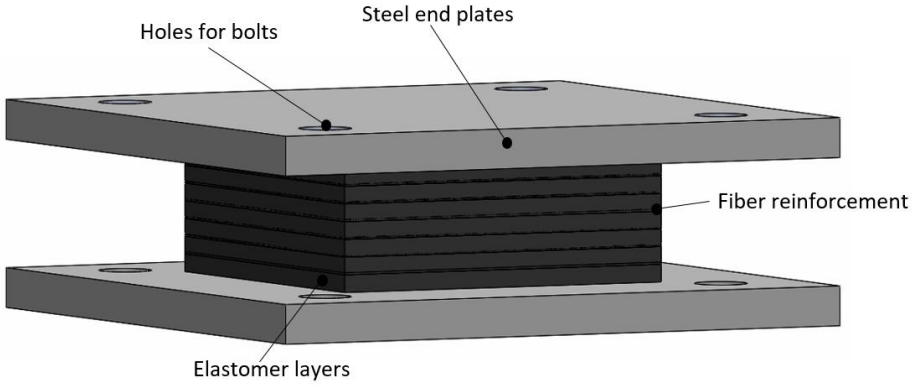

Figure 12: Components of a bonded fiber-reinforced elastomeric isolator (BC-FREI)

The horizontal and vertical operational characteristics of BC-FREIs have been experimentally explored on several occasions. The different types of fiber reinforcements to be used for FREIs have been experimentally tested by Moon et al. (2002). They found out that carbon-fiber has the highest vertical stiffness compared to the other types of fiber materials. They also conducted experiments to compare the performance of BC-FREIs with traditional SREIs, which concluded that BC-FREIs have almost 3 times the vertical stiffness of SREIs. However, it should be noted that the difference in thickness of fiber and steel reinforcement was accounted for by using more layers of fiber and rubber. As a result, the higher primary shape factor in the C-FREI causes lower lateral bulging of the rubber layers allowing it to have a very high vertical stiffness. Horizontal tests indicated that BC-FREIs have lower shear modulus and almost 2.5 times the equivalent viscous damping compared to those of SREIs.

The variations in the mechanical and dynamic properties of BC-FREIs compared to SREIs have been explored by Bakhshi et al. (2014). It was observed that the BC-FREIs have a 20%

lower weight compared to SREIs. The vertical test results indicated that the BC-FREIs had a lower vertical stiffness which was only 0.37 times lower compared to the SREIs. The lateral experimental results indicated that the shear modulus was 0.27 times lower, and the equivalent viscous damping was 0.21 times higher for BC-FREIs when compared to SREIs. Naghshineh et al. (2013) conducted experiments on a new kind of BC-FREIs where carbon-fiber mesh instead of fabric was used as the reinforcement layers. They found out that BC-FREIs when compared to SREIs have a notable reduction in horizontal stiffness when subjected to high magnitudes of compressive stress and lateral strain. BC-FREIs showed a lower vertical stiffness which was comparable to the SREIs and is primarily dependent on the primary shape factor of the bearings. These experimental findings ensure that BC-FREIs is an excellent alternative, if not superior to the traditional SREIs.

A number of finite element studies have been performed on BC-FREIs to further their understanding. Several BC-FREIs having the same loading area were analyzed in FEM by applying compressive-shear loadings to find out the effect of five different aspect ratios on the lateral performance. Two kinds of carbon-fiber reinforcements were used which were unidirectional carbon-fiber (U-CFP) and bidirectional carbon-fibers (B-CFP). It was observed that the stresses in U-CFP reinforcements were larger compared to B-CFP reinforcements, which enables the isolators reinforced with B-CFP to withstand larger lateral strains. Lower aspect ratios of the bearings yielded superior lateral behavior than the bearings with higher aspect ratios (Salim & Ananthakumar, 2017). 2-D finite element simulations on 20 C-FREIs having the same base width to study the influence of the thickness of each elastomeric layer on the vertical and horizontal stiffness was conducted by Toopchi-Nezhad et al. (2013). They found out that the primary shape factor has a large effect on the compression modulus which is dependent on the thickness of each elastomeric layer, while the lateral stiffness is largely affected by the total height of the elastomer layers (secondary shape factor). Hedayati Dezfuli & Alam (2013) conducted a parametric study by numerically testing 27 C-FREIs to study the dependency of three different

factors (number of elastomer layers, thickness of FRP sheets, shear modulus of elastomer) on the lateral and vertical operational characteristics. The results showed that the dependency of the different factors has a larger effect on the vertical characteristics compared to the horizontal characteristics. Riyadh et al. (2020) further identified that the thickness of the carbon fiber sheets has an almost negligible effect on the horizontal stiffness and is mostly dependent on the elastomer material in bonded applications.

Designers and contractors may not prefer to use unbonded bearings in bridges due to lack of confidence or due to the higher probability of the deck unseating. However, the failure modes of BC-FREIs are of utmost interest as delamination becomes critical at larger strains due to the limited flexural rigidity of the carbon fiber reinforcement. Regarding this, one study observed that delamination and debonding became the primary mode of failure in such bonded applications. Delamination was observed between the elastomer and reinforcement layers, and between the elastomer and the steel end plates at 50% shear strain. However, the BC-FREIs remained functional up to 100% shear strain (Hedayati Dezfuli & Alam, 2014). It should be noted that these failure modes are unsatisfactory and means of improving the failure mechanism of bonded C-FREIs is essential.

2.3.2 Unbonded carbon-fiber reinforced elastomeric isolators (UC-FREIs)

A large number of studies are focused on unbonded carbon-fiber reinforced elastomeric isolators (UC-FREIs) due to researchers wanting to take advantage of the rollover deformation taking place at larger strains. This rollover deformation increases the lateral flexibility at cyclic-shear displacements, thereby reducing the horizontal stiffness and the tensile stresses acting on the elastomer layers. One of the early studies on the functionality of UC-FREIs was done by Toopchi-Nezhad et al. (2008). They found out that the vertical stiffness of the isolators in the unbonded application remains satisfactory at all levels of lateral displacements. The horizontal tests showed that the rollover deformation reduces the horizontal stiffness and increases the

efficiency of the device, although a stable rollover only occurs for suitable aspect ratios (Al-Anany & Tait, 2017). Figure 13 shows the rollover behavior of unbonded carbon-fiber reinforced elastomeric isolators subjected to lateral displacements.

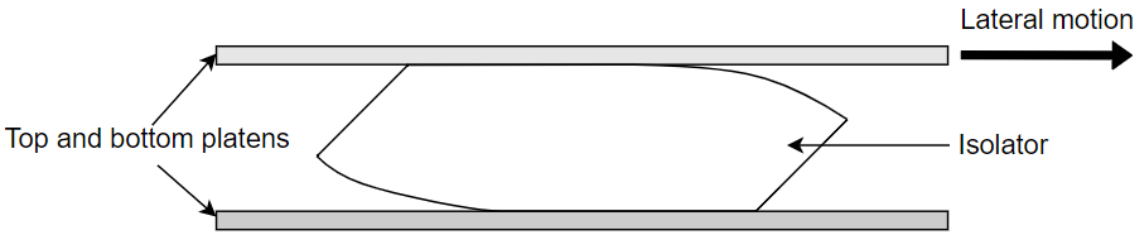

Figure 13: Rollover behavior of unbonded fiber reinforced elastomeric isolators

The effect of static rotations on the vertical stiffness of UC-FREIs resulting from service loads in bridges was investigated by Al-Anany & Tait (2017). It was determined that the static rotations only had a considerable effect on the vertical stiffness at lower levels of vertical loads. Isolators having a suitable aspect ratio for a stable rollover deformation works efficiently against static rotations. The effect of aging and shape factors on the lateral behavior of UC-FREIs has been probed by Russo et al. (2013). A higher shape factor depicts a higher horizontal stiffness but in turn, reduces the damping ratio. The process of aging induces a rise in horizontal stiffness and a fall in the damping ratio. Russo et al. (2013) also studied the effect of using bi-directional and quadri-directional carbon-fiber fabrics as the reinforcement. Quadri-directional carbon-fiber fabrics have a more prominent resistivity to the vertical loads and are more dissipative against horizontal loads.

Hamid et al (2007) performed reduced scale shake table tests on a two-story moment-resisting frame structure by isolating the base with UC-FREIs. The test results revealed that the isolators were able to reduce the top story drift by up to 42% and the orientations of the UC-FREIs had a negligible effect on their performance. To reduce the cost of such isolators even further, recycled rubber has been employed to C-FREIs and tested in unbonded applications. The results showed successful lateral behavior takes place during cyclic lateral tests where the horizontal

stiffness reduces by 82% by increasing the lateral strain by 78% after rollover behavior takes place (Spizzuoco et al., 2014).

Finite element studies along with analytical approaches have further proved the viability of unbonded fiber-reinforced elastomeric isolators. Farzad & Kelly (1999) developed an analytical model able to predict the behavior of U-FREIs, providing a very good approximation in the post elastic behavior and not in the elastic region. The bi-linear model proposed by Pauletta et al. (2017) provides a very good approximation in both the elastic and post-elastic regions up to shear strains of 150%. The secant horizontal stiffnesses for both bonded and unbonded specimens were addressed by Thuyet et al. (2017). They compared the finite element results with the experimental results and proposed an analytical equation to predict the effective horizontal stiffness. The approach showed reasonable approximation at lateral strains lower than 100% of the total thickness of the rubber layers. Sistla & Mohan (2020) conducted finite element analyses to obtain the hysteresis curves of both bonded and unbonded fiber-reinforced isolators. Figure 14 shows the hysteresis curve comparison for the bonded and unbonded specimens at a lateral strain of $1.2T_e$, where T_e is the total thickness of the elastomer.

UC-FREIs when compared to BC-FREIs have lower initial horizontal stiffness and this stiffness reduces even further when rollover deformations take place at larger strain values, making the isolator even more efficient in seismic isolation. Furthermore, they also isolated a two-story building with the specimens and obtained from the time history analyses that the top story shear and displacement is lower for the unbonded specimens.

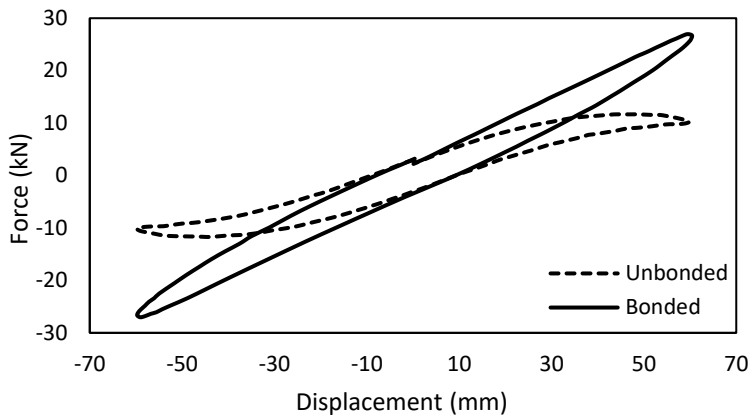

Figure 14: Shear hysteresis behavior comparison of bonded and unbonded fiber-reinforced isolator (adapted from (Sistla & Mohan, 2020))

There are several shortcomings of UC-FREIs when considered for practical applications. They have a low energy dissipation capacity and often possess inadequate horizontal stiffness to resist service loads, such as wind loads at service (Toopchi-Nezhad et al., 2008). UC-FREIs may experience roll-out instability when the overturning moment due to the horizontal forces exceeds the stabilizing moment from the vertical forces (Pauletta et al., 2015). The sliding instability of UC-FREIs was pointed out by Russo & Pauletta (2013), which is dependent on the friction between the contact surfaces of the concrete and the isolator. They illustrated that the sliding instability becomes a concern, and unstable behavior of the isolator is observed at high lateral displacements subjected to low values of applied compression. Moreover, all the points of the surface of the isolator in contact with the concrete undergo a rigid permanent deformation after the unloading cycle at lower compressive stresses. These shortcomings can be overcome using an energy dissipation device having an initial high stiffness and high damping.

2.4 Polyurethane (PE) performance evaluation

The techniques to improve the energy dissipation and stability of elastomeric isolators have been long explored in many studies. For example, silicone instead of natural elastomer has proven to be more durable and independent of the working temperature. The equivalent viscous

damping of silicone bearings was approximately twice of natural or high damping elastomeric isolators (Hayashi et al., 1993). Other high damping materials in the form of filler cores in elastomeric isolators have been proven useful in mitigating seismic energy.

Talaeitaba et al. (2019) tested the performance of a new kind of elastomeric bearing where the lead plug used in lead rubber bearings was replaced with a rubber cylinder enclosed with steel rings. The mechanical properties of the isolator revealed a superior energy dissipation capacity and lower effective lateral stiffness. The performance of circular steel-reinforced elastomeric isolators consisting of single or multiple rubber cores has been investigated numerically by Rahnavard & Thomas (2019). The authors concluded that the use of rubber cores improves the energy dissipation of the isolators which in turn weaken the input forces transmitted to the structure. Moreover, multiple rubber cores when compared to the single-core have higher energy dissipation at larger lateral strains. Furthermore, isolators having multiple rubber cores are more proficient in dissipating energy and are more stable when the cores have a wider radial distribution. The stability of square isolators with single or multiple rubber cores was further investigated by Rahnavard et al. (2020) using the quasi-static method. Figure 15 shows the fabrication steps which were used for a single rubber core isolator bonded with a cold-vulcanizing agent. They found out that the size of the core has minimal effect on stability, and a small number of cores result in superior performance compared to having a large number of holes with the same area.

The core of the isolators can be filled with a viscous material having high damping energy. One such isolator with the acronym “Added Damping Rubber Isolator (ADRI)” was proposed by Dolce et al. (2003). The proposed isolation device depicted more than 2 times the damping ratio compared to isolators without a viscous filling. The authors also suggested that the equivalent viscous damping in the order 20% or even higher can be achieved with ADRIs, higher than that of lead rubber bearings. Furthermore, rather than illustrating a hysteretic behavior like lead rubber bearings, ADRIs show a viscous nature of damping which is more advantageous for near-fault

earthquakes. It was also pointed out by the authors that the ADRIs have a more stable mechanical behavior compared to high damping elastomeric isolators subjected to repeated cyclic loading.

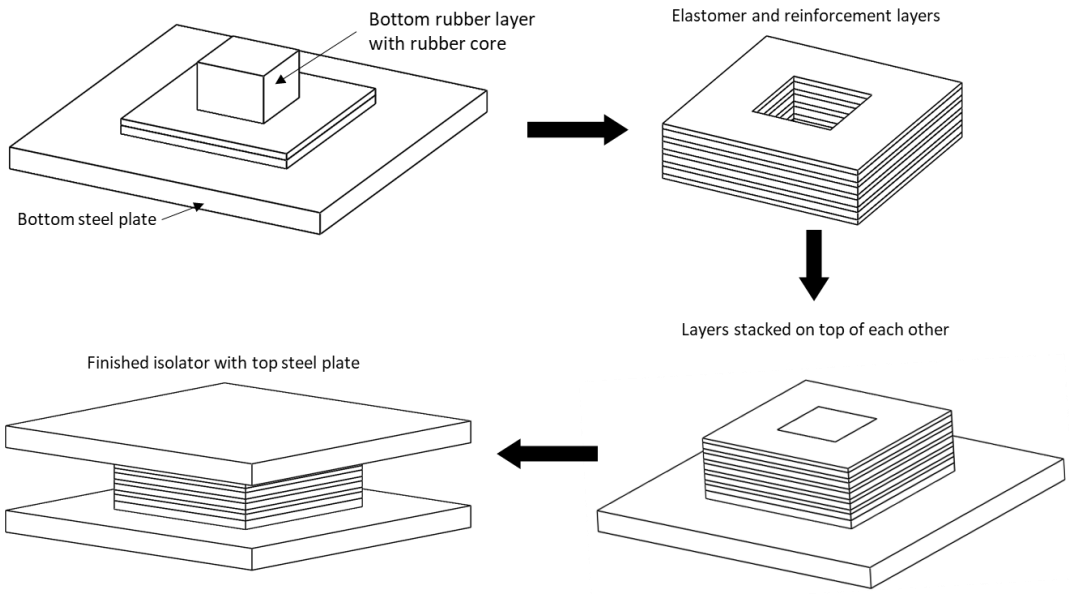

Figure 15: Representation of the fabrication procedure of square rubber isolators with rubber cores (adapted from (Rahnavard et al., 2020))

One such material which can be incorporated as the core in elastomeric isolators is polyurethane (PE). PE portrays a relatively high hardness, ranging from 60A to 70D on a durometer scale. Furthermore, PE materials display high anti-abrasion performance which enables them to be used in a wide variety of devices (Qi & Boyce, 2005). In civil engineering seismic isolation applications, PE is commonly used in Eradi-Quake Systems (EQS) which consists of cylindrical PE springs. The functionality of the EQS has been tested and determined that the PE springs do not recover completely and retain a sliding displacement when no pre-compression is introduced (Choi et al., 2017). Although, it was also determined that PE illustrates an ideal self-centering capability when tested with a precompression, which is always the case for elastomeric isolators due to the dead load of the superstructure. The flag-shaped hysteresis behavior of pre-compressed polyurethane is similar to super elastic shape memory alloys (SMA),

which are often referred to as smart materials (Choi et al., 2017; Rahman Bhuiyan & Alam, 2013). The excellent re-centering, high energy dissipation, high abrasion performance capabilities deem polyurethane as a potential material to be used in elastomeric bearings.

Chapter 3: Experimental Investigation of Carbon-Fiber Reinforced Elastomeric Isolators with Polyurethane Cores

3.1 General

In Chapter 2, a thorough literature review was done for acquiring insight into the performance of isolation devices and carbon-fiber reinforced elastomeric isolators (C-FREIs). The performance of polyurethane (PE) in seismic isolation devices has been well established to realize an improvement in the functionality of C-FREIs.

This chapter presents the information related to the design specifications and materials utilized in the fabrication of the C-FREIs and the novel carbon-fiber reinforced elastomeric isolators with polyurethane cores (C-FRPEs). The C-FRPEs were designed and proposed to serve as an isolation system having enhanced energy dissipation and re-centering capabilities. The detailed fabrication steps, mechanical properties, testing program, and test setup are briefly discussed in this chapter.

3.2 General design features of fiber-reinforced isolators

Fiber-reinforced elastomeric isolators (FREIs) should provide adequate stiffness in the vertical direction and be flexible and sufficiently stable to dissipate the lateral forces experienced during seismic excitation. The shape factor is a critical design factor to denote the stability of such bearings. Kelly (1993) proposed a simplified theory to address issues with stability in fiber-reinforced elastomeric isolators. The theory relates the critical load capacity of elastomeric bearings being a function of the primary and secondary shape factors. The primary shape factor (S_F) is a measure of the local geometry of an elastomeric bearing which quantifies the inverse of each elastomeric layer's slenderness. Moreover, the magnitudes of the primary shape factor greatly influence the stresses acting on the elastomer-reinforcement interfaces. The secondary shape factor (S_{F2}) is a measure of the inverse of the global slenderness which describes the bearing's tendency to remain stable under lateral displacements. In the US, early applications of

elastomeric bearings in the period from 1985-1991 considered the primary and secondary shape factor values in the range 7 < S_F < 11 and 1.5 < S_{F2} < 3, respectively. Values of S_F > 5 and S_{F2} > 3 is recommended to maintain good performance in both vertical and horizontal directions (Montuori et al., 2016). Gauron et al. (2018) explored how the critical load of elastomeric bearings when subjected to compressive-shear loads are influenced by the primary shape factor and the slenderness ratio (${S_{F2}}^{-1}$). Increments in S_F and S_{F2} were made up to maximum values of 12.5 and 1.4 respectively. It has been observed that S_{F2} has a greater influence on stability than S_F when lateral loads are considered. Equations (3.1) and (3.2) define the primary and secondary shape factors of the elastomeric isolators. According to the equations, S_F is defined as the ratio of the loaded area to the load free area of each elastomer layer. S_{F2} is also known as the aspect ratio and is calculated by dividing the bearing's length or width by the total elastomer thickness.

$$S_F = \frac{L\,W}{2t_e\,(L+W)} \tag{3.1}$$

$$S_{F2} = \frac{W}{n_e t_e} \tag{3.2}$$

Where, L and W are the length and width of the bearing respectively, t_e is the thickness of an individual elastomer layer, n_e is the number of elastomer layers.

This study is conducted on square-shaped bearings ($L = W$) and their primary shape factor can be given by equation (3.3).

$$S_F = \frac{L^2}{4Lt_e} = \frac{L}{4t_e} \tag{3.3}$$

3.3 Design features of the fabricated isolators

Reduced scale isolators having plan dimensions ($L \times W$) of 140×140mm were chosen for investigating their vertical and lateral properties. The thickness of individual elastomer layers (t_e) was taken to be 6.5mm with a total number of 5 layers ($n_e = 5$). This leads to the total elastomeric height (T_e) of the isolators to be 32.5mm. As mentioned previously, a primary shape factor higher than 5 and a secondary shape factor higher than 3 are required to have good

performance in both vertical and horizontal directions. According to equation (3.2) and equation (3.3), the values of S_F and S_{F2} are 5.4 and 4.3, respectively. These values of shape factors provide adequate performance in both vertical and horizontal directions. Reinforcement was provided between the five elastomer layers by 4 carbon-fiber sheets ($n_f = 4$). The thickness of the individual carbon-fiber sheets (t_f) is 0.25mm. The geometric parameters associated with the isolator design are shown in Figure 16. Table 1 tabulates the geometric details of the carbon-fiber reinforced elastomeric isolators (C-FREIs) designed in this study.

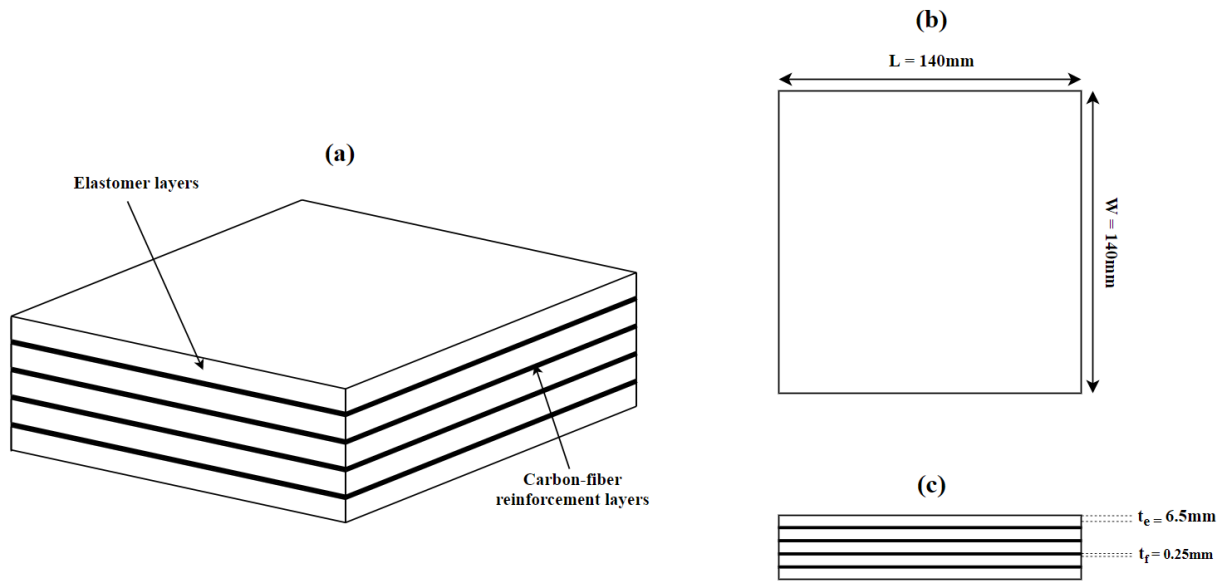

Figure 16: Geometric details of the carbon-fiber reinforced elastomeric isolator design (a) isometric view (b) top view (c) side view

Table 1: Details of the geometric properties of the C-FREI design

$L \times W$ (mm×mm)	t_e (mm)	t_f (mm)	n_e (-)	n_f (-)	T_e (mm)	S_F (-)	S_{F2} (-)
140 × 140	6.5	0.25	5	4	32.5	5.4	4.3

Three different modifications were made to the plain C-FREIs by incorporating polyurethane (PE) cores. The basis of the modification was for the C-FREIs to have a single polyurethane core or multiple polyurethane cores. Single and multiple core configurations are used following the study by Rahnavard & Thomas (2019). In their study, it was determined that multiple rubber cores are more efficient to dissipate energy at higher lateral strains compared to

a single core. The functionality of single or multiple polyurethane cores has not been explored in terms of both vertical and lateral directions, justifying the basis of the modifications.

The first modification was done having a single PE core at the center of the isolator, denoted as C-FRPE1. The second modification was done having 5 PE cores, with each core having the same area, denoted as C-FRPE2. Finally, the third modification was done also having 5 PE cores, with the center core having four times the area as each of the four other cores, denoted as C-FRPE3. It should be noted that the total area cut off from the isolators for the placement of the PE cores in all the modifications was kept constant at 2450mm^2. This cut-out and polyurethane core area equals 12.5% of the total area ($L \times W$) of the isolators.

Table 2 describes three modifications made on the C-FREIs with the polyurethane cores. Figure 17 shows a detailed schematic representation of the three modifications made to the carbon-fiber reinforced elastomeric isolators. In the figure, both plan views and isometric views are shown, with the isometric views depicting both before and after polyurethane cores are placed.

Table 2: Description of the modifications done on the C-FREIs based on number of cores and core size

Specification	Abbreviation	No. of Polyurethane cores (-)	Area of each core (mm^2): A = 2450mm^2
No modification	C-FREI	-	-
Modification 1	C-FRPE1	**1** at the center	A
Modification 2	C-FRPE2	**5** equal area cores: 1 at the center and 4 other cores radially distributed	$\frac{1}{5}A$
Modification 3	C-FRPE3	**5** unequal area cores: 1 large core at the center and 4 radially distributed smaller cores	Center core: $\frac{1}{2}A$ All other cores: $\frac{1}{8}A$

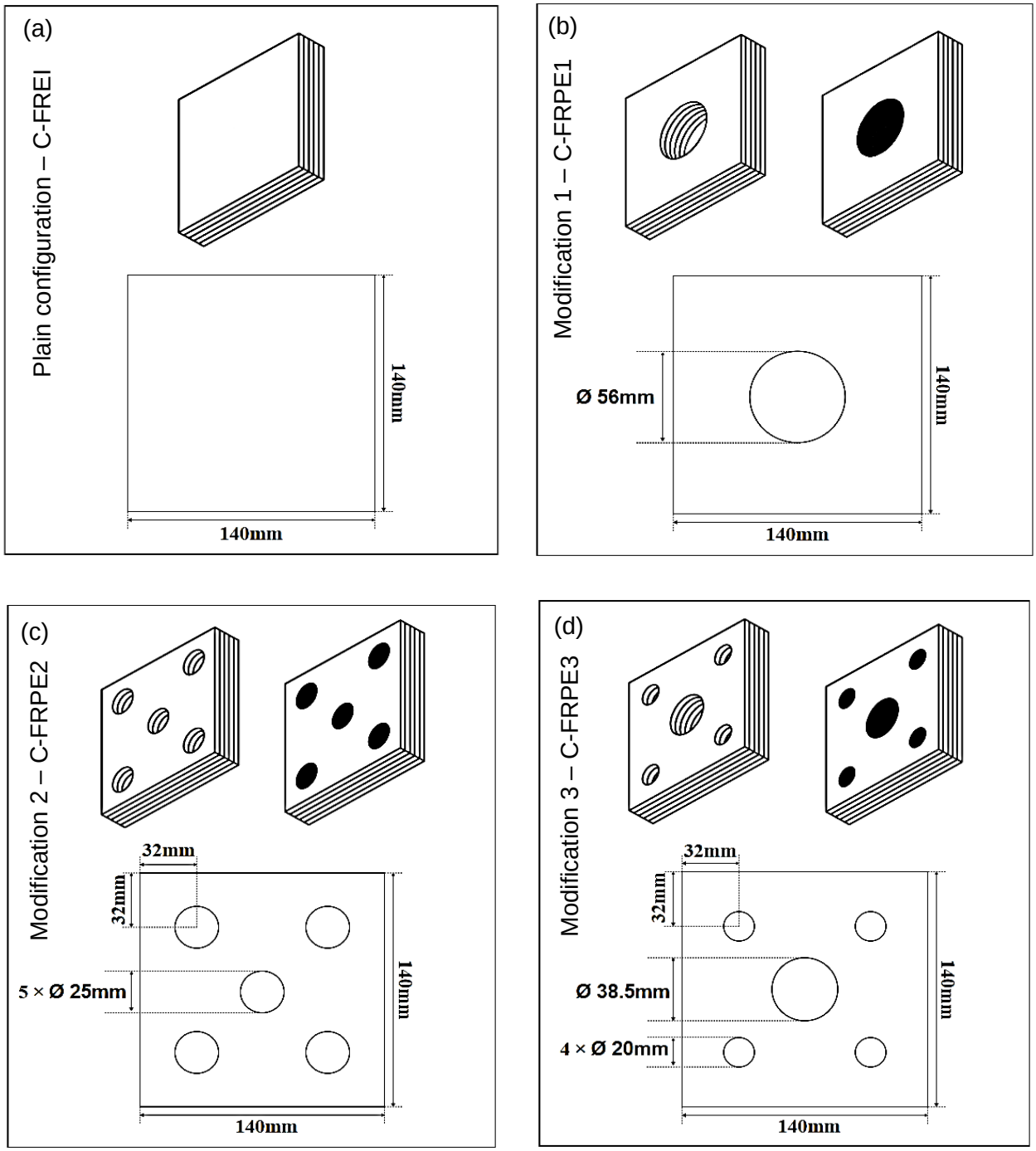

Figure 17: Isometric and plan views of the plain/ modified carbon-fiber reinforced elastomeric isolator (a) C-FREI (b) C-FRPE1 (c) -FRPE2 (d) C-FRPE3

3.3.1 Cost-efficiency of the fabricated C-FREIs and C-FRPEs

Cost is one of the major concerns when it comes to expanding the usage of C-FREIs to even moderate seismic zones and low-rise residential buildings. There is not a significant variation in the material cost of the fabricated C-FREIs and C-FRPEs in this study when compared to the estimated material cost of the same dimension SREIs (if reinforcement was replaced with steel shims). However, the majority of the cost reduction of the fabricated isolators comes from the elimination of labor-intensive manufacturing processes. In SREIs, the steel plates have to be cut, sand-blasted, cleaned with acid, and coated with a bonding compound before laying the elastomer and steel layers for vulcanization in a mold. The interleaved layers in a mold are heated under pressure for an extended period of time to complete the manufacturing process. This process is labor-intensive and hikes the price of the SREIs (James M Kelly, 1999a). In contrary to the SREIs, the elastomer and reinforcement layers in FREIs do not require a hot vulcanization process to initiate the bonding between them. In one method, the bonding between the carbon-fiber reinforced sheets and the rubber layers was initiated and propagated using a cold bonding compound (Toopchi-Nezhad et al., 2008). Alternatively, a microwave heating mechanism can replace traditional bonding methods of vulcanization under pressure at elevated temperatures. The production of FREIs could also be multiplied as the FREIs could be produced in the form of long rectangular strips and cut to the required sizes (James M Kelly, 1999a). As a result, the labor expenses will be reduced as they can be manufactured via automated processes. Due to the cost-efficiency of eliminating the labor-intensive hot vulcanization process, the C-FREIs and C-FRPEs in this study are fabricated using an efficient cold vulcanization method.

3.4 Fabrication process

A total of twenty reduced scale C-FREIs and C-FRPEs were manufactured using high-quality neoprene, polyurethane, and carbon-fiber sheets. All the specimens produced have identical geometric properties as described in Table 1 and Figure 17. The neoprene for the

elastomer layers is produced from natural rubber and rated as 55±5 shore A hardness on a durometer scale, conforming to a minimum tensile strength of 17MPa as specified by the Canadian Highway Bridge Design Code CHBDC S6:19. The polyurethane material used for the cores is characterized with a hardness of 60±3 Shore A on the durometer scale, with a tensile strength of 37MPa (Redwood Plastics and Rubber, n.d.; CSA-S6-19, 2019). Reinforcement was provided between the elastomer layers using plain weave bi-directional carbon-fiber sheets which provide uniform strength in both horizontal and vertical directions.

The bonding between the elastomer layers and the carbon-fiber sheets was achieved with the method of cold vulcanization by using curing adhesive rubber cement. The cement is a two-component adhesive that needs to be catalyzed with an appropriate amount of elastoplastic hardener. Figure 18 shows the fabrication process of the C-FREIs with/without polyurethane cores. Initially, the elastomer layers are roughened and buffed with the use of a wire brush. This provides more surface area for bonding to take place. Next, the adhesive is applied according to the manufacturer's instructions and the layers are stacked on top of each other and pressure applied for two days. The bond reaches 80% of its strength in the first 24 hours while the rest of the strength is achieved within a course of 14 days.

It is worth mentioning that this type of bonding is very cost-effective as it does not require a mold under high temperature and pressure. The C-FREIs are then cut to the design sizes and cut-outs for the placement of the polyurethane cores are made using the waterjet technology. Finally, the polyurethane cores also cut using the same waterjet technology are inserted into the cut-outs of the isolators with more adhesive. Finally, to prevent premature delamination, the side faces of the isolators were coated with the same adhesive. The same adhesive was also used for bonding the top and bottom of the isolator surfaces to the steel plates in the bonded experiments.

The fabricated carbon-fiber reinforced elastomeric isolators with/without the polyurethane cores were tested in both the vertical and horizontal directions to obtain their operational characteristics. For this reason, vertical compression and compression-shear tests were

employed, with their testing program and test setup described in the following sections. The testing program was designed based on the test procedures described in the International Organization for Standardization ISO 22762-1:2018: Test methods for elastomeric seismic protection isolators (ISO 22762-1, 2018).

Figure 18: Fabrication process of the carbon-fiber reinforced elastomeric isolators with polyurethane cores.

3.5 Vertical compression test: Testing program, mechanical properties, and test setup

The compressive properties can be determined by measuring the applied vertical force and their corresponding vertical displacements. The vertical force is controlled during the tests and thus the tests are conducted under load control. The vertical testing program is described in this section and the test equipment employed to carry out the testing program is also discussed.

3.5.1 Testing program and mechanical properties

The test piece is loaded monotonically up to the design compressive stress (P_v). When the design P_v is reached, three fully reversed sinusoidal loading with amplitude variation of ±30%P_v is applied with a frequency of 0.2Hz. Finally, after the third cycle, the design P_v is monotonically unloaded until P_v reaches zero. Different values of P_v are applied to the isolators ranging from 2MPa up to 9.5MPa, with increments of 1.5MPa. Figure 19 shows the vertical loading protocols applied to the fabricated isolators. Note that the compressive force (F_v) as obtained from the compressive stress ($F_v = P_v \times L \times W$), corresponding to 39.2kN (for 2MPa) up to 186kN (for 9.5MPa), with increments of 29.4kN (1.5MPa).

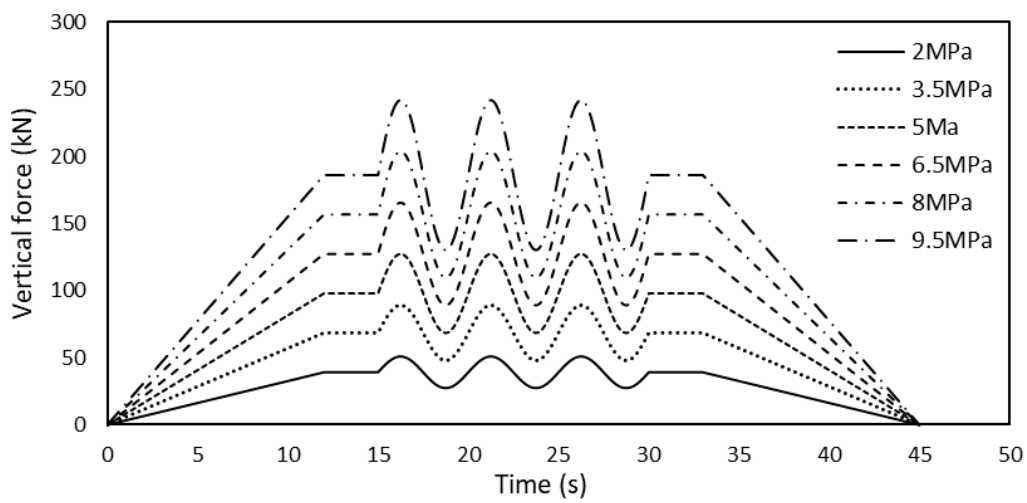

Figure 19: Variation of the design compressive pressures applied with time on the isolators

The vertical operational characteristics are obtained from the vertical force versus vertical displacement curves. Figure 20 shows a typical vertical force vs displacement graph depicting the main parameters to be obtained. Based on the graph, the readings are taken from the third cycle. This load and displacement readings from the third cycle are essential for fiber-reinforced elastomeric isolators as they have a significant run-in behavior before developing the maximum vertical stiffness. This region of significant run-in results from the fiber reinforcements not being initially completely straight and taut at the beginning of the experiment (James M. Kelly, 2008).

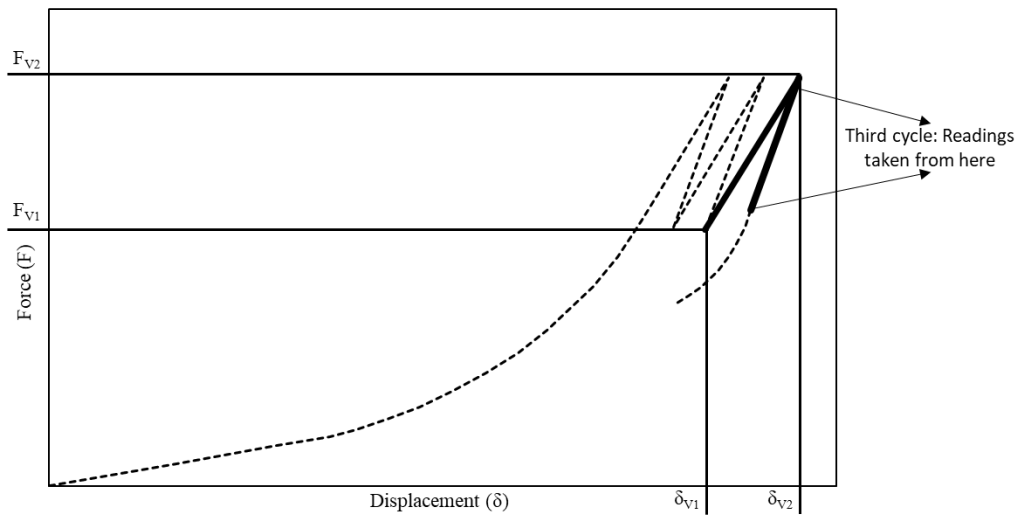

Figure 20: Force-displacement relationship for vertical compression properties to be obtained from the third cycle (adapted from (ISO 22762-1:2018)).

Based on the parameters displayed in Figure 20, the vertical properties can be obtained. The vertical operational characteristics include vertical stiffness (K_v), compression modulus (E_c), equivalent viscous damping (ξ), and the maximum vertical deflection (v_{max}), which are all obtained from the third cycle. The vertical stiffness can be calculated by:

$$K_v = \frac{F_{V2} - F_{V1}}{\delta_{V2} - \delta_{V1}} \tag{3.4}$$

Where F_{V2}, F_{V1}, δ_{V2}, δ_{V1} are the maximum vertical force, minimum vertical force, maximum vertical displacement, minimum vertical displacement, respectively.

Following the vertical stiffness, the compression modulus can be obtained from the vertical stiffness using equation (3.5).

$$E_c = \frac{K_V t_e}{L \times W} \tag{3.5}$$

It is important to note that either K_v or E_c will be sufficient to determine the compressive strength of elastomeric isolators. However, their sensitivity to loading levels can be different despite showing similar trends (Van Engelen et al., 2014). Both of these parameters set important design criteria as the vertical frequency of a structure under a specified dead load relates to its vertical stiffness, while the lateral bulging of the elastomer layers under a specified dead load relates to the compression modulus of an elastomeric bearing (J.M Kelly, 1993). In terms of damping, the equivalent viscous damping due to the vertical loading is calculated in the same process as done for lateral loading according to equation (3.7), although the lateral damping characteristics are more crucial for an isolation system.

3.5.2 Vertical test setup

The test was carried out at the Applied Laboratory for Advanced Materials and Structures (ALAMS) located at the University of British Columbia. The MTS model 370.5 universal testing machine capable of applying axial loads up to 500kN and 150mm actuator dynamic stroke was utilized for this purpose. In order to collect the data and monitor the results while executing the tests, the MTS TestSuite™ software developed by the manufacturer is implemented. Figure 21 shows the main components of the MTS test machine.

The isolator specimens are placed between the top and bottom grippers between two steel plates as shown in Figure 22 by taking into consideration the machine characteristics and dimensional limits. As the load to be applied is purely compression loading, the specimens were placed in such a manner that the wedge grips of the MTS machine are centric to the top and bottom steel plates. Another steel plate with a wider surface area is placed beneath the bottom steel plate to attach four LVDTs to measure the vertical displacements.

Figure 21: Main components for the vertical compression test setup.

The MTS machine utilized is equipped with a load cell and vertical movement transducers to measure the axial load and the movement of the MTS head respectively. The LVDTs as shown in Figure 22 measure the same displacements measured by the vertical movement transducers located in the testing machine, and as a result the LVDTs were only used for determining their accuracy and gaining more insight into the vertical force-displacement behavior of the isolators. The LVDT and the transducer readings within the MTS machine are discussed more briefly in section 4.2.1.

As given in Table 2, three modifications were made to the C-FREIs resulting in a total of four types of isolators to be tested (C-FREI, C-FRPE1, C-FRPE2, and C-FRPE3). For the vertical tests, 3 replicates of each type were used resulting in a total of 12 isolators. Six levels of vertical pressures (P_v) ranging from 2MPa up to a maximum of 9.5MPa, with increments of 1.5MPa are applied to the isolators. The vertical loading protocols are described in Figure 19.

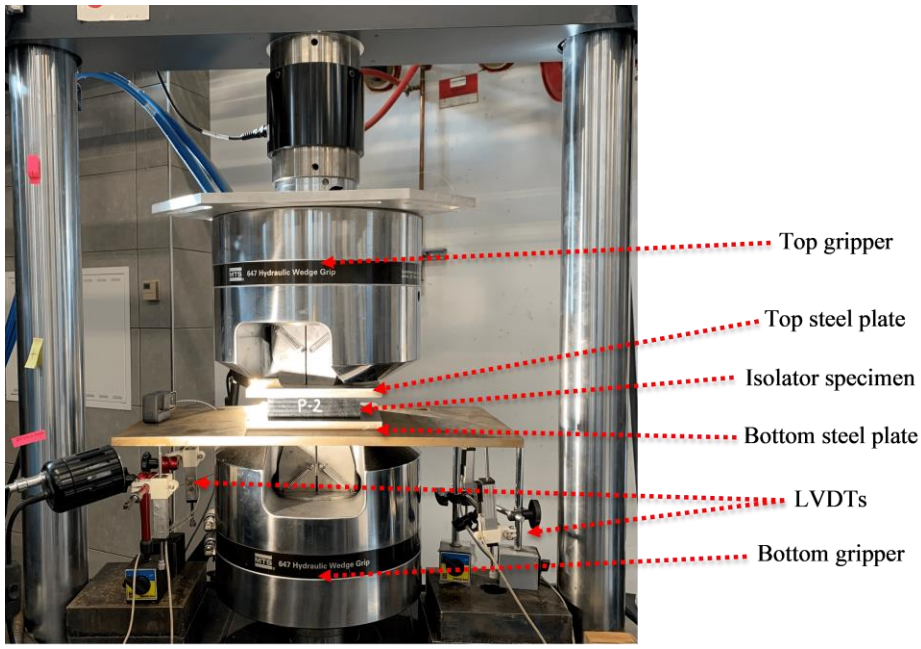

Figure 22: Loading the specimens in the testing machine for vertical compression testing.

3.6 Compressive-shear test: Testing program, mechanical properties, and test setup

The horizontal properties of the C-FREIs and C-FRPEs are obtained from the compressive-shear test. The test is performed by applying a constant vertical load under load control and lateral cyclic displacements under displacement control simultaneously. The vertical load simulates the dead load acting on the isolator and should be kept constant during the entire duration of applying the cyclic shear displacements. The most important parameters which determine the lateral behavior of an isolation system are the horizontal stiffness and the equivalent viscous damping. The flexibility of an isolator in the lateral direction is determined from the horizontal stiffness, while the capability of the isolators to mitigate the seismic energy is determined from the equivalent viscous damping.

3.6.1 Lateral mechanical properties

Figure 23 shows a typical lateral force vs displacement hysteresis behavior of an elastomeric isolator when tested under compressive-shear loads adapted from ISO 22762-1:2018.

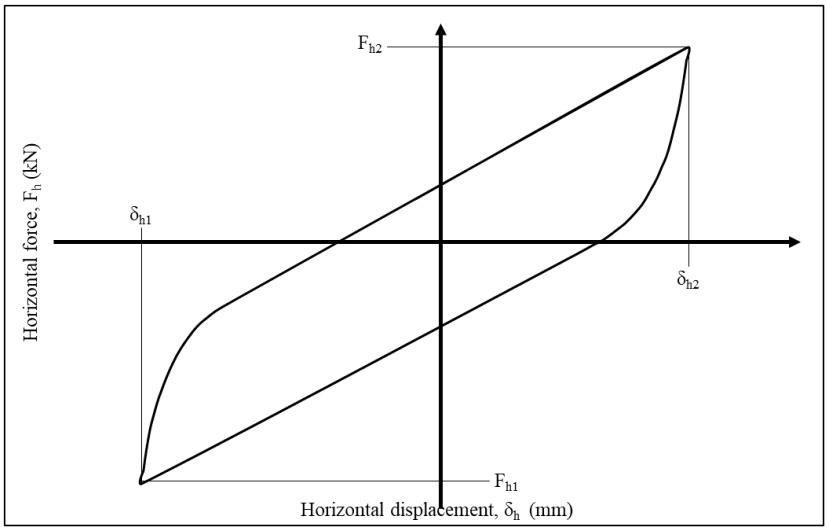

Figure 23: Force-displacement relationship for lateral properties compressive-shear test (adapted from (ISO 22762-1:2018)).

Based on the parameters displayed in Figure 23, the effective horizontal stiffness (K_h) can be obtained from equation (3.6).

$$K_h = \frac{F_{h2} - F_{h1}}{\delta_{h2} - \delta_{h2}} \tag{3.6}$$

Where F_{h2}, F_{h1}, δ_{h2}, δ_{h1} are the maximum horizontal force, minimum horizontal force, maximum horizontal displacement, minimum horizontal displacement respectively.

The equivalent viscous damping (ξ) can also be defined as the ratio of the energy dissipated to the elastic energy restored in the elastomeric bearing given according to equation (3.7).

$$\xi = \frac{W_d}{4\pi W_s} \tag{3.7}$$

Where W_d represents the energy dissipated per cycle. It can be obtained from the area inside the lateral force-displacement hysteresis loop, and W_s is the energy which is restored in the elastomeric bearing. W_s is calculated according to equation (3.8).

$$W_s = \frac{1}{2} K_h (\delta_{avg})^2 \tag{3.8}$$

δ_{avg} is the average lateral displacement calculated using equation (3.9).

$$\delta_{avg} = \frac{|\delta_{h2}|+|\delta_{h1}|}{2} \quad (3.9)$$

It is important to note that placing the polyurethane cores in the C-FREI will cause an effect on the effective horizontal stiffness. Based on the new effective horizontal stiffness, the effective shear modulus (G_h) can be calculated using equation (3.10) from each lateral strain amplitude. G_h is obtained from the following equation:

$$G_h = \frac{K_h \gamma t_e}{L \times W} \quad (3.10)$$

Where γ is the lateral strain when displaced in the lateral direction (Kelly, 1993).

3.6.2 Compression-shear testing program

With the parameters of interest for the fabricated isolators described in the previous section, the horizontal testing program is described in this section. The isolators (both plain C-FREIs and C-FRPEs) were subjected to a constant vertical pressure followed by three fully reversed lateral cyclic displacements of different amplitudes. Initially, the horizontal characteristics for different shear strain amplitudes are tested, followed by several dependence tests.

3.6.2.1 Horizontal properties for different cyclic strain amplitudes

The isolators were put under constant vertical pressure (P_v) of 3.5MPa which corresponds to a vertical force of 68.6kN. Six individual cyclic shear strains with amplitudes of 25% T_e, 50% T_e, 75% T_e, 100% T_e, 125% T_e, and 150% T_e are applied at a constant frequency of 0.05Hz (Time period of 20s). T_e is the total thickness of the elastomer layers calculated as 32.5mm as shown in Table 1. A total of three fully reversed sinusoidal cycles are applied for each strain amplitude. Figure 24 demonstrates the vertical pressure applied and the variation of the cyclic horizontal displacements applied to the specimens.

The horizontal properties for different strain amplitudes are tested for both bonded and unbonded applications of the isolators. The horizontal mechanical properties for both bonded and

unbonded specimens are obtained from equations 3.6 to 3.9. It is important to note that the vertical pressure remains constant (3.5MPa) during all amplitudes of horizontal cyclic strains.

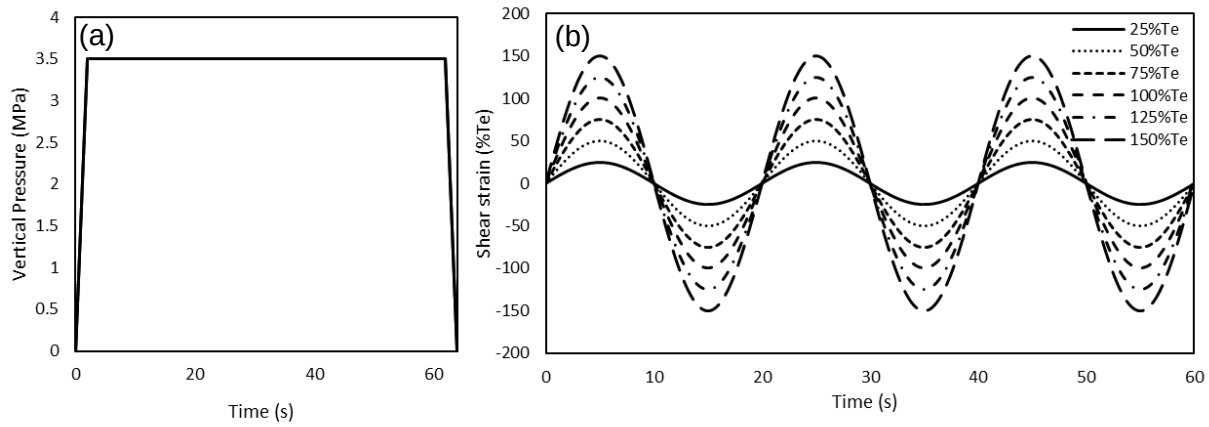

Figure 24: Input loading in the compressive-shear test (a) vertical pressure (b) cyclic shear strains.

3.6.2.2 Dependence tests on the lateral properties

Several dependence tests are performed on the specimens to further evaluate the horizontal stiffness and the equivalent viscous damping of the isolators by changing three different parameters. The parameters are the strain dependence on the lateral properties, compressive force dependence on the lateral properties, and the lateral cyclic rate dependence on the lateral properties.

These dependence parameters are tested for both the bonded and unbonded applications. Previous studies have reported the effect of these parameters on the unbonded applications of FREIs. Vanngo et al. (2017) have reported that the strain dependence on the lateral properties of unbonded specimens has a significant reduction in the effective horizontal stiffness as the amplitude is increased. Similarly, Toopchi-Nezhad et al. (2008) have reported that the influence of the compression loading has a very small effect on the effective horizontal stiffness, however increasing the compression load by twice causes an increase in the damping characteristics. They have also observed that the horizontal properties of unbonded specimens

are independent of the cyclic rate as long as no damage occurs in the bearing components. It is important to explore how the dependency tests will affect the performance of the novel C-FRPEs.

3.6.2.2.1 Strain dependence on the lateral properties

The objective of the strain dependence test is to identify how the horizontal stiffness and the equivalent viscous damping of the isolators change when multiple levels of cyclic shear strain are applied simultaneously. This is tested by subjecting the isolators to a constant compressive pressure of P_v = 3.5MPa while simultaneously applying multiple levels of cyclic shear strains measuring 25% T_e, 50% T_e, and 75% T_e (T_e is the total thickness of the rubber layers). Three fully reversed sinusoidal cyclic displacements are applied for each strain level having a frequency of 0.05Hz, resulting in a total of nine complete cycles for three levels of strain. The variation of the vertical pressure and the cyclic horizontal displacements versus time for the strain dependence test is illustrated in Figure 25.

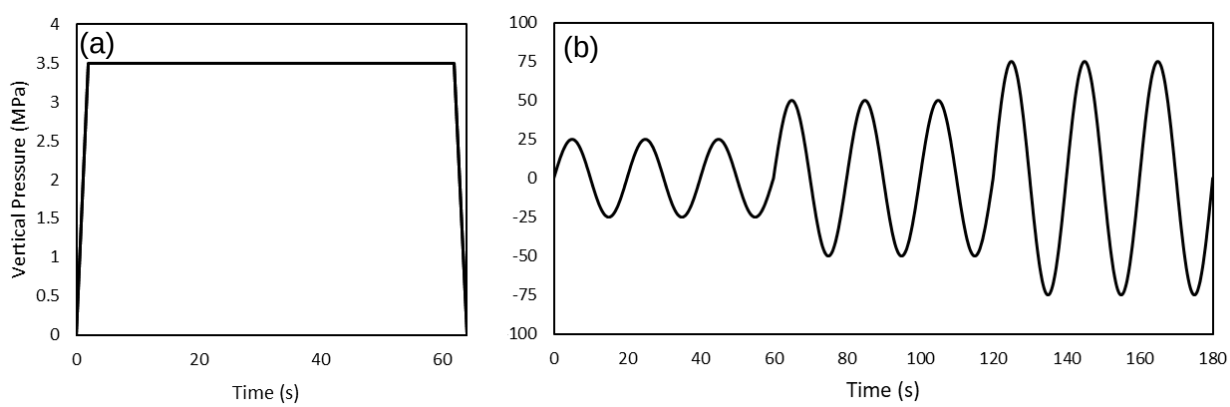

Figure 25: Input loads in the horizontal strain amplitude dependence tests (a) vertical pressure (b) lateral shear strain.

3.6.2.2.2 Compression force dependence on the lateral properties

The objective of the compressive force dependency test is to evaluate the effect of the compressive pressure on the horizontal stiffness and the equivalent viscous damping of the isolators. In this regard, the effect of the compressive pressure is explored by varying the vertical compressive load while keeping the amplitude and frequency of the lateral strain constant. The

vertical compressive load is interchanged between three levels (2MPa, 3.5MPa, and 5MPa) while applying a lateral cyclic strain of 50%T_e at a frequency of 0.05Hz. Figure 26 shows the variation of the vertical compressive load and the cyclic shear strain applied to the isolators.

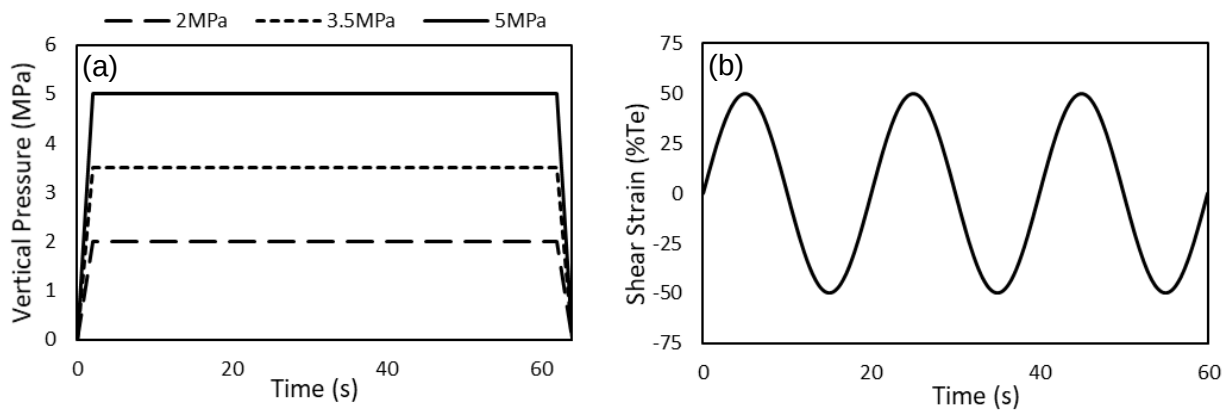

Figure 26: Input loads in the vertical compressive pressure dependence tests (a) vertical pressure variation (b) lateral shear strain at 50% T_e.

3.6.2.2.3 Lateral cyclic rate dependence on the lateral properties

The objective of the lateral cyclic rate dependence tests is to evaluate the effect of the lateral cyclic rate on the horizontal stiffness and equivalent viscous damping of the isolators. Various kinds of earthquakes with different magnitudes and frequency contents can strike a base-isolated structure. Thus, the effect of the lateral cyclic rate is an important measure.

The lateral cyclic rate dependency test is performed by introducing three different levels of lateral cyclic frequencies measuring 0.005Hz, 0.1Hz, and 0.5Hz. These frequencies lead to a time-period of each sinusoidal cycle to be 200s, 10s, and 2s, respectively. The magnitude of the vertical compression is kept constant at 3.5MPa while the amplitude of the lateral cyclic strains is also kept constant at 50%T_e. The procedure of this test is similar to the tests described before where the vertical compressive load is kept constant while applying 3 fully reversed sinusoidal lateral strains, repeating each test with a different lateral cyclic rate. The variation of the lateral cyclic rate frequencies versus time is depicted in Figure 27.

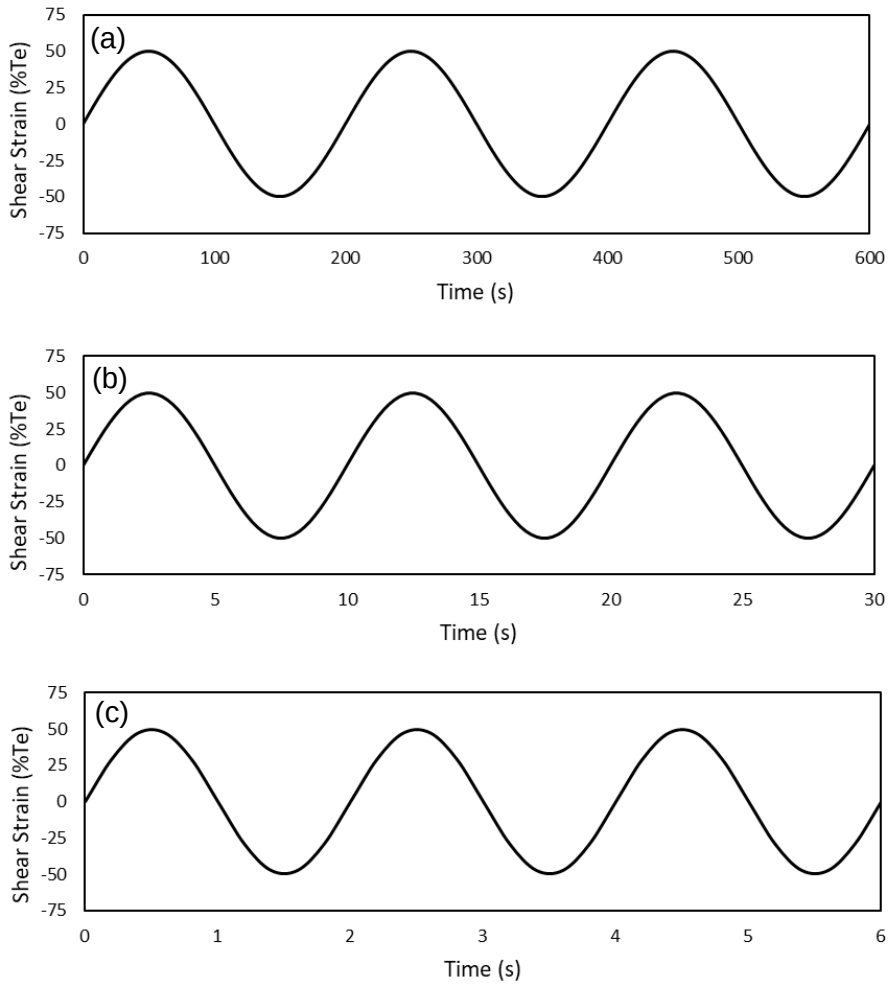

Figure 27: Lateral cyclic frequency rates for the lateral cyclic rate dependency test (a) 0.005Hz (b) 0.1Hz (c) 0.5Hz.

3.6.3 Compression-shear test setup

With the objective to determine the horizontal properties of the isolator specimens, a test setup capable to apply bi-directional loading in both vertical and horizontal directions was designed and fabricated. For this reason, a two-block shear-type test setup was utilized for the compression-shear test. Figure 28 shows the general idea of the two-block shear-type test setup.

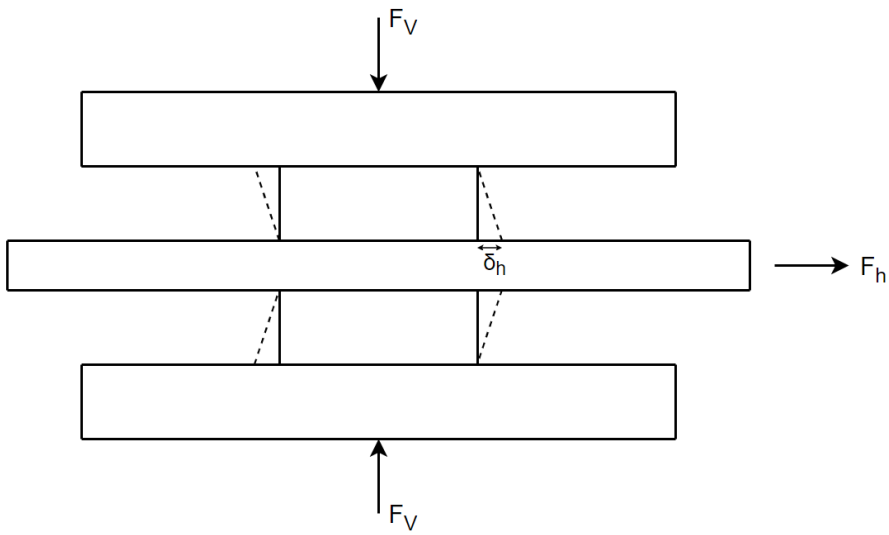

Figure 28: General idea of a two-block shear-type test.

Where F_v is the constant vertical force, F_h is the horizontal force, and δ_h is the horizontal displacement. The test setup was built in the Applied Laboratory for Advanced Materials and Structures (ALAMS) located at the University of British Columbia. Figure 29a and 29b show the main components of the test setup. The components of the test setup were assembled on top of a concrete block which was anchored to a strong floor by post-tensioning the four corners of the block with high-strength steel (HSS) rebars. The axial load was applied using an ENERPAC CLSG1502 hydraulic pump rated with a maximum capacity of 800kN. The axial load effect was kept constant and held together rigidly by post-tensioning four high strength (Grade B7) threaded rods. The threaded rods were anchored to the bottom of the concrete block base and the top steel plate. The axial load was varied by changing the pressure of the hydraulic jack applied to the movable steel directly below the isolator specimens. The applied axial pressure was monitored using a calibrated load cell placed between the hydraulic jack and the steel heightener plates.

To apply lateral cyclic displacements, a push-pull steel T-section between the two specimens was attached to a hydraulic MTS actuator rated with a load capacity of ±250kN and a displacement capacity of ±125mm, where the MTS actuator was mounted to a reaction frame. The head of the actuator was extended in such a way that the zero-displacement position of the

specimen was the halfway extension of the actuator to have sufficient clearance in both directions when applying the lateral cyclic displacements. Figure 29a shows the assembly of the different components on top of the concrete block before placing the lateral bracing sections.

The specimen configuration was restrained laterally with the help of bolted moment carrying I-sections and stiffened angle sections as shown in Figure 29b. This lateral bracing system also restrains the assembly to move laterally while applying the lateral cyclic displacements and allows the deformation of only the elastomeric isolators. Figure 30 shows the profile view of all components and after the actuator connection is made.

(a)

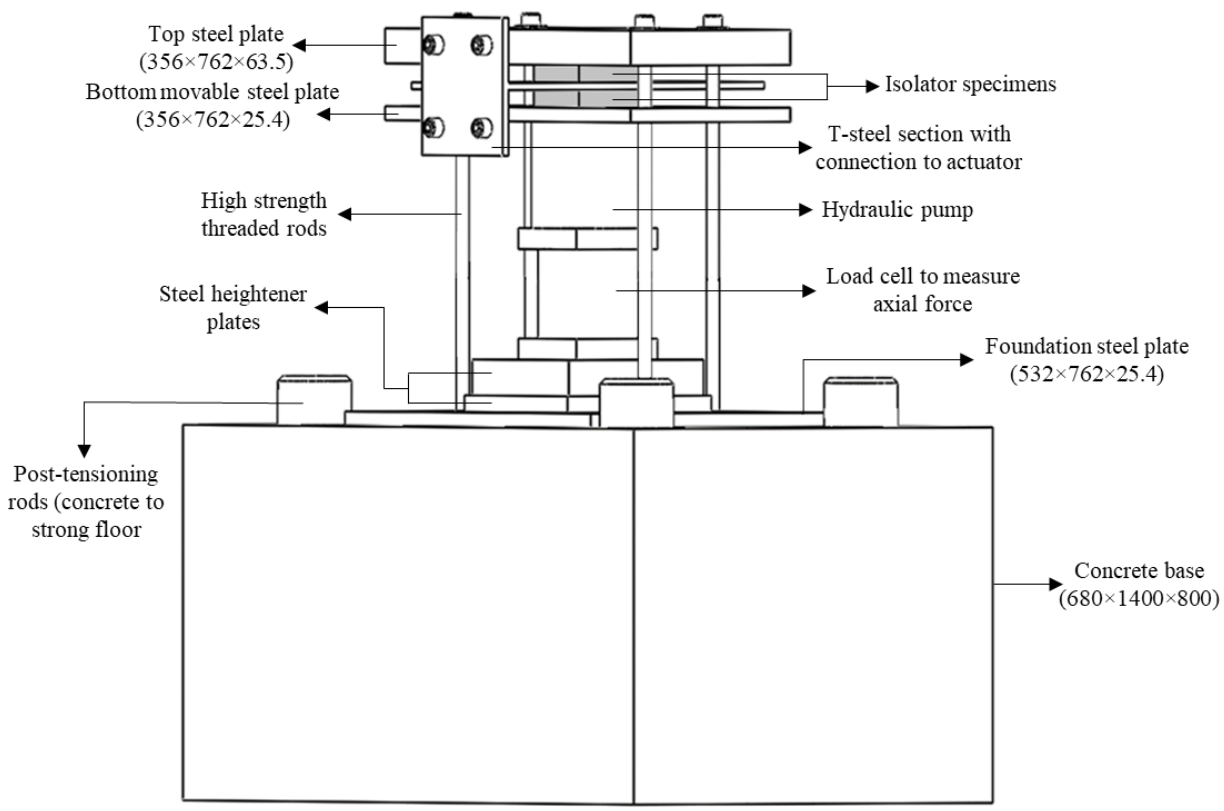

(b)

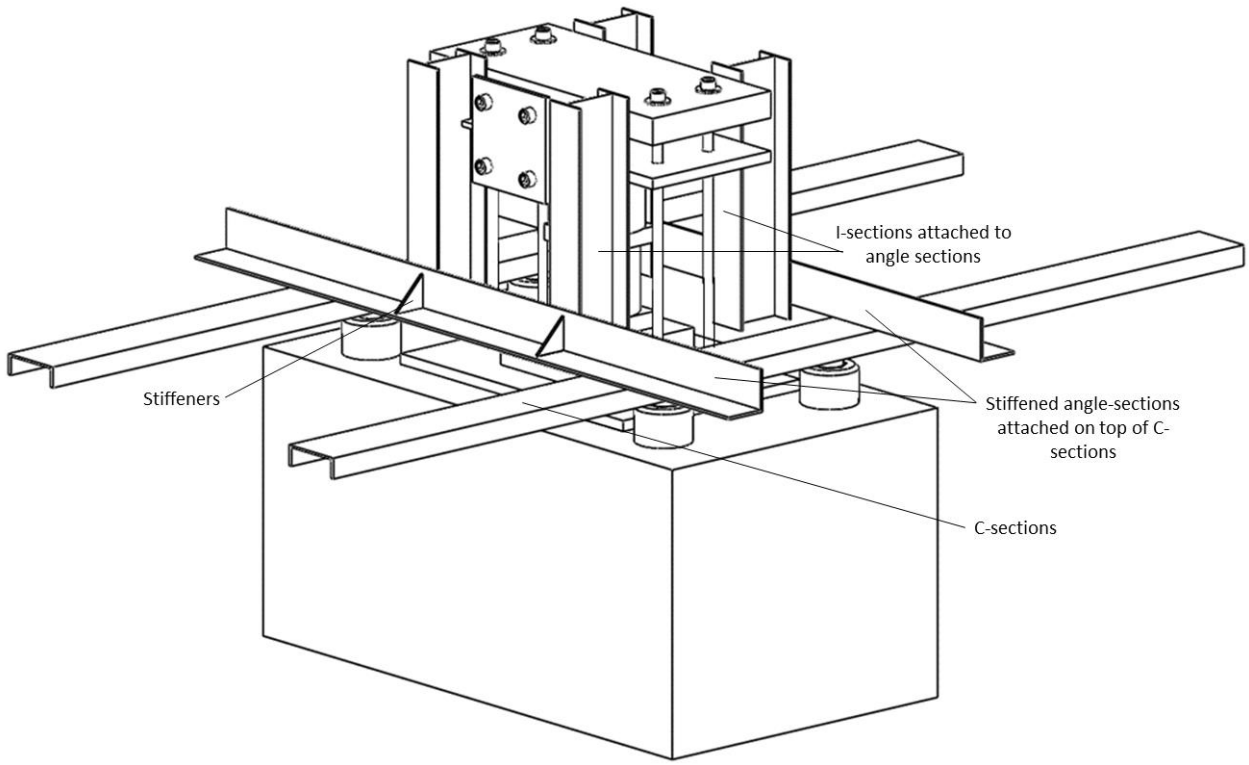

Figure 29: Component assembly for the compression-shear test on top of the base concrete block (a) without the lateral bracing system (b) with the lateral bracing system

Figure 31 shows the final test setup build in the ALAMS lab in UBC. The axial compression was applied using the hydraulic pump which exerts pressure on the specimens by a movable steel plate. The horizontal MTS actuator was set to apply the cyclic shear displacements by pushing and pulling the middle push-pull T-plate. The load cell measures the applied axial force, and in addition to the lateral force and displacement readings from the MTS machine, a strain pot was used to monitor the lateral displacements of the push-pull plate as shown in Figure 32. The MTS controller in the actuator measures the lateral force and displacements, although the displacement readings from the MTS controller were compared with the strain pot displacements to check their accuracy as the pinned connections at both ends of the actuator may cause slight deviations in the displacement readings.

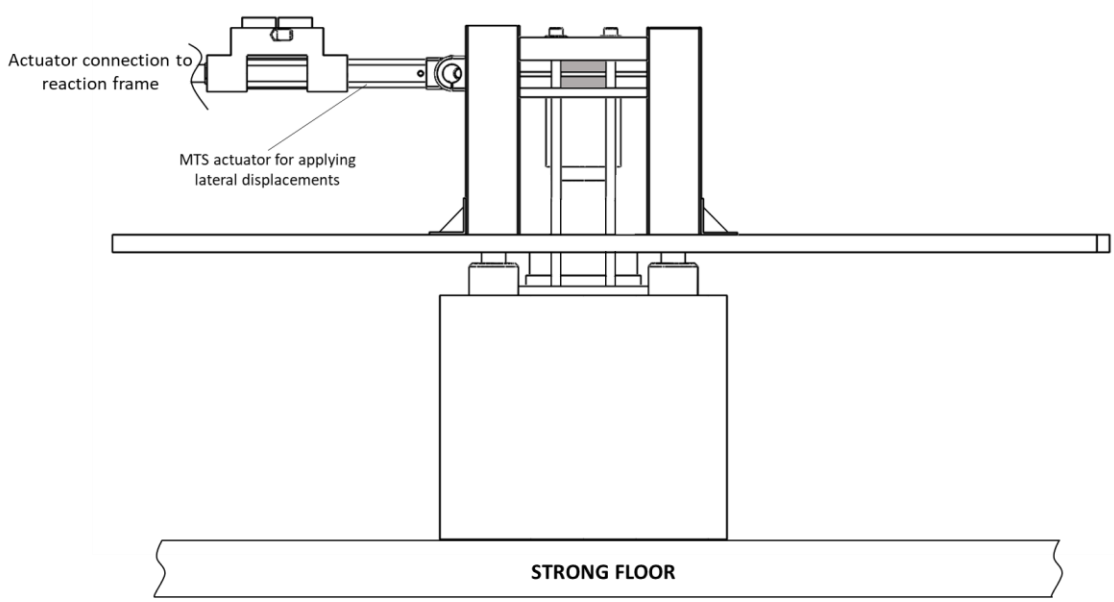

Figure 30: Profile view of the component arrangement for the compression-shear testing

Figure 31: Final configuration of the compressive-shear test setup

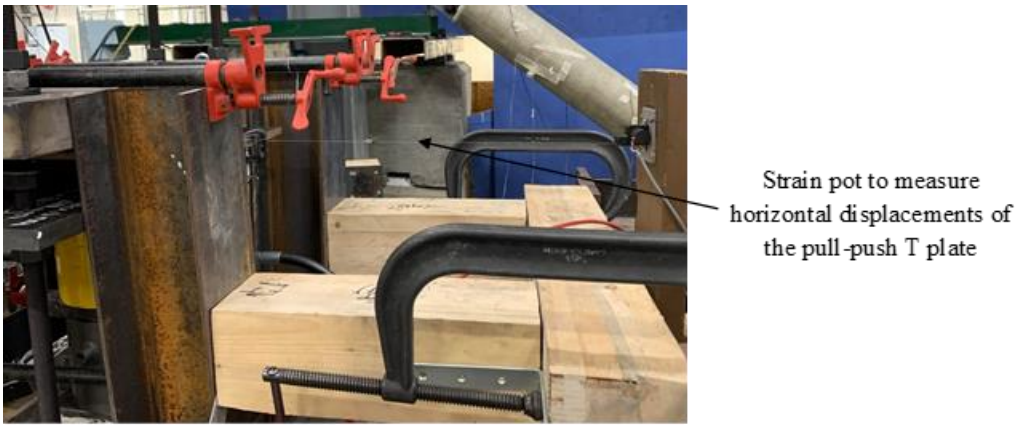

Figure 32: Strain pot to measure the lateral displacements

Before carrying out the compressive-shear tests, the lateral bracing I-sections were strengthened more to eliminate any lateral displacements occurring in the top and bottom steel plates of the test setup. The displacement of the specimens is only of interest and any displacements occurring outside the specimens were carefully examined and eliminated. This was done with the help of strong clamps and extension timber beams extended from post-tensioned pedestals to reduce the moment arm of the I-sections. Appendix A shows images of the step-by-step process of strengthening the test setup.

Four types of isolator configurations, i.e., plain C-FREI, and three configurations of C-FRPEs result in a total of eight isolators tested in the two-block shear test. The precision and accuracy of the results in a two-block shear test are satisfactory as the displacement and force values obtained correspond to the average of two specimens. The lateral force values are halved to account for the performance of a single specimen. For bonded applications, the top and bottom surfaces of the isolators were bonded to the surfaces in contact with the steel plates using the same bonding agent used for bonding the layers of the isolators. The unbonded tests were conducted by placing the isolators in position on roughened steel plates.

3.7 Limitations on the proposed specimen design and test program

The C-FRPEs were designed with three configurations where the area of the polyurethane cores was kept constant in each of the configurations. Other than the PE core distributions, the area of the PE core in the isolators can have a significant impact on the vertical and lateral response of the isolators, and hence future studies can be conducted by varying the area of the polyurethane cores. Another limitation of the proposed compression-shear testing program is that the lateral strain was limited to a maximum of 150%T_e. Unbonded applications of C-FREIs can be subjected to even higher lateral strains where the vertical surfaces of the isolators would come in contact with the top and bottom steel plates which causes an increase in the horizontal stiffness, thereby limiting the maximum lateral displacement. This limitation in the maximum lateral strain applied is due to the slender configuration of the test setup built for the compression-shear test. At more than 150%T_e, global displacement of the test setup was observed which affected the lateral force vs displacement behavior of the isolators.

3.8 Summary

Carbon-fiber reinforced elastomeric isolators (C-FREIs) are a relatively new kind of isolators that have the steel reinforcement of traditional isolators replaced with carbon fiber sheets. The fabrication of the C-FREIs is less complex and inexpensive when compared to traditional isolators, increasing their popularity to be used in even low-rise residential structures in earthquake-prone zones. The layers in the C-FREIs can be bonded using a cold vulcanization agent and can be cut to any required size during the manufacturing process. This chapter presents the fabrication of C-FREIs using the cold vulcanization process where 20 reduced scale C-FREIs were fabricated using the simple and fast manufacturing process. Furthermore, the C-FREIs can be utilized in both bonded and unbonded applications which is another advantage of FREIs. However, previous studies have shown that C-FREIs in bonded applications go through early delamination due to the fiber sheets having almost no flexural rigidity. Unbonded

applications are always not preferred due to the unseating of the bridge decks and a lower energy dissipation capacity. Therefore, in order to improve their performance and increase their dissipating energy, three different modifications were introduced and made to the C-FREIs by utilizing polyurethane cores. Different hole sizes and distributions were made for the placement of the polyurethane cores. This chapter also describes the fabrication process of the modified carbon-fiber reinforced elastomeric isolators with polyurethane cores (C-FRPEs).

To test the performance of the introduced C-FREIs and C-FRPEs, the testing program and the test setup capable to carry out the experimental program were also introduced in this chapter. The isolators will be tested in both vertical and horizontal directions by applying compressive and lateral cyclic loads. The operational characteristics which define the performance of the isolators in both vertical and horizontal directions were also discussed.

Chapter 4: Test Results and Discussion

4.1 General

Bonded applications of elastomeric isolators will generally be preferred as they are securely attached to the substructure and superstructure whereas, unbonded applications have advantages in having a lower horizontal stiffness and their ability to take larger lateral strains. However, both kinds of applications have drawbacks such as in bonded applications, premature delamination is observed due to the carbon-fiber reinforcement lacking any flexural rigidity, while in unbonded applications roll-out instability and lower energy dissipation is observed at higher lateral strains. Therefore, for the sole purpose of improving their energy dissipation capability and delamination performance, experimental investigations are carried out where polyurethane cores are inserted in the C-FREIs.

With the purpose of performing experimental investigations on the carbon-fiber reinforced elastomeric isolators with/without the polyurethane cores, Chapter 3 presents the fabrication process of the isolators, testing program, test setup, and the mechanical properties of interest. The fabrication process involved a cold-vulcanization process which is cost-effective and does not involve a labor-intensive process. The testing program is designed with a series of tests under two major tests, which are the vertical compression tests and compressive-shear tests. The compressive-shear testing consists of general horizontal behavior tests as well as three dependence tests on the horizontal properties. Regarding the test setup, a uniaxial testing machine is utilized for the vertical compression tests, and a test setup capable to apply bi-directional loading in both vertical and horizontal directions was designed and fabricated to carry out the compression-shear testing.

This Chapter discusses the test results obtained from carrying out the experimental program described in Chapter 3. The efficiency of the isolators is determined by investigating their vertical and horizontal operational characteristics from the test results. In this regard, the vertical

operational characteristics primarily consist of vertical stiffness, equivalent viscous damping, and maximum vertical deflection. The main parameters of interest from the horizontal tests are the horizontal stiffness and the equivalent viscous damping. This chapter also discusses the failure stresses of the isolators and the performance of the isolators after failure. The results are discussed in terms of the performance comparison between the plain C-FREIs with the modified C-FREIs. Comparisons between bonded and unbonded applications of the isolators are also made.

4.2 Vertical compression test results

The vertical compression test was done to primarily evaluate the vertical stiffness. Other parameters such as the maximum vertical deflection and equivalent viscous damping were also investigated to gain more clarity on how the vertical specifications change when plain C-FREIs are modified by placing polyurethane cores. The vertical testing is done according to section 6.2.1 in ISO 22762-1:2018. A brief description of the testing program and test setup is illustrated in section 3.5 in Chapter 3.

4.2.1 Instrument comparison

The displacements obtained from the vertical transducers due to the movement of the MTS head were compared to the mean displacements from the 4 LVDTs installed in the test setup to ensure the accuracy of the MTS displacements. Figure 33 shows a graph of comparison between the MTS and the LVDT readings, displayed for the different types of isolators at different vertical pressures. It is observed that the difference between the two readings is not significant and the majority of the deviation occurred within a percentage of 1-3% with the maximum deviation at 5%. Hence due to the relatively small difference and for simplification, only the vertical transducer readings from the MTS were utilized for the analysis and discussion.

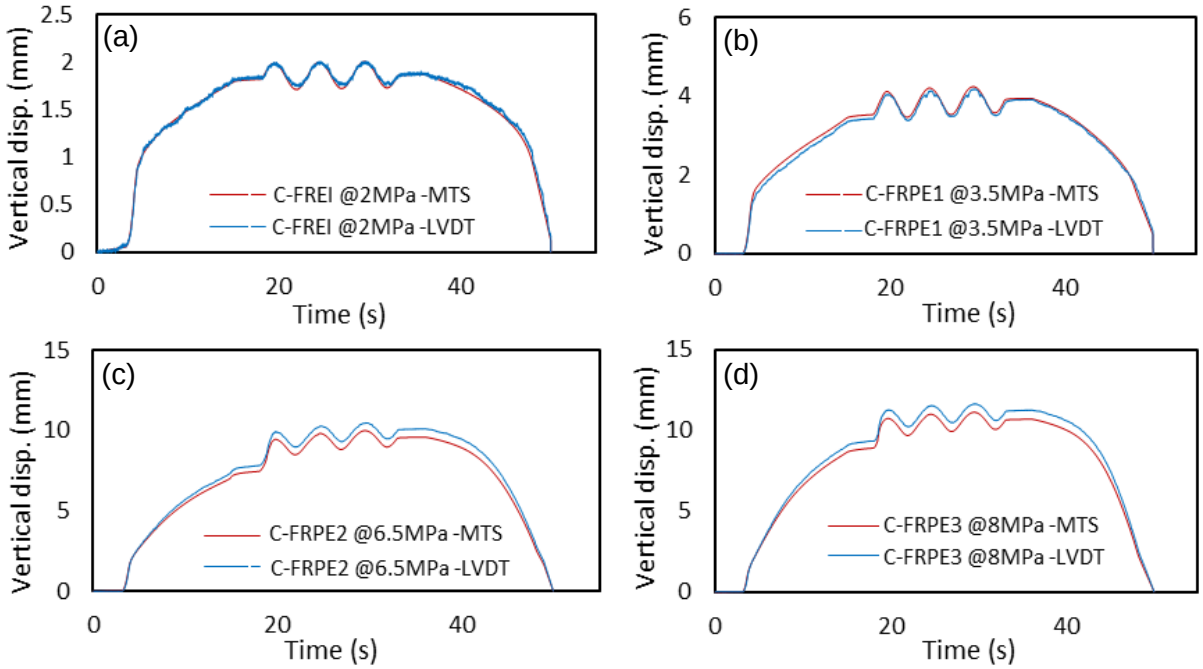

Figure 33: Vertical displacement reading comparison between the MTS transducers and LVDTs for (a) C-FREI at 2MPa (b) C-FRPE1 at 3.5MPa (c) C-FRPE2 at 6.5MPa (d) C-FRPE3 at 8MPa.

4.2.2 Failure tests

One replicate from each type of isolator was chosen for the failure tests. The specimens were loaded in increments of 1.5MPa starting from 2MPa up to a maximum of 9.5MPa. It was observed that all types of isolators showed acceptable vertical behavior and depicted no initial bond failure up to the loading protocol of 6.5MPa. As expected, the plain configuration (C-FREI) was able to take much higher vertical loads before initial failure due to the plain configuration having a larger area containing the carbon-fiber reinforcement. Figure 34 shows the stages at which the isolators encountered an extra bulging and showed local delamination between the CFR and elastomer layers. This happens as the carbon-fiber reinforcement layers could not prevent the extra deformation experienced at such high loads.

The loads at which the initial failure was observed were 9.3MPa, 8.1MPa, 7.7MPa, and 7.2MPa for C-FREI, C-FRPE1, C-FRPE2, and C-FRPE3, respectively. For the modified isolators with the PE cores, C-FRPE1 withstood higher pressure than the other modifications despite

having a similar area removed for each. This implies that a single PE core at the center can take larger loads before failure compared to the modifications where the PE cores were distributed. However, the maximum bearing pressure at SLS for elastomeric isolators does not typically exceed 7MPa (GoodCo Z-Tech, 2010) and therefore, the failure performance of the C-FRPEs was deemed to be adequate.

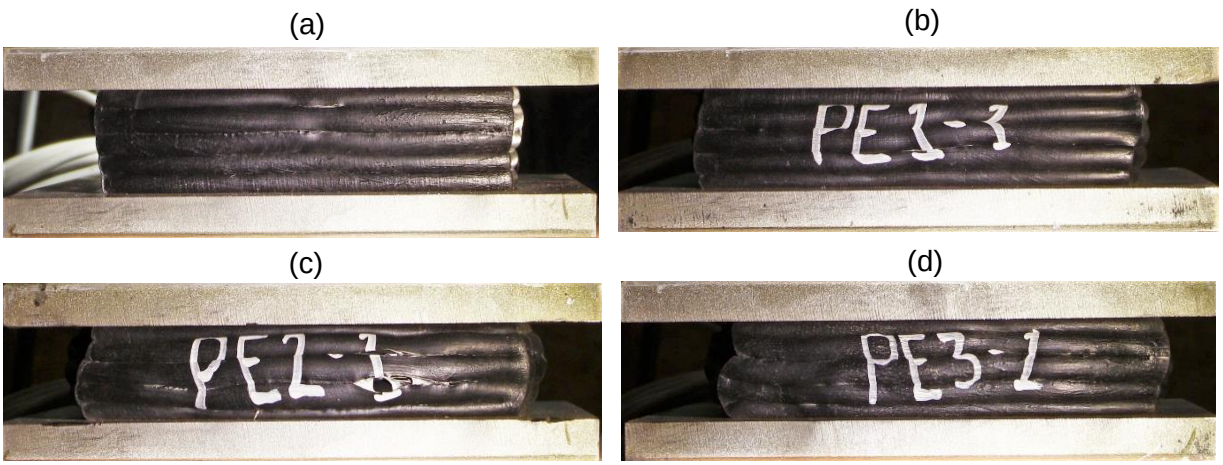

Figure 34: Initial bond failure observation for (a) C-FREI at 9.3MPa (b) C-FRPE1 at 8.1MPa (c) C-FRPE2 at 7.7MPa (d) C-FRPE3 at 7.2MPa

Figure 35 compares the force-displacement relationships of the failed specimens with the loading protocol of $P_v = 9.5$MPa. At this loading protocol, all the specimens have long failed. As observed from the Figure, the plain C-FREI degrades in its centering capability and there is an unstable behavior in making the successive cycles. This happens as the elastomer and the reinforcement layers go out of the plane due to the local delamination. The isolators equipped with the polyurethane cores remain much more stable in performing the successive cycles due to the cores holding the layers in position.

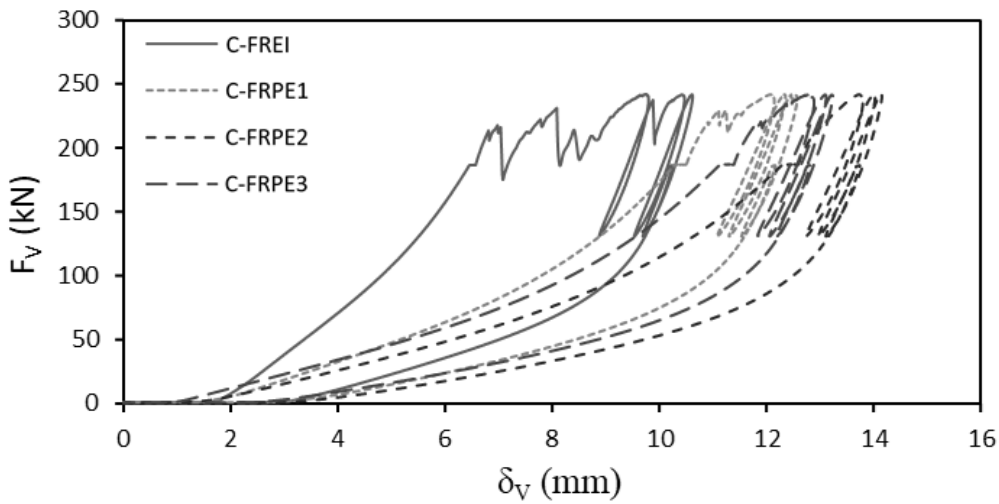

Figure 35: Vertical force vs distance relationship for the isolators after failure at a vertical pressure of 9.5MPa.

4.2.3 Vertical operational characteristics

In this section, the vertical specifications describing the vertical behavior of the novel C-FRPEs are evaluated and compared to that of the plain C-FREI. As stated previously, the vertical properties are computed from the third cycle of the vertical loading protocol due to the significant run-in behavior of fiber-reinforced elastomeric isolators not being initially taut and straight in compression loading. As also determined from the failure tests, only the vertical force vs displacement relationships pertaining to vertical loadings of 2MPa, 3.5MPa, 5MPa, and 6.5MPa was analyzed. Figure 36 illustrates the vertical force (F_v) versus the vertical displacement (δ_v) for four different pressure levels for each type of isolator.

Within each Figure (i.e., Figure 36a, 36b, 36c, 36d), the force vs displacement relationships are compared for each type of isolator. The figure shows a non-linear monotonic behavior as the force is increased which happens primarily due to the non-linear behavior of the elastomer under compression loading. Also, when the pressure reaches the target design pressure and before undergoing the cyclic displacements, the vertical deflection continues to increase even when the pressure remains constant (creep behavior). As the pressure is released in the unloading phase, the elastomeric isolators undergo plastic deformation.

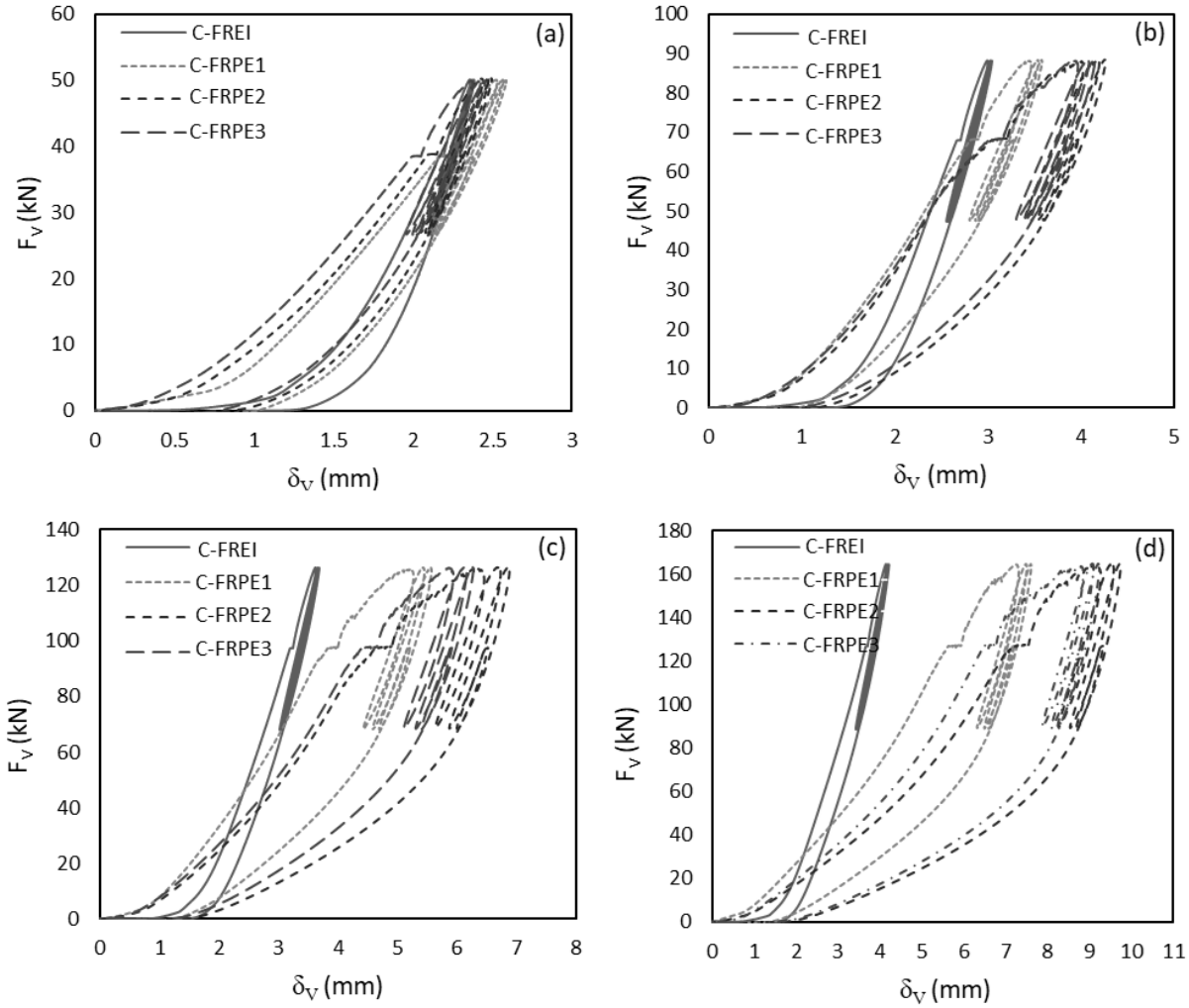

Figure 36: Vertical force vs distance relationship for the plain and polyurethane core C-FREIs at (a) 2MPa (b) 3.5MPa (c) 5MPa (d) 6.5MPa.

At an initial glance, it is observed that the plain isolator (C-FREI) has higher stiffness and undergoes lower displacements compared to the C-FRPEs. Moreover, the isolators with the polyurethane cores (C-FRPEs) cover a much higher area under the force-displacement graphs indicating their superior energy dissipation capability. To gain further clarity, the vertical stiffness (K_v), equivalent viscous damping (ξ), and the maximum vertical deflection (v_{max}) are compared from the third cycle of the force-displacement curves. Figure 37 shows the third cycle hysteresis

loops at the given vertical pressures. Table 3 represents the mean vertical operational characteristics.

Table 3: Vertical operational characteristics of the plain and polyurethane core isolators at different vertical pressures

Vertical Specifications	P_v (MPa)	C-FREI	C-FRPE1	C-FRPE2	C-FRPE3
K_v (kN/mm)	2	88	53	58	54
	3.5	90	60	61	59
	5	95	66	66	67
	6.5	103	75	72	75
ξ (%)	2	9	12	11	14
	3.5	9	13	18	17
	5	9	23	26	22
	6.5	8	19	25	25
v_{max} (mm)	2	2	3	2	2
	3.5	4	4	4	4
	5	4	6	7	6
	6.5	4	8	10	9

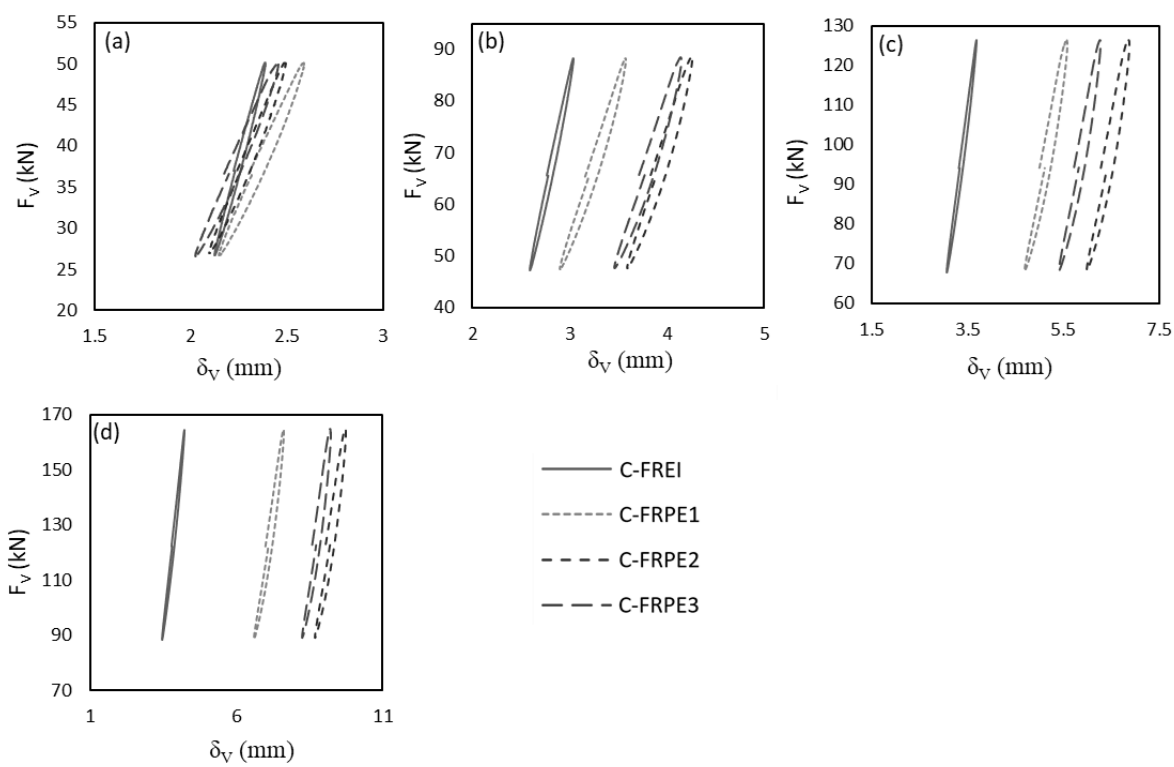

Figure 37: Third cycle vertical hysteresis loops for the plain and polyurethane core C-FREIs (a) 2MPa (b) 3.5MPa (c) 5MPa (d) 6.5MPa.

4.2.3.1 Vertical stiffness (K_v)

The results illustrate that the C-FREI shows higher stiffness compared to the C-FRPEs due to having a higher reinforcement ratio. The values of K_v reduce ~28-38% for the C-FRPEs due to the placement of the PE cores amounting to 12.5% of the total area of the plain C-FREI. The reduction in stiffness for all modifications of C-FRPEs is approximately equal implying that the vertical stiffness is not dependent on the distribution of the PE cores. Moreover, this reduction in vertical stiffness due to the placement of the PE cores is more prominent (38%) for isolators subjected to lower pressure.

Figure 38 shows how K_v vary to changes in the design compressive pressures. K_v increases as we increase the design pressure due to the presence of bi-directional carbon-fiber reinforcement and also due to the elastomer layers stiffening at higher pressures. At large magnitudes of vertical pressures, the carbon-fiber reinforcement stretches more tightly due to the higher transverse shear forces acting between the elastomer and reinforcement layers. This increase in vertical stiffness amounts to ~2-8% for the plain C-FREI and ~8-12% for the C-FRPEs, for every 1.5MPa increment in the vertical pressure. Therefore, it can be interpreted that the placement of polyurethane cores makes the isolator more sensitive to stiffness increase at higher vertical pressures. This can be explained as the polyurethane cores undergo a higher amount of bulging which applies higher transverse stresses to the reinforcement layers at higher pressures.

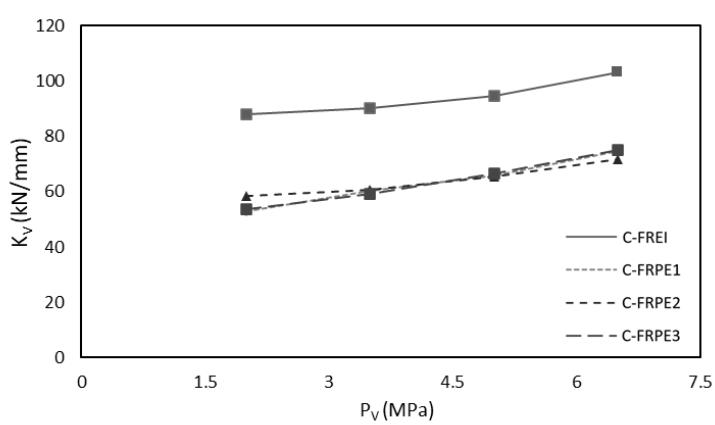

Figure 38: Variation of vertical stiffness to pressure for different types of isolators.

4.2.3.2 Equivalent viscous damping (ξ) and maximum vertical deflection (v_{max})

The third cycle hysteresis loop (see Figure 37) shows a notably higher area for the isolators with the polyurethane cores. Figure 39a shows the magnitudes of ξ at different vertical pressures. A clear consensus cannot be made between the difference in the damping performance of C-FRPEs having the different distribution of polyurethane cores, although their performance is comparable to each other. This implies that as observed for the vertical stiffness, the vertical damping properties are independent of the distribution of the polyurethane cores and only dependent on the area of the cores. For the plain C-FREI, ξ ranges between 8-9% and remains almost constant as the compression pressure is increased. For the C-FRPEs, ξ ranges between 12-25% and show a remarkable increase in damping as the pressure is increased. At low pressure (P_v = 2MPa), the C-FRPEs depict 33% higher damping when compared to the plain C-FREI, which increases to more than 200% at higher pressure (P_v = 6.5MPa). These values suggest that the placement of the polyurethane cores in C-FREIs will be significantly more efficient when the isolators are subjected to higher vertical pressures. The equivalent viscous damping increases more than twice when polyurethane cores are used and therefore the isolators will be much more efficient in the energy dissipation of the vertical component of a seismic record.

Figure 39b illustrates the maximum vertical deflection (v_{max}) experienced by the isolators at each respective vertical pressure. The plain C-FREI almost depicts a linear increase to every 1.5MPa increments in the vertical pressure, whereas the isolators containing the polyurethane cores (C-FRPEs) show increasingly higher displacements at higher pressures. As expected, due to the lower stiffness of the C-FRPEs, they undergo a higher vertical displacement compared to the plain C-FREI. However, at lower vertical loads (e.g., at P_v = 2MPa), v_{max} of the C-FRPEs are very similar to the plain C-FREI. The configuration C-FRPE1 show slightly lower values of v_{max} when compared to C-FRPE2 and C-FRPE3, representing isolators having a single polyurethane core at the center is more efficient in limiting the maximum vertical displacement experienced by

the isolator. Figure 40 shows the experimental photos taken at the maximum vertical deformations of the isolators at the respective pressures.

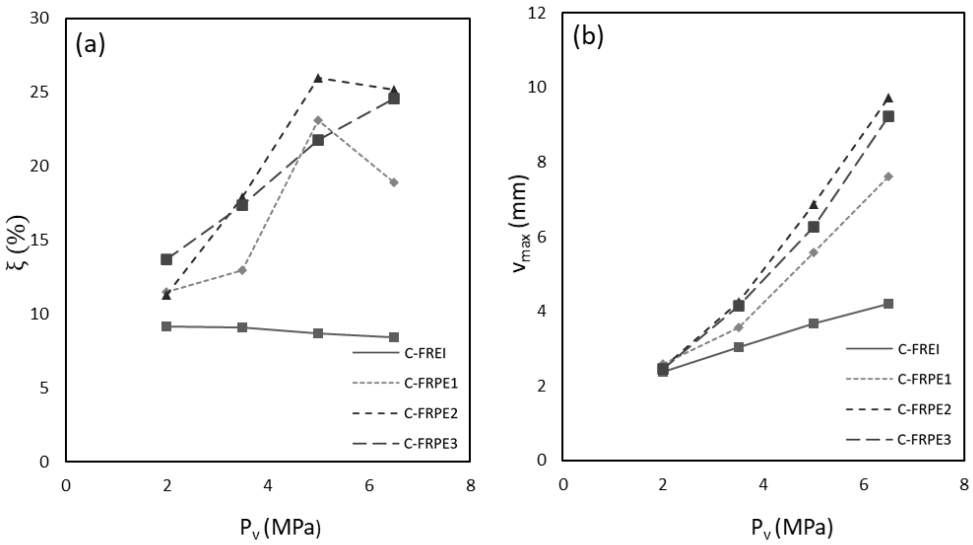

Figure 39: Variation of vertical properties with the vertical pressure for (a) equivalent viscous damping (b) maximum vertical displacement

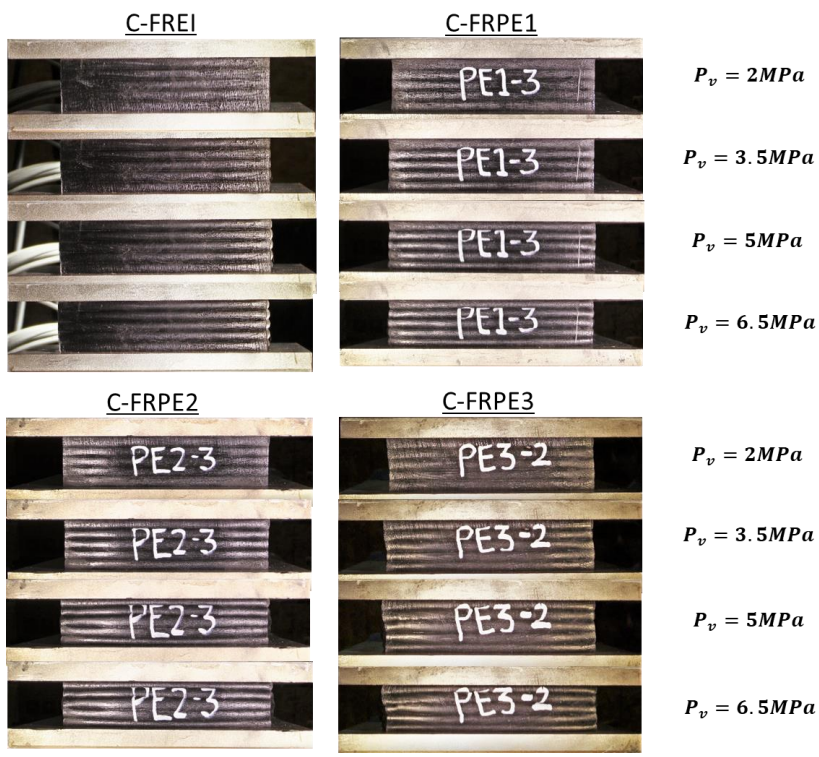

Figure 40: Vertical deformation of the isolators at the design vertical pressure.

4.2.4 Vertical performance after failure

The specimens used for the failure tests in section 4.2.2 were again tested at low pressures to check their vertical performance after failure. The failed isolators were subjected to vertical pressures of 2MPa and 3.5MPa and their vertical stiffness was compared to the vertical stiffness before failure had occurred. Table 4 illustrates the vertical stiffness before failure and the failed specimens at vertical pressures of 2MPa and 3.5MPa. It is observed that for all configurations, the vertical stiffness drops dramatically after failure. However, for the plain C-FREI, this drop in vertical stiffness is more drastic compared to the isolators equipped with the PE cores (C-FRPEs). The maximum drop in vertical stiffness for the C-FREI, C-FRPE1, C-FRPE2, C-FRPE3 is 73%, 62%, 69%, and 66%, respectively. Configuration C-FRPE1 has the highest capability to retain its stiffness after failure.

Table 4: Vertical stiffness before and after failure at low pressure for the plain and polyurethane core isolators

Configurations	Parameters	P_v (MPa)	
		2	**3.5**
C-FREI	Initial K_v (kN/mm)	88	92
	After failure K_v (kN/mm)	24	32
	Drop in stiffness (%)	73	66
C-FRPE1	Initial K_v (kN/mm)	54	61
	After failure K_v (kN/mm)	21	35
	Drop in stiffness (%)	62	43
C-FRPE2	Initial K_v (kN/mm)	60	63
	After failure K_v (kN/mm)	19	26
	Drop in stiffness (%)	69	59
C-FRPE3	Initial K_v (kN/mm)	56	61
	After failure K_v (kN/mm)	19	27
	Drop in stiffness (%)	66	56

4.2.5 Vertical test summary

Plain and polyurethane core carbon-fiber reinforced elastomeric isolators (C-FREIs and C-FRPEs) were subjected to vertical compression loading ranging from 2MPa up to 9.5MPa. The failure tests indicated that the isolators with the polyurethane cores failed within the range of 7.2-

8.1MPa, while the plain C-FREIs failed at a much higher pressure of 9.3MPa. It is also observed that after failure had occurred, C-FRPEs undergo more stable cyclic displacements and are able to retain more of their vertical stiffness.

There is a drop in vertical stiffness due to the placement of the polyurethane cores amounting to 12.5% of the loading area of the isolators, which ranges from 28% to 38%. There is an increase in the vertical stiffness of the isolators as the pressure is increased which is more prominent for the C-FRPEs. There is a remarkable increase in the equivalent viscous damping (more than twice of plain C-FREI at higher pressures) due to the placement of the polyurethane cores. This makes the isolators much more efficient in mitigating the vertical component of the seismic event. It should be noted that both vertical stiffness and damping are not reliant on the distribution of the cores and primarily dependent on the area of the cores.

Surprisingly, the maximum vertical displacements depict almost similar values for C-FREIs and C-FRPEs at lower pressures. At higher pressures, the maximum vertical displacement of C-FRPEs becomes notably higher than the plain C-FREI. Moreover, the isolator with a single polyurethane core at the center is more efficient in limiting the maximum vertical displacements experienced from the total loads.

4.3 Compression-shear test

In compression-shear test, the specimen is subjected to a constant vertical load while applying simultaneous cyclic shear displacements. The test is performed under vertical load control and lateral displacement control. The primary performance specifications of interest from the compression-shear test are the horizontal stiffness and the equivalent viscous damping. The dissipation energy and the restoring energy are also compared as supplementary parameters. The horizontal stiffness would determine the pliability of the isolator in the lateral direction while the equivalent viscous damping, dissipation energy, and restoring energy would determine the capability of the isolator to dissipate the earthquake energies. The testing method described in

section 6.2.2 of ISO 22762-1:2018 was employed to carry out the compression-shear tests. A brief description of the testing program, test setup, and mechanical properties are described in section 3.6 in Chapter 3.

4.3.1 Compression-shear test results

In this section, the horizontal operational characteristics of the isolators containing the polyurethane cores (C-FRPEs) are analyzed and compared to that of the plain C-FREI. As three fully reversed cyclic-shear displacements are applied for each shear strain amplitude, the horizontal operational characteristics are computed from the average of the force-displacement hysteresis curves.

4.3.1.1 Horizontal characteristics for different shear strain amplitudes: Bonded and unbonded applications

In this test, the isolators are subjected to a constant compressive pressure of 3.5MPa followed by different amplitudes of shear strains (25, 50, 75, 100, 125, 150%T_e). At each shear strain amplitude, three fully reversed sinusoidal cycles are applied to have a frequency of 0.05Hz (Time period 20s). A brief detail of the loading protocols is described in section 3.6.2.1.

4.3.1.1.1 Horizontal characteristics of C-FREI and C-FRPEs in unbonded applications

Unbonded applications result in a more efficient form of application for fiber-reinforced elastomeric isolators due to their lack of flexural rigidity. More extensive research has been done in literature focusing on unbonded applications to take advantage of the stable rollover deformation resulting from the lack of flexural rigidity of the fiber reinforcement. Figure 41 shows the lateral force vs. lateral displacement hysteresis loops for the four types of isolators (C-FREI for plain, and C-FRPE1, C-FRPE2, C-FRPE3 as the modified isolators with the polyurethane cores).

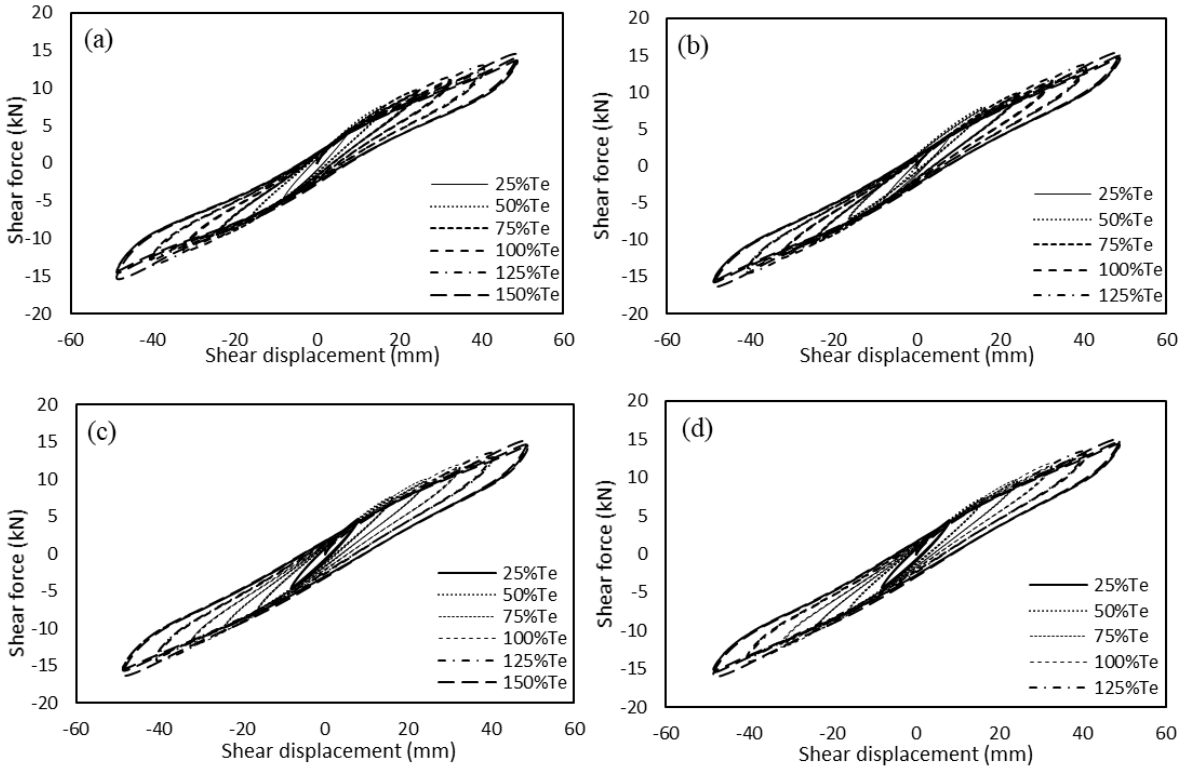

Figure 41: Lateral load-displacement behavior of isolator (a)C-FREI (b)C-FRPE1 (c)C-FRPE2 (d)C-FRPE3 under a constant 3.5MPa compression having shear strain amplitudes of 25, 50,75, 100, 125, 150%T_e (T_e=32.5mm) in unbonded tests.

From the hysteresis behavior illustrated in Figure 41, all the isolators show a very consistent stable behavior for all the shear strain amplitudes tested: 25, 50, 75, 100, 125, 150%T_e (where T_e is the total thickness of the elastomer reading 32.5mm). Comparing Figure 41a, the plain isolator C-FREI depicted an almost linear behavior up to approximately 75%T_e. As the shear strain amplitude is increased (for 100,125, 150%T_e), a nonlinear softening behavior in the loop is observed which occurs mainly due to the unattached boundary conditions of the top and bottom surfaces of the isolator in contact with the testing rig steel plates. Moreover, at higher strains (more than 100%T_e), the softening behavior is not noticeable, and tangential horizontal stiffness stays at its positive value with an insignificant drop. This illustrates that the secondary shape factor ($S_{F2} = 4.3$) chosen for the design of the isolators are deemed to be acceptable and show a stable rollover deformation (SRD). Toopchi-Nezhad et al. (2008) studied the influence of lower

S_{F2} values ($S_{F2} = 1.9$) on the horizontal properties of unbonded C-FREIs. It was observed that at higher lateral strains, the softening behavior continues and shows a negative tangential stiffness which was deemed to be unacceptable.

For the isolators containing the polyurethane cores (see Figure 41a, b, and c), the softening behavior at larger strains is almost negligible for all modifications of C-FRPEs. This implies that the use of polyurethane cores improves the SRD of the isolators for unbonded applications. It is also observed that when compared to the hysteresis loops of C-FRPE1, C-FRPE2 and C-FRPE3 shows a more stable and almost linear behavior up to the maximum shear strain of 150%T_e. This suggests that the PE cores distributed radially are more efficient in improving the SRD compared to a single PE core at the center. Figure 42a-f displays a few photographs taken during the compressive-cyclic tests of the specimens at the extreme lateral strains tested. After the completion of the series of cyclic tests in unbonded applications, no damage or delamination was observed except for C-FRPE3 at extreme shear strain (150%T_e).

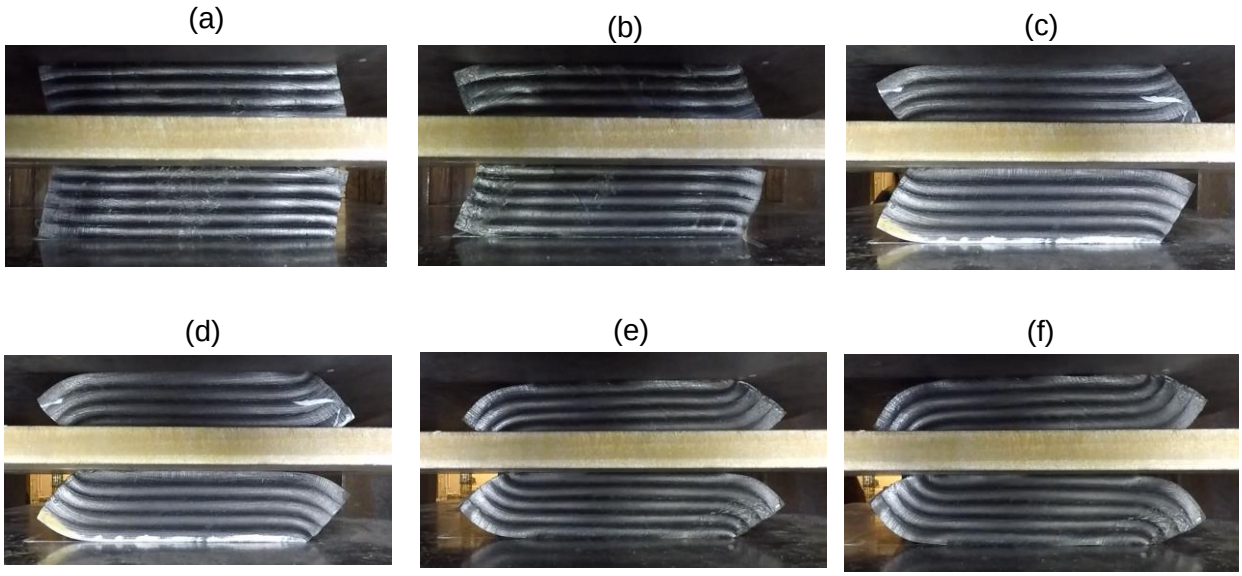

Figure 42: Isolators under 3.5MPa vertical compression and subjected to horizontal strain amplitudes of (a)C-FRPE2 at 25%T_e (b)C-FRPE3 at 50%T_e (c)C-FREI at 75%T_e (d)C-FREI at 100%T_e (e)C-FRPE1 at 125%T_e (f)C-FRPE1 at 150%T_e.

Table 5 depicts the horizontal stiffness (K_h), the dissipating energy (W_d), the restoring energy (W_s), and the equivalent damping ratio (ξ) of the plain and modified isolators calculated using equation (3.6) to equation (3.9). The results reflect the average values based on the three cycles of the hysteresis loops. The results are further clarified by plotting these parameters as a function of the shear strain amplitude as shown in Figure 43.

Table 5: Horizontal specifications of the plain C-FREI and modified C-FRPEs tested for unbonded applications for different strains at P_v = 3.5MPa

Modification	γ (%)	K_h (kN/mm)	W_d (J)	W_s (J)	ξ (%)
C-FREI	25	0.57	17.70	19.00	7.4
	50	0.45	52.75	59.80	7.0
	75	0.38	98.30	114.40	6.8
	100	0.34	153.00	179.45	6.8
	125	0.31	221.35	254.95	6.9
	150	0.29	307.70	341.10	7.2
C-FRPE1	25	0.57	17.65	18.70	7.5
	50	0.46	53.35	60.65	7.0
	75	0.40	99.55	119.25	6.6
	100	0.36	154.90	190.55	6.5
	125	0.33	222.05	273.60	6.5
	150	0.31	304.30	367.90	6.6
C-FRPE2	25	0.57	18.15	18.75	7.7
	50	0.46	54.60	61.00	7.1
	75	0.40	104.00	119.20	6.9
	100	0.36	166.00	189.85	7.0
	125	0.33	248.05	270.60	7.3
	150	0.31	369.95	362.40	8.1
C-FRPE3	25	0.54	17.35	17.90	7.1
	50	0.45	52.80	59.20	7.1
	75	0.39	97.35	116.65	6.6
	100	0.36	153.45	187.90	6.5
	125	0.33	228.90	267.95	6.8
	150	0.30	338.20	360.40	7.5

Comparing Figure 43a, the horizontal stiffness (K_h) for all the isolators show a decreasing behavior as the shear strain is increased. This happens primarily due to the softening nonlinear behavior of the elastomer which enhances due to the rollover deformation of the unbonded application. The degradation in the horizontal stiffness for every increment in 25%T_e strain is more

prominent at lower strains. For example, as γ is increased from 25%T_e to 50%T_e, the reduction in K_h amounts to 18% to 21%, while as γ is increased from 125%T_e to 150%T_e, the reduction in K_h amounts to only 6-8%. The modified C-FRPEs show a slightly higher horizontal stiffness compared to the plain C-FREI. Although higher K_h means lower flexibility of the isolators with lower efficiency, this increase amounts to only an average of 2-4% suggesting the efficiency of the isolators by placing the PE cores do not degrade the efficiency in terms of the horizontal stiffness. In fact, this slight increase in the horizontal stiffness is what contributes to a more stable rollover deformation of the isolators. There is no noticeable variation in the K_h values for the different modifications of C-FRPEs. This depicts that K_h is not dependent on the distribution of the polyurethane cores. A slight increase in the horizontal stiffness will only cause a slight increase in the effective shear modulus (G_h) according to equation (3.10). The main contribution of placing the polyurethane cores is to cause an improvement in the energy dissipation capabilities.

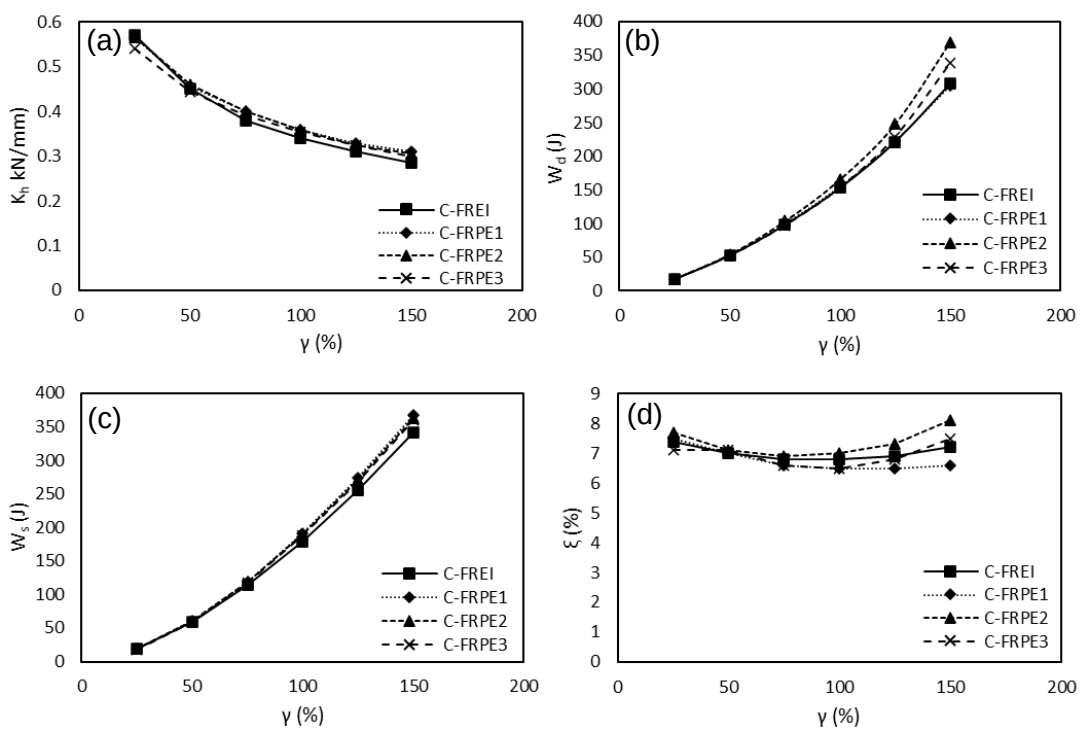

Figure 43: Comparison of the main horizontal parameters for the isolators in unbonded applications for (a) horizontal stiffness (b)dissipation energy (c) restoring energy (d) equivalent viscous damping

The energy dissipation (W_d) and the restoring energy (W_s) (see Figure 43b and 43c) rises with an increasing magnitude of lateral strain for all the isolators. C-FRPE2 shows a higher W_d values compared to C-FRPE1 and C-FRPE3 suggesting that smaller and radially distributed PE cores are more efficient in increasing the dissipation energy of such isolators. This increase in W_d becomes more significant at higher lateral strains showing that the PE cores become more efficient at higher lateral displacements. This will become an advantage to dissipate high magnitude earthquakes. For example, C-FRPE2 has 2.5% and 20.2% higher dissipation energy when compared to the plain C-FREI when subjected to shear strains of 25%T_e and 150%T_e, respectively. The restoring energy (W_s) for all the modifications of C-FRPEs show similar behavior with slightly higher values compared to plain C-FREI. At 150%T_e, an increase of 5.5-8% in W_s is observed for the C-FRPEs compared to the plain C-FREI. This small increase in the restoring energy can be explained according to equation (3.8). W_s is proportional to the horizontal stiffness and the applied lateral strain, where the horizontal stiffness is the only dependent parameter. Hence, a small increase in the horizontal stiffness as described above causes only a small rise in the restoring energy. There is not much improvement in the equivalent viscous damping (ξ) after placing the polyurethane cores in the isolators. Only the modification C-FRPE2 has higher values of ξ compared to the plain C-FREI. This is due to the fact that ξ is proportional to the ratio of the dissipated energy to the restoring energy. Since C-FRPE2 has higher dissipation energy, the equivalent viscous damping is noticeably higher which is approximate ~4% and ~12.5% higher compared to the plain C-FREI at shear strains of 25%T_e and 50%T_e respectively.

4.3.1.1.2 Horizontal characteristics of C-FREI and C-FRPEs in bonded applications

The C-FREIs and C-FRPEs were tested in bonded applications by bonding the isolators to the testing machine using the same rubber cement compound used for bonding the elastomers and fiber reinforcement layers. Figure 44 shows the rubber cement being added to the steel plates

of the test setup. The steel surface had to be grinded and surface conditioned for the bonding agent to work well as per the manufacturer's instructions.

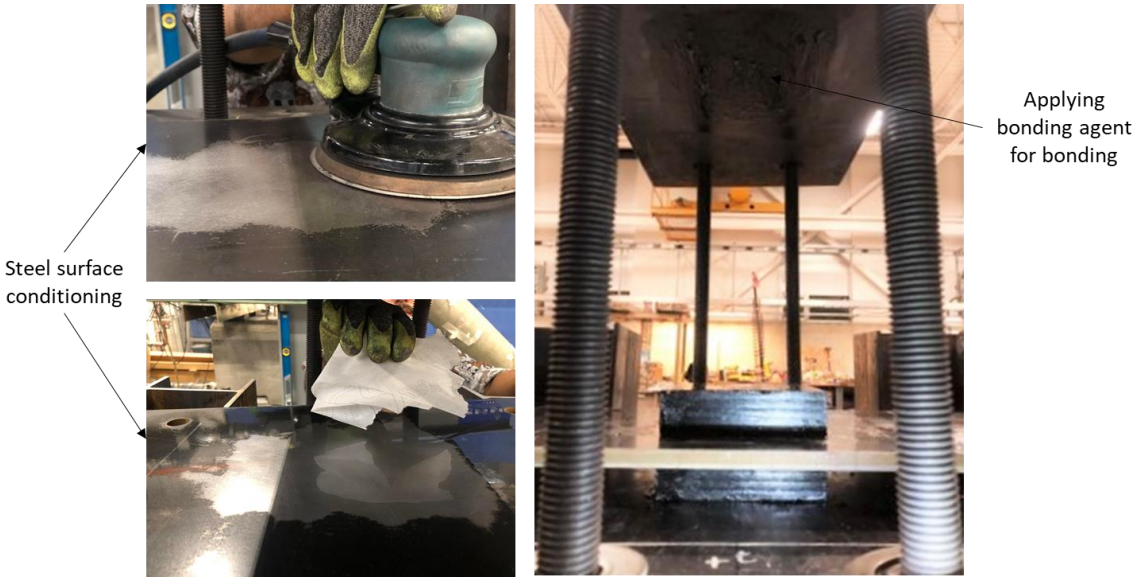

Figure 44: Bonding the isolators to the testing steel plates for testing in bonded applications.

Bonded applications of fiber-reinforced elastomeric isolators are usually not preferred due to their lack of flexural rigidity. The result of rollover deformation at higher lateral strains tends to apply a peel-off force occurring due to tensile forces generating from the top and bottom elastomer layers. These tensile forces create a coupling moment at larger displacements, thereby increasing delamination. However, bonded applications can often be preferred by contractors as they avoid the unseating of bridge decks at larger magnitude earthquakes. Delamination occurs when the tensile forces generated exceed the bonding strength of the rubber cement used during fabrication. Figure 45 shows the delamination behavior for the plain C-FREI and the C-FRPEs subjected to shear strains of 25, 50, and 75%T_e at the extreme positions.

All of the configurations of the isolators shows no delamination for the lowest lateral strain of 25%T_e. The plain C-FREI demonstrates slight delamination at 50%T_e and significant delamination at 75%T_e. In contrary to the C-FREI, the modified isolators with the polyurethane cores (C-FRPEs) showed no delamination at 50%T_e and only slight delamination at some edges at 75%T_e. This proves that the use of these polyurethane cores significantly improves the

delamination behavior of fiber-reinforced elastomeric isolators. One reasonable explanation for the isolators with the PE cores to have improved delamination behavior is a slight increase in the horizontal stiffness and an increase in the dissipation energy. However, the primary reason for this is the bonding characteristics of polyurethane to the testing steel plates. It was observed during the tests that the polyurethane material has a stronger bond with steel compared to the elastomer bond with steel when using the rubber cement as the bonding agent. Figure 46 shows how the cores were still attached to the steel plates after the tensile force was applied to remove the specimens upon completing the bonding tests. These cores prevent the elastomers, and the fiber reinforcement layers from rollover, thereby reducing the delamination.

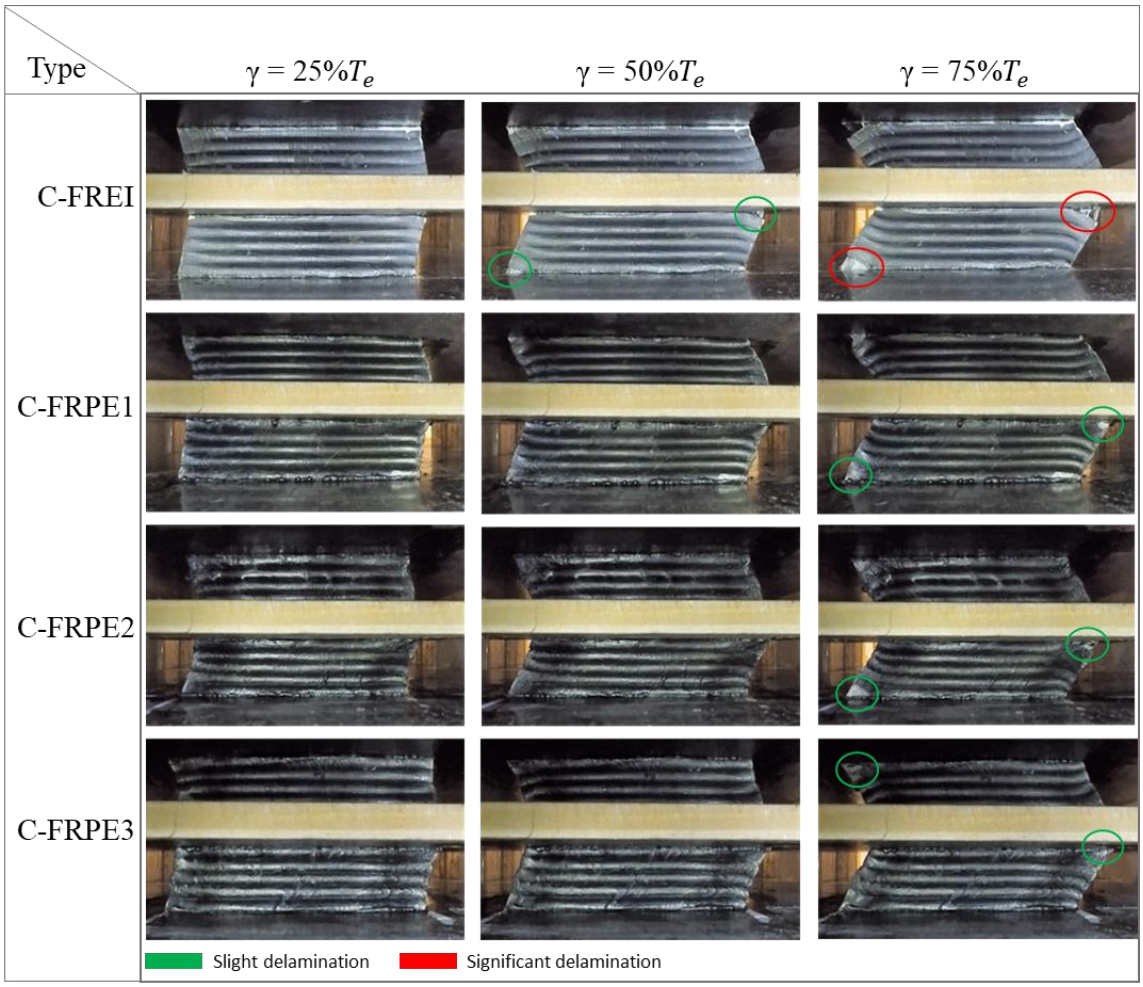

Figure 45: Bonding the isolators to the testing steel plates for testing in bonded applications

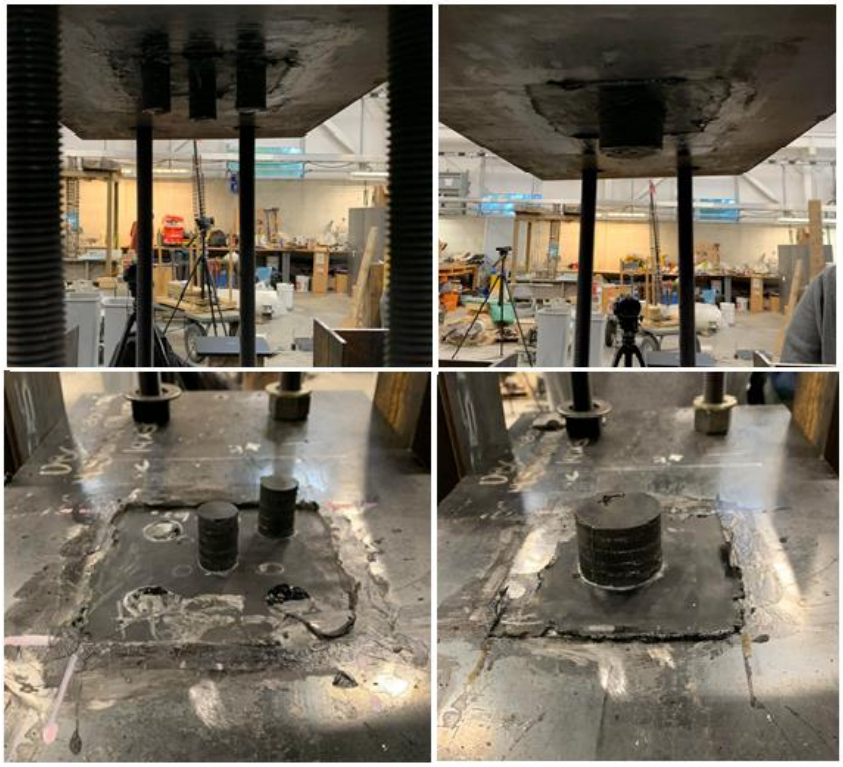

Figure 46: Bonding of the polyurethane cores to the steel plates in improving the delamination behavior in bonded applications.

Figure 47 shows the lateral force vs displacement hysteresis loops for all the shear strains considered. Although delamination mainly occurs at and after γ = 75%T_e, the hysteresis loops remained stable as the isolators acted as partially bonded specimens. Fiber-reinforced elastomeric isolators have also been tested in partially bonded applications to eliminate the disadvantages of unbonded applications while retaining the rollover advantages which proved to be efficient in terms of horizontal stiffness and energy dissipation capacity (Van Engelen et al., 2019).

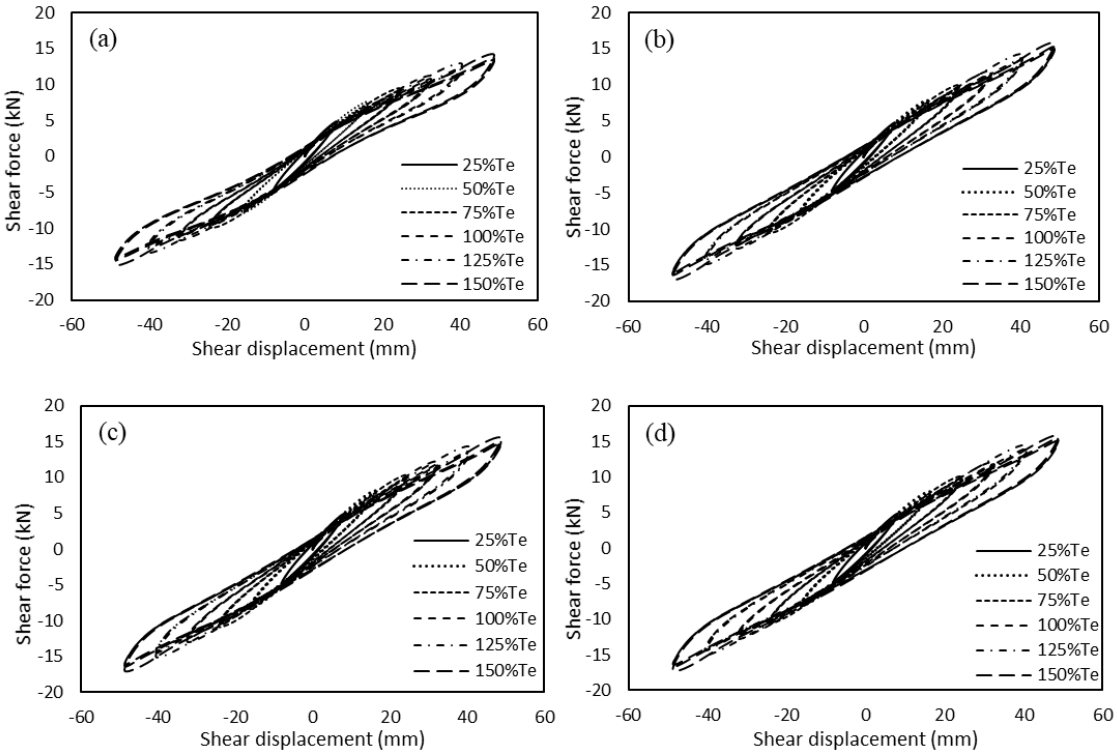

Figure 47: Lateral load-displacement behavior of isolator (a)C-FREI (b)C-FRPE1 (c)C-FRPE2 (d)C-FRPE3 under a constant 3.5MPa compression having shear strain amplitudes of 25, 50,75, 100, 125, 150%T_e (T_e=32.5mm) in bonded tests.

Similar to the unbonded applications, the hysteresis behavior for the bonded application shows a softening behavior for only the plain C-FREI. The behavior is seen to be very consistent for all the shear amplitudes tested. Table 6 shows the horizontal stiffness (K_h), the dissipating energy (W_d), the restoring energy (W_s), and the equivalent damping ratio (ξ) of the plain and modified isolators. As also previously stated, these values were calculated based on the mean of the three cycles. Figure 48 plots these values to be further discussed.

For all the isolators, the horizontal stiffness (K_h) degrade as the shear strain amplitude is increased primarily occurring for the nonlinear softening behavior of the elastomer layers (see Figure 48a). The highest degradation in the horizontal stiffness occurs at lower amplitudes of strain. When γ is increased from 25%T_e to 50%T_e, the degradation in K_h for all the isolators range from 18-22%, while at higher shear strain amplitudes, i.e., when γ is increased from 125%T_e to

150%T_e, the fall in K_h is only 6-7%. Compared to the plain C-FREI, the isolators with the polyurethane cores have approximately 6-8% higher horizontal stiffness. The distribution of the cores within the isolators has no noticeable effect in terms of horizontal stiffness.

Table 6: Horizontal specifications of the plain C-FREI and modified C-FRPEs tested for bonded applications for different strains at P_v = 3.5MPa

Modification	γ (%)	K_h (kN/mm)	W_d (J)	W_s (J)	ξ (%)
C-FREI	25	0.575	18.65	19.1	7.8
	50	0.45	53.9	59.95	7.2
	75	0.38	96.85	113.25	6.8
	100	0.335	148.85	177.3	6.7
	125	0.305	213.6	252.05	6.7
	150	0.285	296.05	337.45	7.0
C-FRPE1	25	0.575	18.6	19.05	7.8
	50	0.47	58.4	62.15	7.5
	75	0.4	109.8	119.9	7.3
	100	0.36	172.05	192.05	7.1
	125	0.34	255.95	280.3	7.3
	150	0.32	344.95	380.05	7.2
C-FRPE2	25	0.595	18.9	19.8	7.6
	50	0.485	58.75	64.4	7.3
	75	0.415	108.55	124.05	7.0
	100	0.37	168.9	195.6	6.9
	125	0.34	249.95	281.55	7.1
	150	0.315	340.05	376.85	7.2
C-FRPE3	25	0.585	19.35	19.45	7.9
	50	0.47	59.6	62.6	7.6
	75	0.405	112	121.85	7.3
	100	0.365	175.8	194.45	7.2
	125	0.345	265.7	283.65	7.5
	150	0.325	371.15	384.35	7.7

Figures 48b-c illustrates the variation of the energy dissipation (W_d) and the restoring energy (W_s) as a function of the shear strain amplitude. At lower amplitudes of lateral strains, W_d and W_s for all the isolators are almost equal. However, as the lateral strain continues to increase, the energy dissipation and the restoring energy continue to increase which is more prominent for the isolators with the PE cores (C-FRPEs). The highest energy dissipation capacity is

demonstrated by C-FRPE3, which is 25% higher than the plain C-FREI at a lateral strain of 150%T_e. This again suggests that radially distributed polyurethane cores are more efficient in dissipating the earthquake energy compared to a single core. The restoring energy for the C-FRPEs is higher than C-FREI with no discernable variation between the different modifications. At the maximum lateral strain when the restoring energy is the maximum, the C-FRPEs have approximately 12-14% higher restoring energy compared to C-FREI. The equivalent viscous damping (ξ) of all the C-FRPEs is higher than that of C-FREI. The maximum difference is observed for C-FRPE3 which has a 10% higher ξ compared to the plain C-FREI at the maximum lateral strain applied.

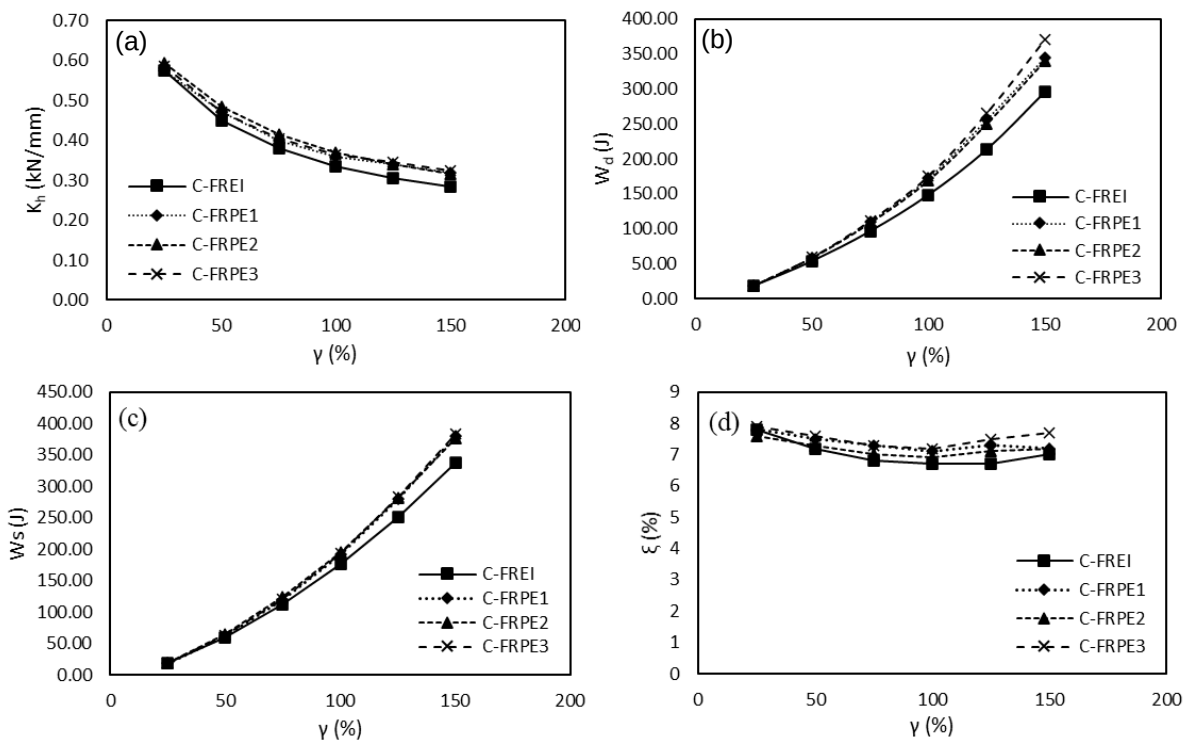

Figure 48: Comparison of the main horizontal parameters for the isolators in bonded applications for (a) horizontal stiffness (b)dissipation energy (c) restoring energy (d) equivalent viscous damping

4.3.1.1.3 Unbonded and bonded application comparison

In the previous sections, the horizontal specifications for the plain C-FREI and modified C-FRPEs were analyzed by subjecting the isolators to a constant compressive load and six levels of lateral strain amplitudes. They were analyzed for both bonded (B) and unbonded (UB) applications. In this section, a brief comparison between both types of applications will be made. Figure 49 plots the horizontal stiffness for the bonded and unbonded specimens for all the lateral strains applied. The plain C-FREI depicts no discernable variation in the horizontal stiffness when tested in bonded and unbonded applications. C-FRPE1 with a single PE core shows only a slight increase (+2%) for bonded applications. C-FRPE2 and C-FRPE3 show a much higher increase in horizontal stiffness when used in bonded applications. When compared to the unbonded applications, C-FRPE2 and C-FRPE3 show approximately +4% and +6% increase in horizontal stiffness, respectively. This rise in horizontal stiffness in bonded applications happens due to the bonding agent holding the specimens to the testing plates. Polyurethane cores having a stronger bond with the bonding agent also increase the stiffness more when compared to the plain specimens. Moreover, radially distributed cores increase the horizontal stiffness even more when used in bonded applications compared to a single core.

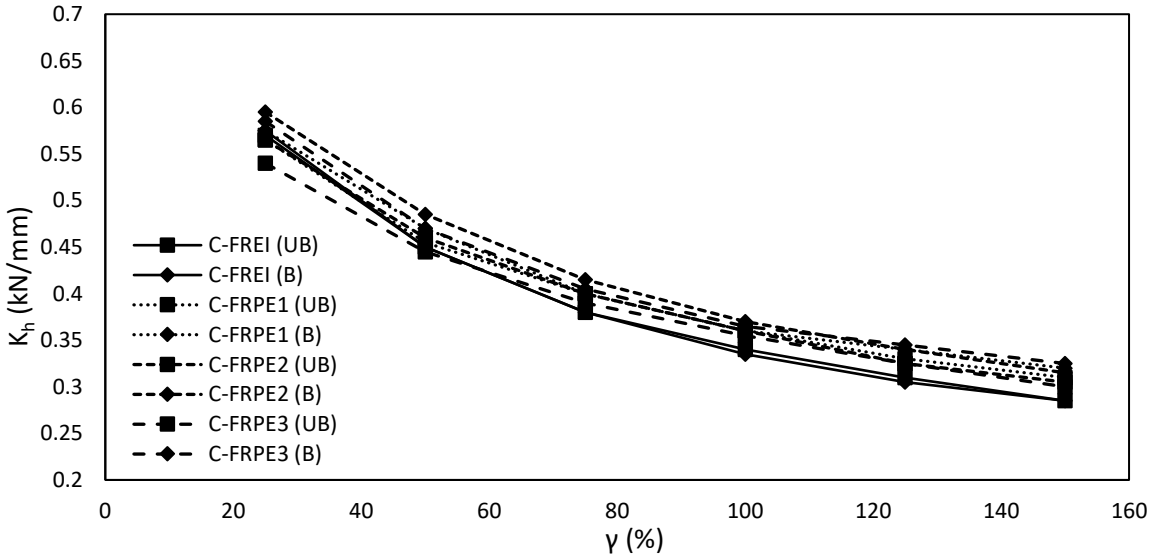

Figure 49: Comparison of the horizontal stiffness between the bonded and unbonded specimens.

There is not much variation in the restoring energy between the bonded and the unbonded specimens. However, the dissipating energy and the equivalent viscous damping are higher for the bonded specimens corresponding to C-FRPE1 and C-FRPE3. The dissipation energy for the bonded C-FRPE1 and C-FRPE3 are on an average of 11% and 13% higher compared to their unbonded counterparts. Figure 50 shows their damping performance plotted for the bonded and unbonded specimens. Due to the restoring energy being almost similar for the bonded and the unbonded, the equivalent viscous damping becomes mainly dependent on the dissipation energy which was seen to be higher for the bonded C-FRPE1 and C-FRPE3. The damping ratio is ~9% higher for the bonded C-FRPE1 and C-FRPE3. This higher damping ratio for only the specific modifications can be explained by the bonding of polyurethane to the steel plates. As previously discussed, polyurethane has a stronger bond compared to the elastomer for the bonding agent used. A larger size of the cores means more surface area of the bond and hence higher horizontal stiffness and dissipation energy. To summarize, bonding the specimens to the testing steel plates does not change the horizontal performance drastically. There is no variation for the plain C-FREI specimens and only a slight increase in the horizontal stiffness and damping ratio for the C-FRPEs.

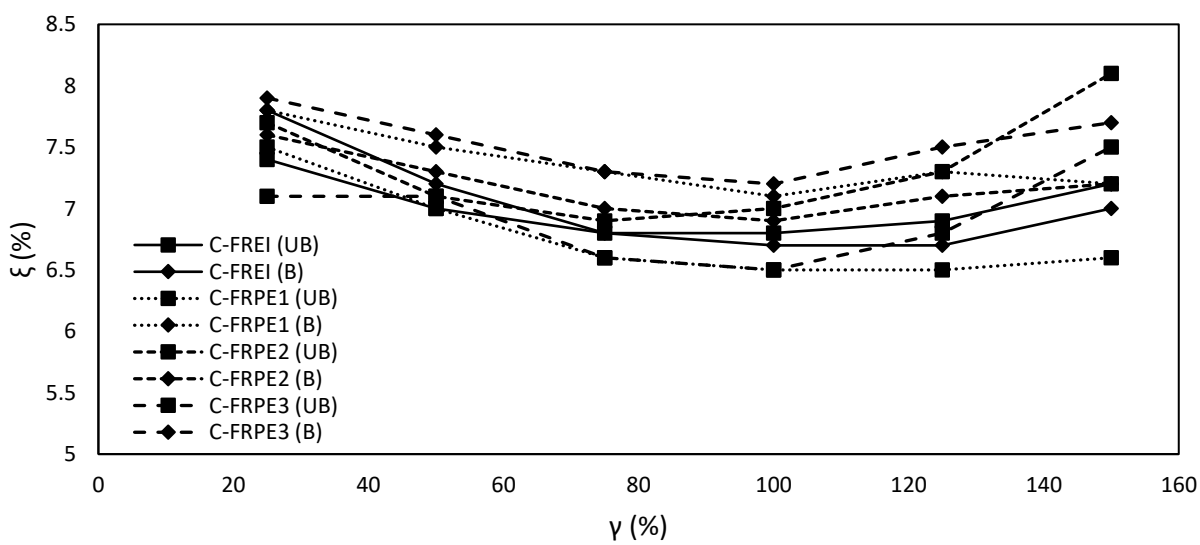

Figure 50: Comparison of the equivalent viscous damping between the bonded and unbonded specimens.

4.3.1.2 Dependence tests on the horizontal characteristics

In this section, three different dependence tests are performed in the lateral direction and their horizontal stiffness and equivalent viscous damping are compared. Only these two parameters are considered as the horizontal stiffness is a measure of the lateral pliability while the equivalent damping ratio is a measure of how efficient an isolator is to dissipate the earthquake energy. The strain dependence, the vertical pressure dependence, and the lateral cyclic rate dependence are the three factors considered in this dependence study.

4.3.1.2.1 Strain dependence on the lateral properties

The objective of the strain dependence tests is to determine how much variation is there in the horizontal properties when different lateral strain amplitudes are applied simultaneously compared to when applied individually. In order to explore this strain dependence, three different amplitudes of lateral strains (25%T_e, 50%T_e, 75%T_e) were applied while keeping the vertical pressure and the loading rate constant. The details of the testing protocols are described in section 3.6.2.2.1. Figures 51 and 52 show the lateral force vs displacement hysteresis loops for the strains considered in unbonded and bonded applications, respectively. The horizontal stiffness and the damping ratio were calculated from the different levels of strain to find any dependency which is given in Table 7 and Table 8 for the unbonded and bonded respectively.

By comparing the hysteresis responses and the values, it can be observed that the drop in horizontal stiffness at the simultaneous increase in shear strain amplitudes is slightly lower compared to when independent values of shear strains are applied (section 4.3.1.1), with no distinguishable variation between the bonded and unbonded applications. For the plain C-FREI, the degradation in the horizontal stiffness from 25%T_e to 50%T_e shear strain is ~18-19% whereas from 50%T_e to 75%T_e, the degradation is ~13%. For the C-FRPEs, the change in horizontal stiffness from 25%T_e to 50%T_e and from 50%T_e to 75%T_e is approximately 13-16% and 10-11% respectively. The degradation in the horizontal stiffness when different amplitudes of cyclic strains

are applied simultaneously is lower compared to when applied independently. Therefore, the strain dependence tests on the isolators are satisfactory and do not show a large difference when tested for individual strains.

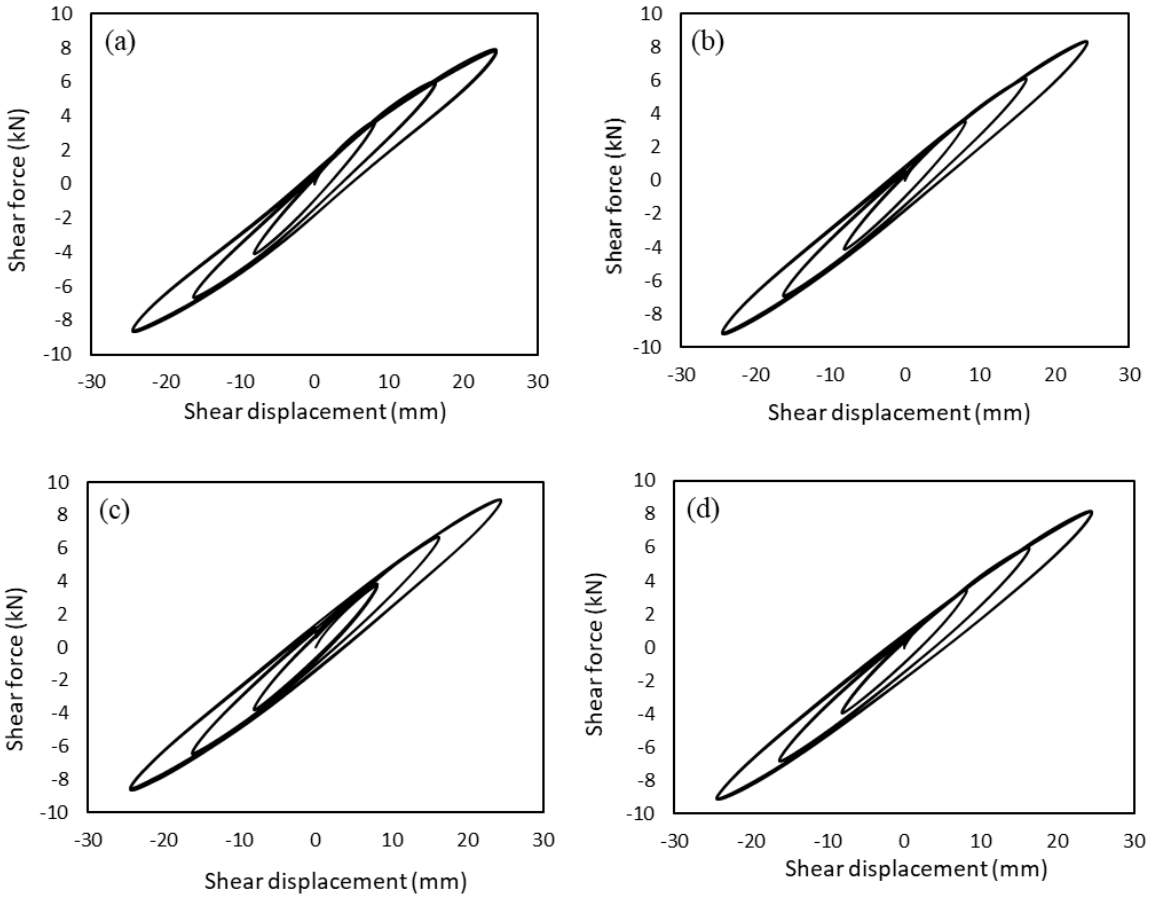

Figure 51: Lateral force vs displacement hysteresis loops for the strain dependence tests (a) C-FREI (b) C-FRPE1 (c) C-FRPE2 (d) C-FRPE3 in unbonded applications.

The mean drop in the equivalent viscous damping for all the isolators is ~6-7% when the cyclic strains are applied simultaneously, whereas this drop equates to ~4-5% when the cyclic lateral strains are applied individually. This proves that there is no significant difference in the damping properties between simultaneous and individual applications of lateral cyclic strains.

The strain dependence tests proved that there is no detrimental performance in the horizontal behavior when different amplitudes of cyclic strains are applied simultaneously. In fact, the degradation in the horizontal stiffness is observed to be much lower which is advantageous

for ground motions having a range of random amplitudes. The C-FRPEs showed a lower degradation compared to the plain C-FREI which is another advantage of placing the polyurethane cores. There was no variation in the degradation properties for the bonded and unbonded applications.

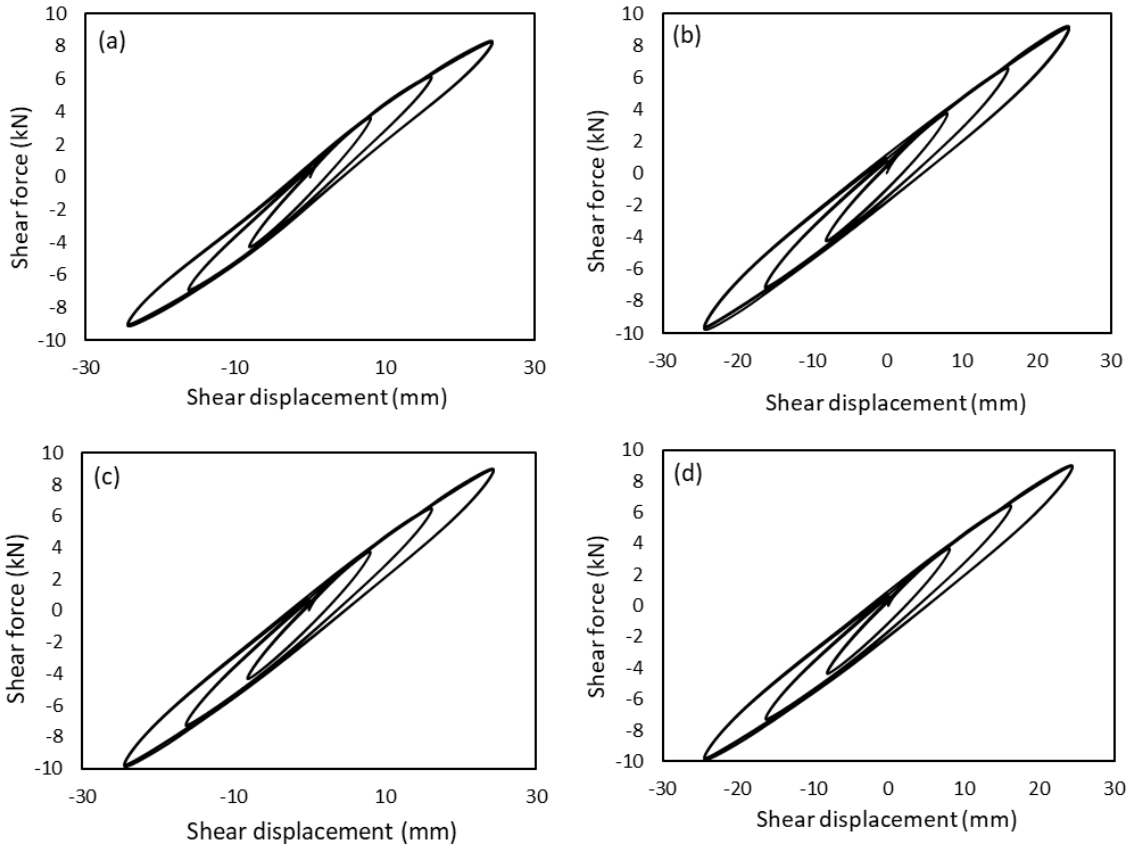

Figure 52: Lateral force vs displacement hysteresis loops for the strain dependence tests (a) C-FREI (b) C-FRPE1 (c) C-FRPE2 (d) C-FRPE3 in bonded applications.

Table 7: Horizontal specifications of the strain dependence test - unbonded

Application	Modification	γ (%)	K_h (kN/mm)	ξ (%)
Unbonded	C-FREI	25	0.48	8.1
		50	0.39	7.6
		75	0.34	7.4
	C-FRPE1	25	0.48	8.2
		50	0.40	7.6
		75	0.36	7.1
	C-FRPE2	25	0.47	8.3
		50	0.40	7.7
		75	0.36	7.2
	C-FRPE3	25	0.46	8.4
		50	0.40	7.8
		75	0.35	7.3

Table 8: Horizontal specifications of the strain dependence test - bonded

Application	Modification	γ (%)	K_h (kN/mm)	ξ (%)
Bonded	C-FREI	25	0.49	8.2
		50	0.40	7.4
		75	0.35	6.9
	C-FRPE1	25	0.49	8.7
		50	0.42	8.1
		75	0.38	7.7
	C-FRPE2	25	0.50	8.4
		50	0.42	7.8
		75	0.38	7.2
	C-FRPE3	25	0.49	8.6
		50	0.42	8.0
		75	0.38	7.4

4.3.1.2.2 Compression force dependence on the lateral properties

In this section, the effect of the vertical pressure on the horizontal stiffness and the equivalent viscous damping is explored. To do this, a lateral strain amplitude of 50%T_e with a frequency of 0.05Hz is applied while varying the vertical pressures at 2MPa, 3.5MPa, and 5MPa. The loading protocols are briefly described in section 3.6.2.2.2. Table 9 shows the K_h and ξ values for the isolators at different pressures for both bonded and unbonded applications. Appendix B and Appendix C show the lateral force vs displacement hysteresis behaviors for the compressive force dependence tests for the unbonded and bonded applications respectively.

Table 9: Horizontal stiffness and equivalent viscous damping at different vertical pressures for bonded and unbonded applications

Application	Modification	P_v (MPa)	K_h (kN/mm)	ξ (%)
Bonded	C-FREI	2	0.40	7.1
		3.5	0.40	7.3
		5	0.40	7.8
	C-FRPE1	2	0.42	7.6
		3.5	0.42	7.9
		5	0.42	8.9
	C-FRPE2	2	0.42	7.5
		3.5	0.42	7.7
		5	0.42	8.4
	C-FRPE3	2	0.42	7.7
		3.5	0.42	7.9
		5	0.42	8.7
Unbonded	C-FREI	2	0.36	7.1
		3.5	0.39	7.4
		5	0.38	7.9
	C-FRPE1	2	0.41	7.1
		3.5	0.41	7.4
		5	0.40	8.6
	C-FRPE2	2	0.40	7.5
		3.5	0.40	7.9
		5	0.40	8.6
	C-FRPE3	2	0.40	7.4
		3.5	0.40	7.7
		5	0.39	8.7

The effect of vertical pressure on horizontal stiffness is explored first. Figure 53 shows a bar chart comparing the horizontal stiffness for the isolators plotted for both bonded and unbonded applications at three different vertical pressures (2MPa, 3.5MPa, 5MPa). The figure shows that the vertical pressure has a negligible effect on the horizontal flexibility for both the plain C-FREI and C-FRPEs. This insensitivity of the horizontal stiffness due to the vertical pressure can be explained by the material of the elastomer and polyurethane used. High damping elastomer is not used in this study which is highly non-linear and is highly sensitive to the environment and loading conditions. The neoprene used is insensitive to the vertical pressure and therefore does not contribute to the horizontal stiffness.

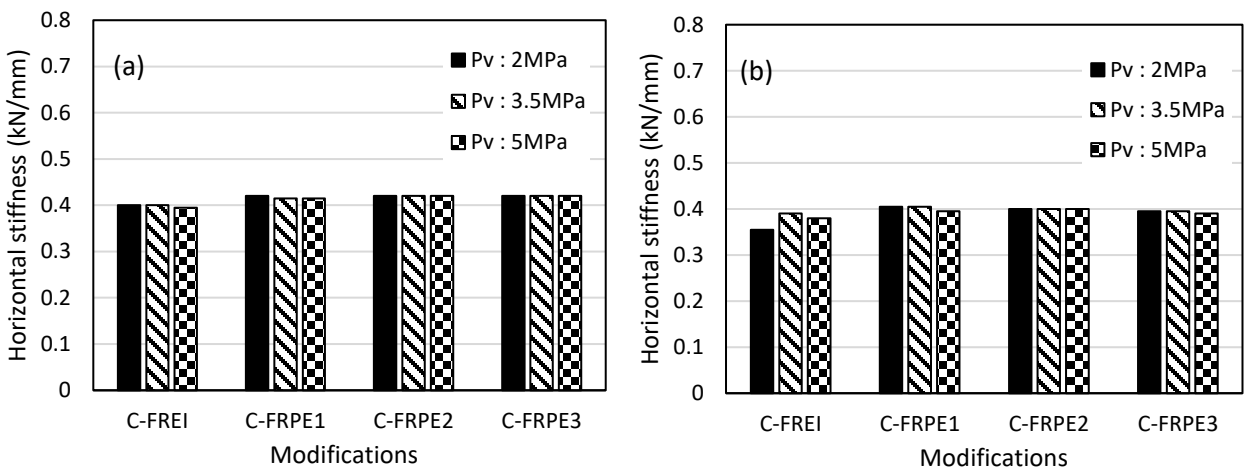

Figure 53: Horizontal stiffness comparison under different vertical pressures of all the isolator modifications for (a) bonded (b)unbonded.

The next considered parameter is the equivalent viscous damping (ξ) of the isolators. Figure 54 compares the effect of the damping properties by changing the vertical compression load. By increasing the vertical pressure, the damping ratio increases which is even more prominent at higher pressures. The bonded and the unbonded applications show almost a similar sensitivity to the change in vertical pressure. To the vertical load variation, the plain C-FREI shows a maximum increase in ξ of 7% as a result of increasing P_v from 3.5MPa to 5MPa. For the isolators with the polyurethane cores (C-FRPEs), the maximum increase in damping is 16% increasing P_v

from 3.5MPa to 5MPa. This increase in damping can be attributed to a rise in the parallel tension of the fiber reinforcement. At higher vertical pressures, due to the bulging of the elastomer layers, the strands of the carbon fiber curve against the elastomer layers due to a lack of flexural rigidity. As the pressure is increased, this curving behavior increases, and more energy is dissipated through friction. As the polyurethane cores are placed without any reinforcement, their bulging is much higher, and more energy is dissipated through friction.

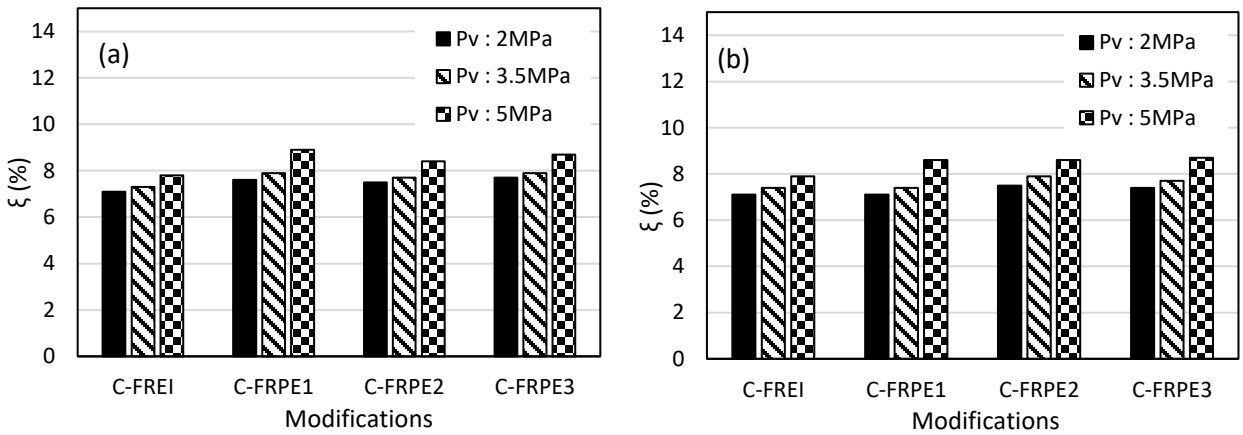

Figure 54: Equivalent viscous damping comparison under different vertical pressures of all the isolator modifications for (a) bonded (b)unbonded.

4.3.1.2.3 Lateral cyclic rate dependence on the lateral properties

Earthquakes can range from having different magnitudes and frequency contents, hitting the base-isolated structures. Therefore, it is important to investigate the effect of the lateral cyclic rate on the horizontal stiffness and damping capability of the isolators. The lateral cyclic tests are conducted by considering three different rates (0.005Hz, 0.1Hz, and 0.5Hz) while the vertical pressure and lateral strain amplitude is kept constant at 3.5MPa and 50%T_e. A brief description of the loading protocol is described in section 3.6.2.2.3. Table 10 denotes the values of the horizontal stiffness and the equivalent viscous damping for the three lateral loading rates considered. Appendix D and E show the lateral force vs displacement hysteresis loops for the unbonded and bonded applications respectively.

Table 10: Horizontal stiffness and equivalent viscous damping at different lateral cyclic rates for bonded and unbonded applications

Application	Modification	f_v (Hz)	K_h (kN/mm)	ξ (%)
Bonded	C-FREI	0.005	0.38	7.9
		0.1	0.41	7.2
		0.5	0.43	7.2
	C-FRPE1	0.005	0.39	8.7
		0.1	0.43	8.1
		0.5	0.45	8.0
	C-FRPE2	0.005	0.40	8.4
		0.1	0.44	7.8
		0.5	0.46	7.6
	C-FRPE3	0.005	0.40	8.8
		0.1	0.44	8.0
		0.5	0.46	7.9
Unbonded	C-FREI	0.005	0.37	8.1
		0.1	0.40	7.3
		0.5	0.42	7.2
	C-FRPE1	0.005	0.38	7.3
		0.1	0.39	8.5
		0.5	0.44	7.9
	C-FRPE2	0.005	0.38	8.8
		0.1	0.42	7.9
		0.5	0.45	7.7
	C-FRPE3	0.005	0.38	9.1
		0.1	0.42	8.0
		0.5	0.44	7.7

Figure 55 shows a bar chart of the effective horizontal stiffness for the bonded and unbonded applications. From the figure, it is observed that increasing the lateral cyclic rate increases the horizontal stiffness and this increase is approximately similar for both the bonded and unbonded applications. This increase in stiffness for the plain C-FREI is approximately 5-6%, whereas, for the C-FRPEs, this increase is ~7-8%. The different modifications (distribution of the cores) do not affect the horizontal stiffness. This increase in horizontal stiffness can be attributed to the stiffening of the elastomer layers at higher loading rates, thus reducing the flexibility of the isolator in the horizontal direction. However, compared to the magnitude of the actual values of

the horizontal stiffness, this increase is negligible and does not affect the performance of the isolators.

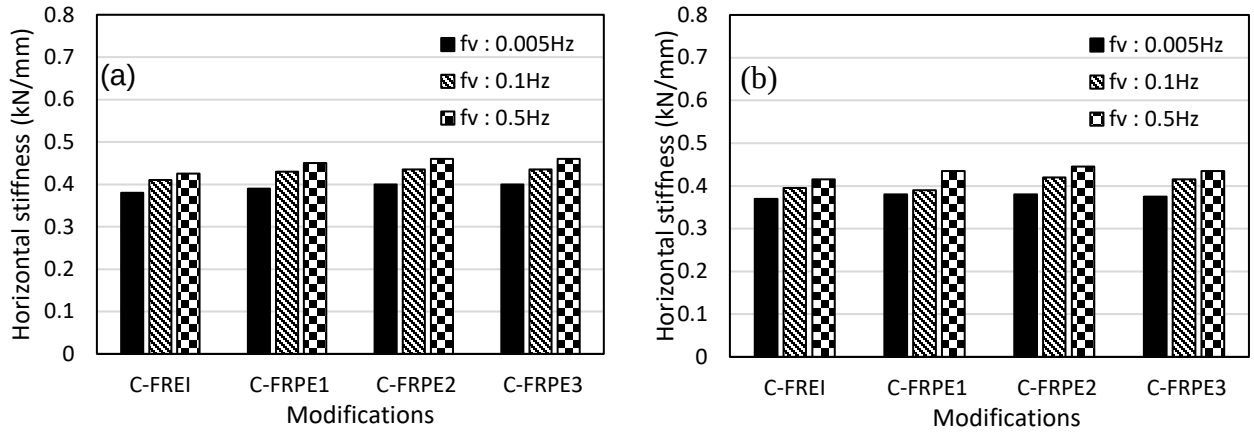

Figure 55: Horizontal stiffness comparison under different lateral loading rates of all the isolator modifications for (a) bonded (b)unbonded

Figure 56 shows the bar chart comparison of the equivalent viscous damping as we change the lateral cyclic rate for the bonded and unbonded applications. As observed previously, similar sensitivity is depicted by both applications. Moreover, the placement of the polyurethane cores does not affect the sensitivity of the lateral loading rate on the isolators, i.e., C-FRPEs behave in a similar manner to C-FREI. In contrary to the horizontal stiffness change, the equivalent viscous damping reduces to an increase in the lateral cyclic rate. An increase in lateral loading rate from 0.005Hz to 0.1Hz reduces the damping by an average of 9.2%, whereas an increase in the loading rate from 0.1Hz to 0.5Hz reduces the damping by an average of 1.8%. This phenomenon of the reduction in the damping coefficient by increasing the loading rate is because of the stiffening of the elastomer layers at higher loading rates. As a result, the flexibility of the isolators in the lateral direction is reduced which causes a reduction in the dissipation energy according to equation 3.7.

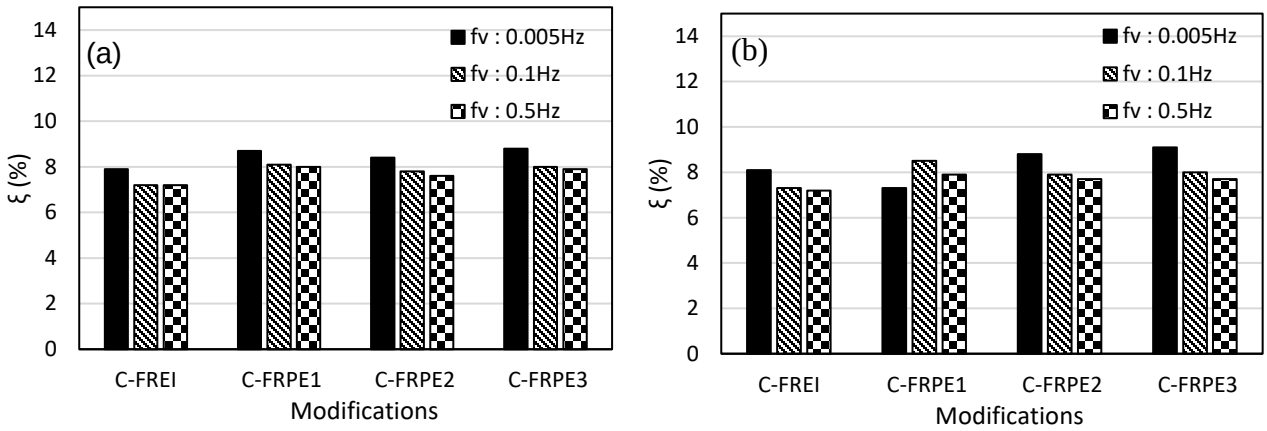

Figure 56: Equivalent viscous damping comparison under different lateral loading rates of all the isolator modifications for (a) bonded (b)unbonded

4.3.2 Compression-shear test summary

In order to shed light on the lateral performance of the carbon-fiber reinforced elastomeric isolators with polyurethane cores (C-FRPEs), compression-shear testing has been done as described in ISO 22762:2018. The isolators were subjected to a constant vertical pressure followed by a series of cyclic shear strains. A series of cyclic shear strains with amplitudes ranging from 25%T_e up to 150%T_e has been applied to determine the horizontal stiffness and energy dissipation characteristics. Moreover, three different dependence tests were also conducted to evaluate the effect on the horizontal characteristics resulting from multi amplitude strains, variation of compressive pressure, and the lateral loading rate.

It is observed from the hysteresis behavior that all the isolators show a very consistent stable behavior with no negative tangential stiffness even at the maximum strains. A non-linear softening behavior is observed for the plain C-FREI at higher strain amplitudes which are eliminated by the placement of the polyurethane cores, thereby increasing the stable rollover deformation (SRD) of the isolators in unbonded applications. This SRD is more efficient for radially distributed polyurethane (PE) cores and illustrates an almost linear behavior up to the maximum strain amplitude of 150%T_e.

There is a very slight increase in the horizontal stiffness for the isolators containing the polyurethane cores. This increase amounts to ~2-4% for unbonded applications and ~6-8% for bonded applications. Although an increase in the horizontal stiffness means lower flexibility, this increase when compared to the actual magnitudes of the horizontal stiffness, is almost negligible. In fact, this slight increase in horizontal stiffness is what contributes to the enhanced rollover deformation of the isolators. There is no distinguishable variation in the horizontal stiffness for the different distribution of the PE cores.

The energy dissipation and the equivalent viscous damping for the C-FRPEs are higher when compared to the plain C-FREIs. Radially distributed cores dissipate higher energy compared to a single core. At higher shear strain amplitudes, this energy dissipation capability for the C-FRPEs becomes even more prominent proving their advantage in higher magnitude earthquakes. At the highest strain considered (150%T_e), C-FRPEs depicted a maximum of 20.2% higher energy dissipation capacity compared to the C-FREI in unbonded applications. For bonded applications, this energy dissipation becomes even higher, with a maximum difference of 25%. Similarly, the maximum increase in the equivalent viscous damping when placing the cores is ~12.5% for unbonded applications and ~10% for bonded applications.

The delamination behavior of the C-FREI and C-FRPEs in bonded applications was also assessed by subjecting the isolators to various shear strain amplitudes. As fiber-reinforced isolators have a lack of flexural rigidity, premature delamination was observed in previous experiments conducted for bonded applications. The use of polyurethane cores greatly reduced the delamination behavior and depicts only minor delamination up to 75%T_e. In contrast to the C-FRPEs, the plain C-FREI delaminates much earlier and shows considerable delamination at even 50%T_e. The primary reason for the improved delamination behavior when PE cores are used is due to the enhanced bond between the PE cores and the testing steel plates when using rubber cement as the bonding agent.

The dependency effect of multi amplitude shear strains, variable vertical pressure, and the lateral loading rate was found to be similar for both bonded and unbonded applications. The degradation in horizontal stiffness and the equivalent viscous damping when the simultaneous amplitude of cyclic shear strains is applied are lower compared to when the strains are applied individually. This proves that no detrimental effect will occur when the isolators are subjected to random ground motions having multiple random amplitudes. The effect of changes in the vertical pressure had a negligible effect on the horizontal stiffness of the isolators. However, the damping co-efficient increases at high vertical pressures for all the isolators. This increase in damping at higher vertical pressures amounts to a maximum of 7% for the plain C-FREI and 16% for the C-FRPEs. Lastly, the increase in the lateral loading rate causes the horizontal stiffness to rise by ~5-8% and causes the equivalent viscous damping to reduce by a maximum of 9.2% for all the isolator configurations.

Chapter 5: Conclusion

5.1 Summary and conclusions

In this study, a novel form of carbon-fiber reinforced elastomeric isolators consisting of polyurethane cores (C-FRPEs) were designed and tested in vertical and lateral directions. Four different configurations of isolators having identical length and width (140mm by 140mm), number of elastomer layers, and thickness of elastomer and fiber reinforcement layers were designed. The configurations differed from each other with one having no polyurethane (PE) core (plan C-FREI), one having a single PE core at the center (C-FRPE1), and the other two having two different radial distributions of PE cores (C-FRPE2 and C-FRPE3). The area of the PE cores used in each configuration was kept constant at 12.5% of the total area of the isolators. Polyurethane is a highly anti-abrasive with a high energy dissipation capability. Polyurethane also shows an ideal self-centering capability when tested with a precompression which is always the case for elastomeric isolators due to isolators having to support the weight of the superstructure. Therefore, polyurethane material is chosen as the material of the cores in this study.

The isolators were fabricated using a simple and efficient manufacturing process where a cold vulcanization method was used to bond the elastomer and the reinforcement layers. The hardness of the elastomer and the polyurethane materials reads to 55 shore A and 60 shore A on a durometer scale. Reinforcement was provided between the layers using bidirectional carbon fiber sheets. The isolators were subjected to two different types of testing, namely the vertical testing and the compression-shear testing, which were conducted according to the testing methods described by ISO 22762:2018. A series of tests under each type of the main tests were introduced to evaluate the vertical and the horizontal performance, as well as the delamination behavior of the isolators. The tests were conducted for both bonded and unbonded applications where the same bonding agent used for bonding the layers was used to bond the specimens to the testing steel plates. A uniaxial testing machine was used for the vertical tests whereas, a bi-

directional testing machine capable of applying both compressive and horizontal loads simultaneously was designed and fabricated for the compressive-shear tests. Chapter 3 details the fabrication, test protocols, and the test setup used in this study.

The experimental results showed considerable improvement in the performance of C-FREIs when polyurethane cores are placed. The vertical tests showed that upon placing the PE cores, there was a reduction in the vertical stiffness. This reduction in stiffness was expected as parts of the isolator containing the reinforcement were removed to place the PE cores. However, the vertical failure tests showed that the C-FRPEs were able to withstand loads up to 8.1MPa which is well above the loads expected at service. The placement of the PE cores suggested a remarkable increase in the equivalent viscous damping and energy dissipation characteristics. This increase in damping was seen to be more than twice at higher pressures which will make the C-FRPEs very efficient to dissipate the vertical component of a seismic event. Moreover, the isolator with a single PE core at the center (C-FRPE1) was found to be the most efficient in terms of vertical loads and limiting the maximum vertical displacements from the total loads.

The compressive-shear testing also showed a considerable improvement in the performance of C-FREIs by placing the PE cores. By increasing the shear strain for all the isolators, a degradation in the horizontal stiffness occurs due to Mullin's effect which is the stress softening phenomenon, and the rollover deformation. Shear strain amplitudes ranging from 25%T_e up to 150%T_e (T_e is the total thickness of the elastomer layers) were applied and the hysteresis loops showed a very consistent and stable behavior for all the shear strain amplitudes. The Stable Rollover Deformation (SRD) was improved by the placement of the PE cores by reducing the softening behavior occurring at higher lateral displacements. A slight increase in the horizontal stiffness ranging from 2-8% was observed for the C-FRPEs when compared to the plain C-FREIs. Therefore, this slight increase will only cause a small increase in the effective shear modulus of the isolators when compared to the plain C-FREI. This shows that the energy dissipation in the lateral direction is improved without affecting the flexibility of the isolators in the

lateral direction. Furthermore, the polyurethane cores do not have a negative impact on the rollover behavior of the isolators, which is necessary for fiber-reinforced isolators when used in unbonded applications. The location or distribution of the PE cores had little to no effect on the horizontal stiffness. Moreover, the energy dissipation and the equivalent viscous damping increased by the placement of the PE cores in the C-FREIs. For unbonded applications, radially distributed PE cores dissipate higher energy whereas, for bonded applications, a single PE core at the center dissipates higher energy. This increase in energy dissipation of C-FRPEs showed a maximum increase of 20% and 25% for unbonded and bonded applications respectively, compared to C-FREIs. Similarly, the equivalent viscous damping showed an increase of 10-12.5% for the C-FRPEs compared to the plain specification.

The delamination behavior upon placing PE cores was also tested followed by a few dependency tests. The dependency tests consisted of finding the effect of multi amplitude strains, compressive pressure, and the lateral loading rate on the horizontal characteristics. The plain C-FREI showed major delamination even at 50%T_e. In contrast to the plain specification, the C-FRPEs showed a significant improvement in the delamination behavior and shows only minor delamination even at higher strains of 75%T_e. This is a major finding which can expand the usage of carbon-fiber reinforced elastomeric isolators in bonded applications. The primary reason for the improved delamination behavior is due to the enhanced bond between the PE cores and the testing steel plates when using rubber cement as the bonding agent. Multiple amplitudes of cyclic strains when applied simultaneously do not have a negative impact on the horizontal performance of the isolators. In fact, the degradation of horizontal stiffness is lower when the strains are applied simultaneously. The variation in the vertical pressure does not cause any change to the horizontal stiffness for all the isolators. However, the damping coefficient increase at higher vertical loads. This increase in damping amounts to approximately 7% for the plain C-FREI and 16% for the C-FRPEs. An increase in the lateral loading rate causes the horizontal stiffness to increase by 5-8% and the damping coefficient to increase by 9.2% for all the isolator configurations. The tests

proved that the use of PE cores in C-FREIs can improve their performance and be viable to be used in full-scale applications.

5.2 Limitations and future study

Based on the vertical tests performed, there was a reduction in the vertical stiffness when polyurethane cores are placed. Moreover, slight delamination between the elastomer and the reinforcement layers was observed after a vertical pressure of 5MPa due to the extra bulging of the polyurethane cores. In order to improve the vertical stiffness when the PE cores are used, the cores can be wrapped with carbon fiber sheets before placing them, thereby limiting the lateral bulging of the cores.

Based on the compressive-shear tests, a limitation of this thesis is that the amplitude of the lateral cyclic strains was limited to a maximum of 150% of the total thickness of the elastomer layers. Although beyond this strain, the vertical faces of the isolator would come in contact with the testing steel plates (complete rollover deformation) and cause an increase in the horizontal stiffness, it is worth exploring how PE cores can cause an effect on this behavior. Local delamination was observed in bonded applications starting from 50%T_e, which was significantly improved by the placement of the PE cores. In order to reduce even more or to eliminate the local delamination, the strength of the bonding agent used for attaching the layers should be increased. Other methods of bonding can also be used by changing the manufacturing process or by the use of supplementary elements.

Factors such as ambient temperature, aging, and humidity were not considered in this study. Elastomeric isolators are usually installed outdoors exposing them to different temperatures and climates in different regions. Therefore, the effect of extreme temperatures, humidity, and aging should be explored in future work when considering PE cores in C-FREIs.

One of the major limitations of this thesis is the area and distribution of the PE cores used in the isolators. Three different core distributions were used, which were a single PE core, and

two distributed configurations of five PE cores. The area of the PE cores was kept constant in all the configurations which were 12.5% of the total surface area of the isolators. Future studies can be conducted by changing the area of the PE cores and using more cores having different distributions.

5.2 Research contribution

Overall, it was demonstrated that the use of polyurethane cores improved the performance of carbon-fiber reinforced elastomeric isolators in both vertical and horizontal directions. Previous studies related to the experimental investigation of C-FREIs showed premature delamination in bonded applications and a limited energy dissipation capability in unbonded applications. In order to address and improve on these shortcomings of C-FREIs, polyurethane cores were used.

The carbon-fiber reinforced elastomeric isolators with polyurethane cores (C-FRPEs) showed an enhanced energy dissipation for both bonded and unbonded applications. Premature delamination was also improved significantly proving their viability to be used in bonded applications. The non-linear softening occurring at higher displacements in unbonded applications were also reduced by the use of such cores.

Bibliography

Ahmadipour, M., & Alam, M. S. (2017). Sensitivity analysis on mechanical characteristics of lead-core steel-reinforced elastomeric bearings under cyclic loading. *Engineering Structures*, *140*, 39–50. https://doi.org/10.1016/j.engstruct.2017.02.014

Al-Anany, Y. M., & Tait, M. J. (2017). Experimental assessment of utilizing fiber reinforced elastomeric isolators as bearings for bridge applications. *Composites Part B: Engineering*, *114*, 373–385. https://doi.org/10.1016/j.compositesb.2017.01.060

Amin, A. F. M., Wiraguna, S., Bhuiyan, A., & Okui, Y. (2006). Hyperelasticity model for finite element analysis of natural and high damping rubbers in compression and shear. *Journal of Engineering Mechanics*, *132*(1), 54–64. https://doi.org/10.1061/(ASCE)0733-9399(2006)132

Bakhshi, A., Jafari, M. H., & Valadoust Tabrizi, V. (2014). Study on dynamic and mechanical characteristics of carbon fiber- and polyamide fiber-reinforced seismic isolators. *Materials and Structures/Materiaux et Constructions*, *47*(3), 447–457. https://doi.org/10.1617/s11527-013-0071-z

Buckle, I. G. (2000). Passive control of structures for seismic loads. *Bulletin of the New Zealand Society for Earthquake Engineering*, *33*(3), 209–221. https://doi.org/10.5459/bnzsee.33.3.209-221

Calabrese, A., Quaglini, V., Strano, S., & Terzo, M. (2020). Online estimation of the friction coefficient in sliding isolators. *Structural Control and Health Monitoring*, *27*(3), 1–16. https://doi.org/10.1002/stc.2459

Canadian Standard Association (CSA). 2019. Canadian highway bridge design code (CHBDC) CAN/CSA-S6-19. Rexdale, Ontario, Canada. (2019).

Cenan, O. (2010). Development of a new seismic isolator named “ball rubber bearing. In Middle East Technical University.

Choi, E., Jeon, J. S., & Seo, J. (2017). Cyclic compressive behavior of polyurethane rubber springs for smart dampers. *Smart Structures and Systems*, *20*(6), 739–757. https://doi.org/10.12989/sss.2017.20.6.739

Constantinou, B. M., Member, A., Mokha, A., & Reinhorn, A. (1990). Teflon bearings in base isolation: Modeling. J*ournal of Structural Engineering 116*(2), 455–474.

Daniell, J. E., Vervaeck, A., & Wenzel, F. (2011). A timeline of the socio-economic effects of the 2011 Tohoku Earthquake with emphasis on the development of a new worldwide rapid earthquake loss estimation procedure. *Australian Earthquake Engineering Society 2011 Conference, Nov*, *May 2014*, 18–20.

Dezfuli, F. Hedayati, & Alam, M. S. (2014). Performance of carbon fiber-reinforced elastomeric isolators manufactured in a simplified process: Experimental investigations. *Structural Control and Health Monitoring*, *21*, 1347–1359. https://doi.org/10.1002/stc.1653

Dezfuli, Farshad Hedayati, & Alam, M. S. (2016). Experiment-based sensitivity analysis of scaled carbon-fiber-reinforced elastomeric isolators in bonded applications. *Fibers*, *4*(1). https://doi.org/10.3390/fib4010004

Dolce, M., Cardone, D., & Marnetto, R. (2000). Implementation and testing of passive control devices based on shape memory alloys. *Earthquake Engineering and Structural Dynamics*, *29*(7), 945–968. https://doi.org/10.1002/1096-9845(200007)29:7<945::aid-eqe958>3.0.co;2-%23

Dolce, M., Cardone, D., Marnetto, R., Nigro, D., & Palermo, G. (2003). A New added damping rubber isolator (ADRI): Experimental tests and numerical simulations. *8th World Seminar on Seismic Isolation, Energy Dissipation and Active Vibration Control of Structures Yerevan, Armenia*, *October*, 6–10.

Farzad Naeim, J. M. K. (2000). Design of seismic isolated structures: From theory to practice. *Earthquake Spectra*.

Gauron, O., Saidou, A., Busson, A., Siqueira, G. H., & Paultre, P. (2018). Experimental

determination of the lateral stability and shear failure limit states of bridge rubber bearings. *Engineering Structures*, *174*, 39–48. https://doi.org/10.1016/j.engstruct.2018.07.039

Govardhan, & Paul, D. K. (2016). Effect of lead in elastomeric bearings for structures located in seismic region. *Procedia Technology*, *25*, 146–153. https://doi.org/10.1016/j.protcy.2016.08.091

Hamid, T.-N., Michael, T., & Robert G, D. (2007). Shake table study on an ordinary low-rise building seismically isolated with SU-FREIs (stable unbonded-fiber reinforced elastomeric isolators). *Pacific Conference on Earthquake Engineering*, *056*, 1–6. https://doi.org/10.1002/eqe

Hayashi, S., Watanabe, H., Nakamura, Y., Yoshizawa, T., & Nakamura, T. (1993). Response characteristics of base-isolated structure with silicone rubber bearings. *Elsevier Science Publishers*.

Hedayati Dezfuli, F., & Alam, M. S. (2013). Multi-criteria optimization and seismic performance assessment of carbon FRP-based elastomeric isolator. *Engineering Structures*, *49*, 525–540. https://doi.org/10.1016/j.engstruct.2012.10.028

Hedayati Dezfuli. (2015). Hysteretic behaviour of steel and fibre-reinforced elastomeric isolators fitted with superelastic shape memory alloy wire. The University of British Columbia.

Hedayati Dezfuli, Farshad, & Alam, M. S. (2017). Effect of different steel-reinforced elastomeric isolators on the seismic fragility of a highway bridge. *Structural Control and Health Monitoring*, *24*(2), 1–15. https://doi.org/10.1002/stc.1866

ISO 22762-1:2018*:* Elastomeric seismic protection isolators: Part 1 test methods. (2018).

Jangid, R. S. (2007). Optimum lead-rubber isolation bearings for near-fault motions. *Engineering Structures*, *29*(10), 2503–2513. https://doi.org/10.1016/j.engstruct.2006.12.010

Kalpakidis, I. V., & Constantinou, M. C. (2009a). Effects of heating on the behavior of lead-rubber bearings. I: Theory. *Journal of Structural Engineering*, *135*(12), 1440–1449.

https://doi.org/10.1061/(asce)st.1943-541x.0000072

Kalpakidis, I. V., & Constantinou, M. C. (2009b). Effects of heating on the behavior of lead-rubber bearings. II: Verification of Theory. *Journal of Structural Engineering*, *135*(12), 1450–1461. https://doi.org/10.1061/(asce)st.1943-541x.0000071

Kelly, J.M. (1993). Earthquake-resistant design with rubber. In *Springer-Verlag London Limited 1993*. Springer-Verlag London Limited 1993. https://doi.org/10.1017/CBO9781107415324.004

Kelly, James M. (2002). Seismic isolation systems for developing countries. *Earthquake Spectra*, *18*(3), 385–406. https://doi.org/10.1193/1.1503339

Kelly, James M. (2008). Analysis of the run-in effect in fiber-reinforced isolators under vertical load. *Journal of Mechanics of Materials and Structures*, *3*(7), 1383–1401. https://doi.org/10.2140/jomms.2008.3.1383

Kelly, James M., & Konstantinidis, D. A. (2011a). Mechanics of rubber bearings for seismic and vibration isolation. *Mechanics of Rubber Bearings for Seismic and Vibration Isolation*. https://doi.org/10.1002/9781119971870

Kelly, James M., & Konstantinidis, D. A. (2011b). Mechanics of rubber bearings for seismic and vibration isolation. In *John Wiley and Sons Ltd*. https://doi.org/10.1002/9781119971870

Kelly, James M. (1999a). Analysis of fiber-reinforced elastomeric isolators. *Journal of Structural and Earthquake Engineering*, *2*, 19–34.

Kelly, James M. (1999b). Analysis of fiber-reinforced elastomeric isolators. *Journal of Structural and Earthquake Engineering*, *2*(1), 19–34.

Khazai, B., Daniell, J., & Wenzel, F. (2011). The March 2011 Japan earthquake. *TATuP - Zeitschrift Für Technikfolgenabschätzung in Theorie Und Praxis*, *20*(3), 22–33. https://doi.org/10.14512/tatup.20.3.22

Kim, J. H., Kim, M. K., & Choi, I. K. (2019). Experimental study on seismic behavior of lead-rubber bearing considering bi-directional horizontal input motions. *Engineering Structures*,

198(June), 109529. https://doi.org/10.1016/j.engstruct.2019.109529

Liu, T., Zordan, T., Briseghella, B., & Zhang, Q. (2014). An improved equivalent linear model of seismic isolation system with bilinear behavior. *Engineering Structures*, *61*, 113–126. https://doi.org/10.1016/j.engstruct.2014.01.013

Lu, Y., Song, J., Xiong, F., Dai, K., Zhou, G., Wei, M., & Zhang, S. (2020). Simplified procedures for seismic design verification and evaluation of lead rubber bearing base-isolated buildings based on free-vibration response. *Structural Design of Tall and Special Buildings*, *29*(12), 1–16. https://doi.org/10.1002/tal.1751

Madera Sierra, I. E., Losanno, D., Strano, S., Marulanda, J., & Thomson, P. (2019). Development and experimental behavior of HDR seismic isolators for low-rise residential buildings. *Engineering Structures*, *183*, 894–906. https://doi.org/10.1016/j.engstruct.2019.01.037

Marioni, A. (n.d.). The use of high damping rubber bearings for the protection of the structures from seismic risk. *Jornadas Portuguesas de Engenharia de Estruturas*.

Markou, A. A., Oliveto, G., & Athanasiou, A. (2016). Response simulation of hybrid base isolation systems under earthquake excitation. *Soil Dynamics and Earthquake Engineering*, *84*, 120–133. https://doi.org/10.1016/j.soildyn.2016.02.003

Masato, A., Junji, Y., & Yozo, F. (2004). Multiaxial behaviors of laminated rubber bearings and their modeling. I: Experimental Study. *Journal of Structural Engineering*, *130*(8), 1119–1132. https://doi.org/10.1061/(ASCE)0733-9445(2004)130

Milani, G., & Milani, F. (2012). Stretch–stress behavior of elastomeric seismic isolators with different rubber materials: Numerical insight. *Journal of Engineering Mechanics*, *138*(5), 416–429. https://doi.org/10.1061/(asce)em.1943-7889.0000340

Montuori, G. M., Mele, E., Marrazzo, G., Brandonisio, G., & De Luca, A. (2016). Stability issues and pressure–shear interaction in elastomeric bearings: The primary role of the secondary shape factor. *Bulletin of Earthquake Engineering*, *14*(2), 569–597.

https://doi.org/10.1007/s10518-015-9819-x

Moon, B.-Y., Kang, G.-J., Kang, B.-S., & Kelly, J. M. (2002). Design and manufacturing of fiber reinforced elastomeric isolator for seismic isolation. *Journal of Materials Processing Technology*, *2*, 145–150.

Muntasir Billah, A. H. M., & Shahria Alam, M. (2015). Seismic fragility assessment of concrete bridge pier reinforced with superelastic shape memory alloy. *Earthquake Spectra*, *31*(3), 1515–1541. https://doi.org/10.1193/112512EQS337M

Naghshineh, A., Akyuz, U., & Caner, A. (2013). Comparison of fundamental properties of new types of fiber-mesh- reinforced seismic isolators with conventional isolators. *Earthquake Engineering and Structural Dynamics*, *43*, 301–316. https://doi.org/10.1002/eqe.2345

Okui, Y., Nakamura, K., Sato, T., & Imai, T. (2019). Seismic response of isolated bridge with high damping rubber bearings: Self-heating effect at subzero temperatures. *Steel Construction*, *12*(1), 2–9. https://doi.org/10.1002/stco.201800029

Osgooei, P. M., Tait, M. J., & Konstantinidis, D. (2014). Three-dimensional finite element analysis of circular fiber-reinforced elastomeric bearings under compression. *Composite Structures*, *108*(1), 191–204. https://doi.org/10.1016/j.compstruct.2013.09.008

Ozbulut, O. E., Mir, C., Moroni, M. O., Sarrazin, M., & Roschke, P. N. (2007). A fuzzy model of superelastic shape memory alloys for vibration control in civil engineering applications. *Smart Materials and Structures*, *16*(3), 818–829. https://doi.org/10.1088/0964-1726/16/3/031

Pauletta, M., Cortesia, A., Pitacco, I., & Russo, G. (2017). A new bi-linear constitutive shear relationship for Unbonded Fiber-Reinforced Elastomeric Isolators (U-FREIs). *Composite Structures*, *168*, 725–738. https://doi.org/10.1016/j.compstruct.2017.02.065

Pauletta, M., Cortesia, A., & Russo, G. (2015). Roll-out instability of small size fiber-reinforced elastomeric isolators in unbonded applications. *Engineering Structures*, *102*, 358–368. https://doi.org/10.1016/j.engstruct.2015.08.019

Qi, H. J., & Boyce, M. C. (2005). Stress-strain behavior of thermoplastic polyurethanes. *Mechanics of Materials*, *37*(8), 817–839. https://doi.org/10.1016/j.mechmat.2004.08.001

Rahman Bhuiyan, A., & Alam, M. S. (2013). Seismic performance assessment of highway bridges equipped with superelastic shape memory alloy-based laminated rubber isolation bearing. *Engineering Structures*, *49*, 396–407. https://doi.org/10.1016/j.engstruct.2012.11.022

Rahnavard, R., Craveiro, H. D., & Napolitano, R. (2020). Static and dynamic stability analysis of a steel-rubber isolator with rubber cores. *Structures*, *26*, 441–455. https://doi.org/10.1016/j.istruc.2020.04.048

Rahnavard, R., & Thomas, R. J. (2019). Numerical evaluation of steel-rubber isolator with single and multiple rubber cores. *Engineering Structures*, *198*, 109532. https://doi.org/10.1016/j.engstruct.2019.109532

Redwood Plastics and Rubber. (n.d.). Elastomeric Bridge bearings.

Riyadh, M. ., Hedayati Dezfuli, F., & Alam, M. S. (2020). Parametric study on the lateral stiffness of carbon-fibre reinforced elastomeric isolators against cyclic loads. *IABSE-JSCE Joint Conference on Advances in Bridge Engineering-IV, August 26-27, 2020, Dhaka, Bangladesh*, 449–457.

Robinson, W., & Greenbank, L. (1976). An extrusion energy absorber suitable for the protection of structures during an earthquake. *Earquake Engineering Structural Dynamics*, *4*(3), 251–259. https://onlinelibrary.wiley.com/doi/10.1002/eqe.4290040306

Russo, G., & Pauletta, M. (2013). Sliding instability of fiber-reinforced elastomeric isolators in unbonded applications. *Engineering Structures*, *48*, 70–80. https://doi.org/10.1016/j.engstruct.2012.08.031

Russo, G., Pauletta, M., & Cortesia, A. (2013). A study on experimental shear behavior of fiber-reinforced elastomeric isolators with various fiber layouts, elastomers and aging conditions. *Engineering Structures*, *52*, 422–433. https://doi.org/10.1016/j.engstruct.2013.02.034

Salim, J., & Ananthakumar, N. (2017). Finite element analysis of fibre reinforced elastomeric bearings with different aspect ratio. *International Journal of Advance Engineering and Research Development*, *4*(04), 7–14. https://doi.org/10.21090/ijaerd.38737

Satish, N., Andrei, M. R., & Michalakis, C. C. (1991). Nonlinear dynamic analysis of 3-D- base-isolated structures. *Journal of Structural Engineering*, *117*(7), 2035–2054.

Siqueira, G. H., Sanda, A. S., Paultre, P., & Padgett, J. E. (2014). Fragility curves for isolated bridges in eastern Canada using experimental results. *Engineering Structures*, *74*, 311–324. https://doi.org/10.1016/j.engstruct.2014.04.053

Sistla, S., & Mohan, S. C. (2020). Numerical modelling of bonded and unbonded flax fiber reinforced elastomeric isolator and their application to RC building. *Materials Today: Proceedings*, *38*, 2890–2898. https://doi.org/10.1016/j.matpr.2020.09.143

Skinner, R., Robinson, W., & McVerry, G. (1993). *An Introduction to Seismic Isolation*. John Wiley & Sons Ltd., U.K.

Spizzuoco, M., Calabrese, A., & Serino, G. (2014). Innovative low-cost recycled rubber-fiber reinforced isolator: Experimental tests and finite element analyses. *Engineering Structures*, *76*, 99–111. https://doi.org/10.1016/j.engstruct.2014.07.001

Talaeitaba, S. B., Pourmasoud, M. M., & Jabbari, M. (2019). An innovative base isolator with steel rings and a rubber core. *Asian Journal of Civil Engineering*, *20*(3), 313–325. https://doi.org/10.1007/s42107-018-00107-9

Toopchi-Nezhad, H., Tait, M., & Drysdale, R. (2011). Bonded versus unbonded strip fiber reinforced elastomeric isolators: Finite element analysis. *Composite Structures*, *93*(2), 850–859. https://doi.org/10.1016/j.compstruct.2010.07.009

Toopchi-Nezhad, H., Tait, M. J., & Drysdale, R. G. (2008). Testing and modeling of square carbon fiber-reinforced elastomeric seismic isolators. *Structural Control and Health Monitoring*, *15*(6), 876–900. https://doi.org/10.1002/stc.225

Toopchi-Nezhad, H., Tait, M. J., & Drysdale, R. G. (2013). Influence of thickness of individual

elastomer layers (first shape factor) on the response of unbonded fiber-reinforced elastomeric bearings. *Journal of Composite Materials*, *47*(27), 3433–3450. https://doi.org/10.1177/0021998312466686

Tsai, H., & Kelly, J. M. (2002). Bending Stiffness of fiber-reinforced circular seismic isolators. *Journal of Engineering Mechanics*, *128*, 1150–1157.

Van Engelen, N. C., Osgooei, P. M., Tait, M. J., & Konstantinidis, D. (2014). Experimental and finite element study on the compression properties of Modified Rectangular Fiber-Reinforced Elastomeric Isolators (MR-FREIs). *Engineering Structures*, *74*, 52–64. https://doi.org/10.1016/j.engstruct.2014.04.046

Van Engelen, N. C., Tait, M. J., & Konstantinidis, D. (2019). Investigation of partially bonded fiber-reinforced elastomeric isolators (PB-FREIs) with nominal vertical tensile loads. *Canadian Journal of Civil Engineering*, *46*(8), 669–676. https://doi.org/10.1139/cjce-2018-0014

Vanngo, T., Dutta, A., & Deb, S. (2017). Evaluation of horizontal stiffness of fibre-reinforced elastomeric isolators. *Earthquake Engineering and Structural Dynamics*, *46*, 1747–1767. https://doi.org/10.1002/eqe

Warn, G. P., & Ryan, K. L. (2012). A review of seismic isolation for buildings: Historical development and research needs. *Buildings*, *2*(3), 300–325. https://doi.org/10.3390/buildings2030300

Warn, G. P., Whittaker, A. S., & Constantinou, M. C. (2007a). Vertical Stiffness of elastomeric and lead–rubber seismic isolation bearings. *Journal of Structural Engineering*, *133*(9), 1227–1236. https://doi.org/10.1061/(ASCE)0733-9445(2007)133:9(1227)

Warn, G. P., Whittaker, A. S., & Constantinou, M. C. (2007b). Vertical stiffness of elastomeric and lead–rubber seismic isolation bearings. *Journal of Structural Engineering*, *133*(9), 1227–1236. https://doi.org/10.1061/(asce)0733-9445(2007)133:9(1227)

Xiang, N., Alam, M.S., Li, J. (2018) Shake table studies of a highway bridge model by allowing

the sliding of laminated-rubber bearings with and without restraining devices. *Engineering Structures*, 171, 583–601.

Yoshida, J., Abe, M., & Fujino, Y. (2002). Constitutive model of high damping rubber materials. *Doboku Gakkai Ronbunshu*, *2002*(710), 209–224. https://doi.org/10.2208/jscej.2002.710_209

Yuan, Y., Wei, W., Ping, T., Akira, I., Hongping, Z., Hirokazu, I., & Tetsuhiko, A. (2016). A rate-dependent constitutive model of high damping rubber bearings: Modeling and experimental verification. *Earthquake Engineering & Structural Dynamics*, *45*, 1875–1892. https://doi.org/10.1002/eqe

Z-Tech, G. (2010). *Goodco Z-Tech - Elastomeric bearings*. 1–20.

Zhao, Y. X., Hu, W. J., Mei, J., Wei, N., & Xie, J. J. (2011). Experimental study on mechanical properties of rubber used for damping bearing. *Advanced Materials Research*, *189–193*, 1132–1136. https://doi.org/10.4028/www.scientific.net/AMR.189-193.1132

Appendices

Appendix A: Stepwise procedure for strengthening the lateral bracing system for the compression-shear test setup

The compression shear test setup before extra strengthening

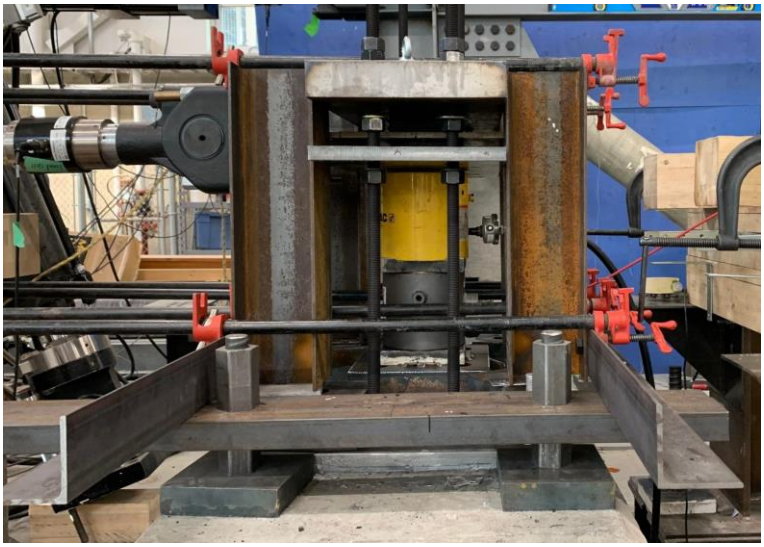

Strong clamps were added to increase the torsional strength of the L-sections and make the test setup to act as a frame

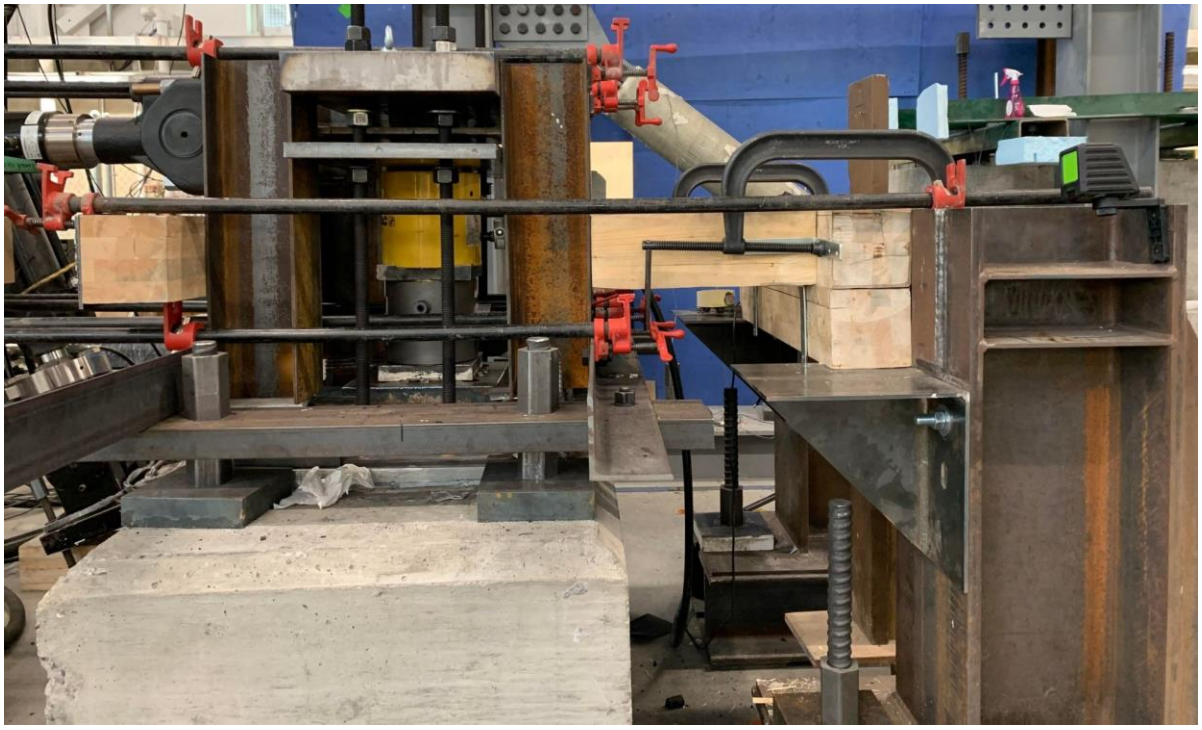

Timber beams and strong clamps were extended to reduce the moment arm of the I-sections.

The beams and clamps were held by a pedestal post-tensioned to the strong floor.

Appendix B: Lateral force vs lateral displacement hysteresis loops by varying the vertical compression for unbonded application

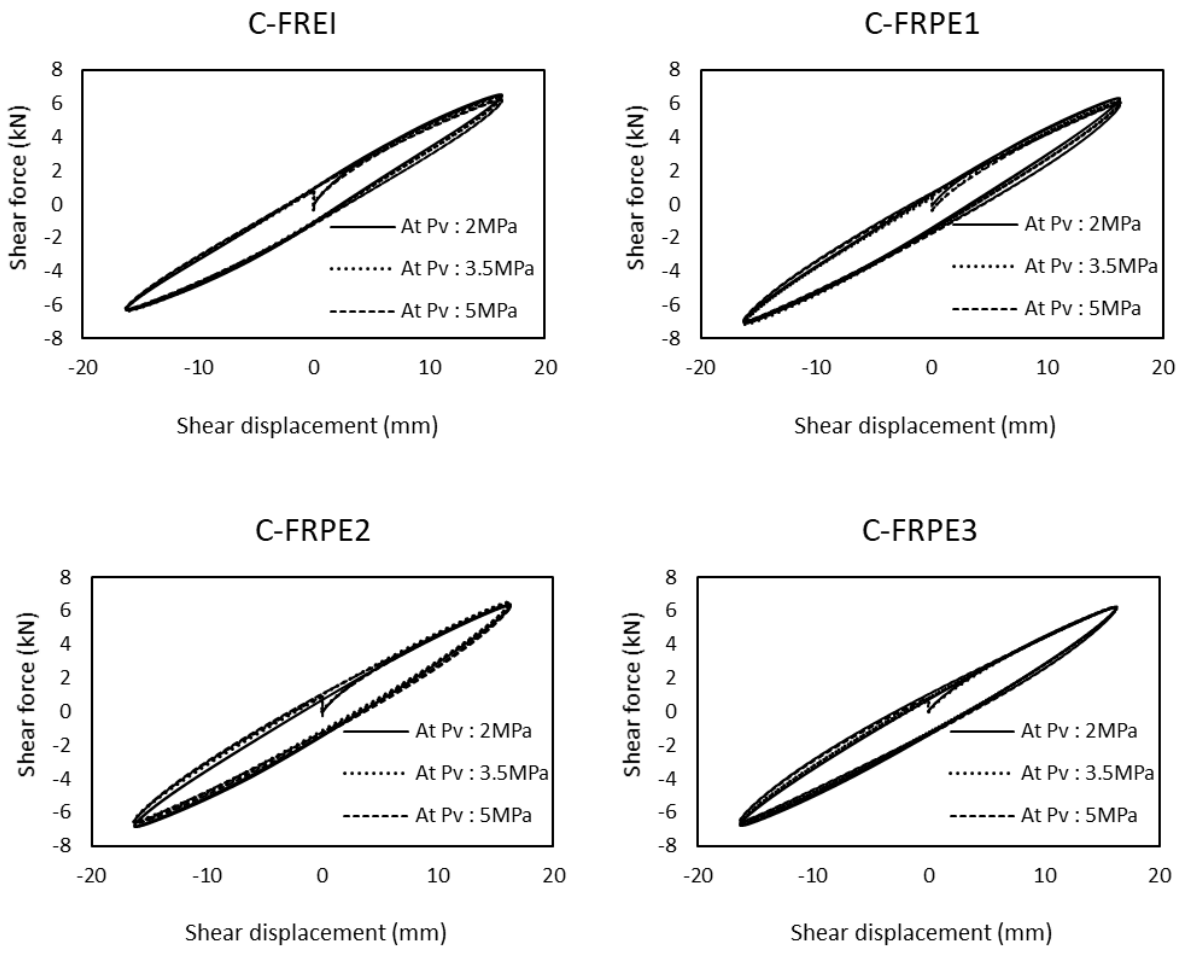

Appendix C: Lateral force vs lateral displacement hysteresis loops by varying the vertical compression for bonded application

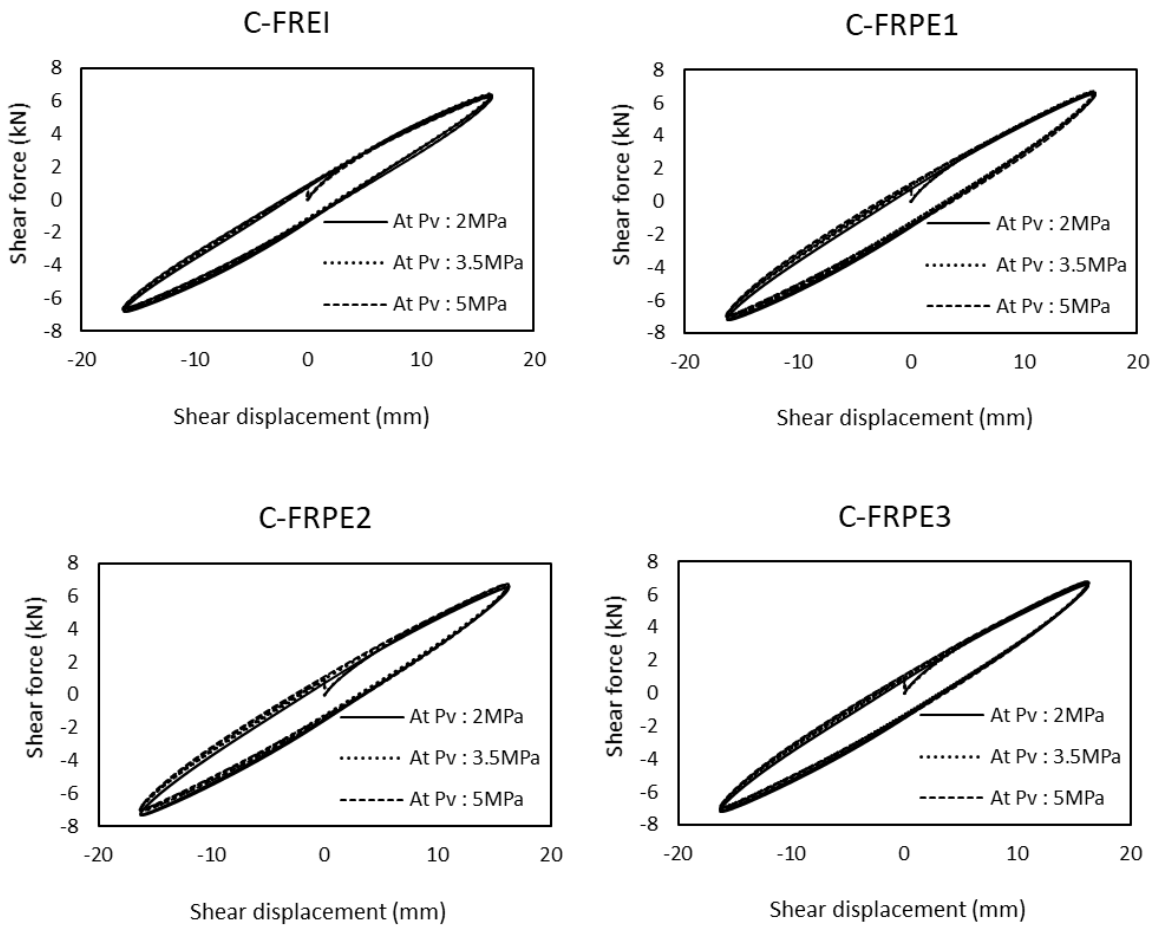

Appendix D: Lateral force vs lateral displacement hysteresis loops by varying the lateral loading rate for unbonded application

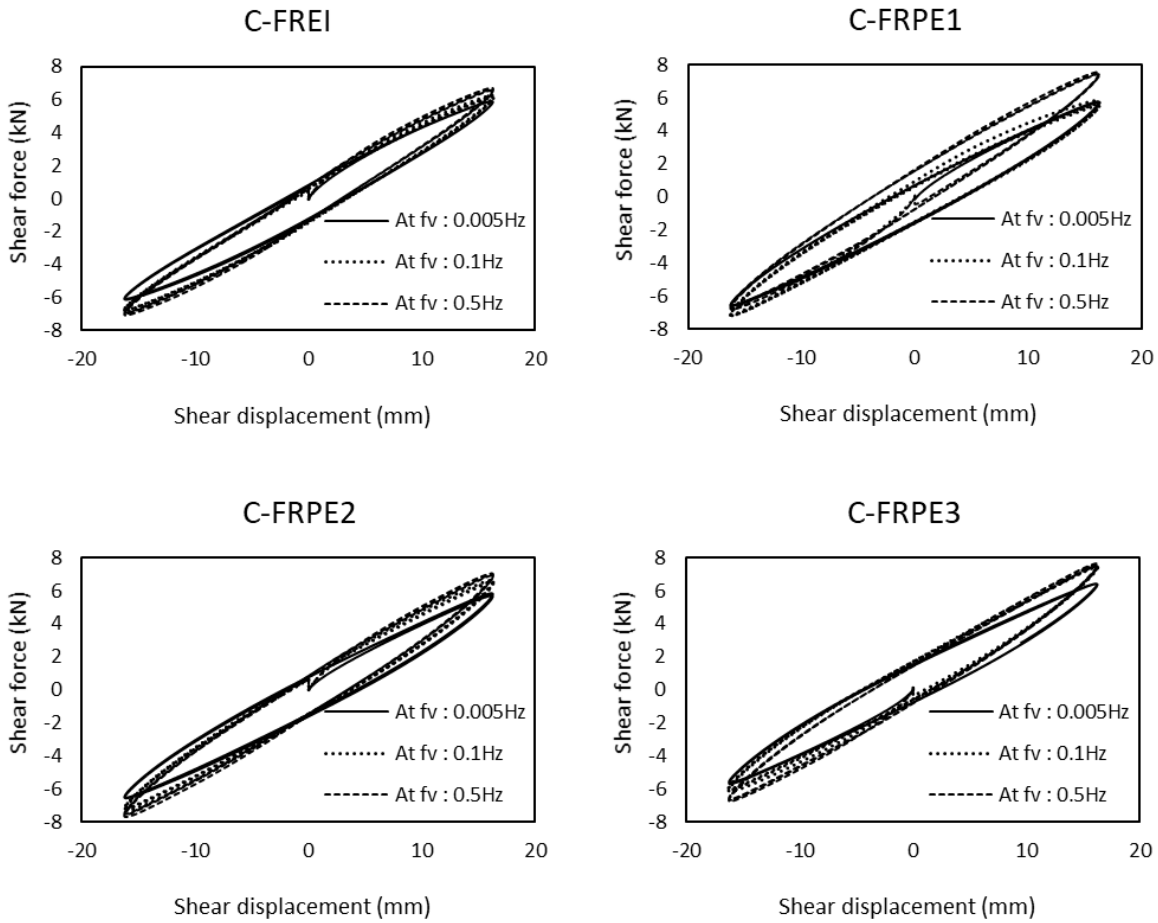

Appendix E: Lateral force vs lateral displacement hysteresis loops by varying the lateral loading rate for bonded application